A DYNAMICAL UNDERSTANDING OF STRATOSPHERIC INFLUENCES ON TROPOSPHERIC CLIMATE AND THE OCEAN

by

Junsu Kim

A dissertation submitted to the faculty of
The University of Utah
in partial fulfillment of the requirements for the degree of

Doctor of Philosophy

Department of Atmospheric Sciences

The University of Utah

May 2014

THE UNIVERSTITY OF UTAH GRADUATE SCHOOL

STATEMENT OF DISSERTATION APPROVAL

The dissertation of **Junsu Kim**

has been approved by the following supervisory committee members:

Thomas Reichler,	Chair	**1/6/2014** Date Approved
John Horel,	Member	**1/6/2014** Date Approved
Larry Horowitz,	Member	**1/24/2014** Date Approved
Jan Paegle,	Member	**1/6/2014** Date Approved
Zhaoxia Pu,	Member	**1/6/2014** Date Approved

and by **Kevin Perry**, Chair of

the Department of **Atmospheric Sciences**

and by David B. Kieda, Dean of The Graduate School.

ABSTRACT

Changes in the stratospheric circulation have the potential to affect weather and climate in the troposphere, especially over the high latitudes. In order to better understand such influences, we analyze the relationships among stratospheric, tropospheric, and oceanic variability. We reach our goal with the aid of coupled chemistry-climate models and coupled atmosphere-ocean models.

Over the past decades, ozone depletion in the Antarctic stratosphere has been accelerating the poleward side of the stratospheric polar vortex. We suspect that the change in the winds in turn affects the concentrations of ozone. This idea is investigated with coupled chemistry-climate models. We find a strong indication for the existence of a positive feedback between ozone depletion and change in the circulation: the chemical ozone loss feeds back into the stratospheric circulation, and changes in the circulation produce more ozone deficit.

Climate models tend to systematically overestimate the persistence time scale of extratropical variability, in particular over the Southern Hemisphere. The systematic overestimation in climate models raises the concern that the models are overly sensitive to external forcings and that future projections based on those models are unreliable. We investigate issues concerning the persistence time scale of the annular mode using reanalysis and model data. We find that the 50-year record of historical observations is probably too short to derive a stable estimate of the annular mode time scale that may be

used to evaluate climate models. We also find a robust relationship between the magnitude and the seasonal timing of the time scale in both stratosphere and troposphere, confirming and extending earlier results of a dynamical coupling between the stratosphere and the troposphere and of influences of stratospheric variability on the troposphere.

Extreme events in the stratosphere are known to alter tropospheric weather and climate. However, it is still unclear whether the stratosphere also has the capacity to affect the ocean and its circulation. This possibility is suggested from observations which show low-frequency covariability between the stratosphere and the Atlantic thermohaline circulation. We use simulations from coupled atmosphere-ocean models to explore more systematically a possible stratospheric influence on the oceanic circulation over the North Atlantic Ocean on multidecadal time scales. Our analysis identifies the stratosphere as a previously unknown source for decadal climate variability in the troposphere and suggests that the stratosphere forms an important component of climate that should be well represented in models.

TABLE OF CONTENTS

ACKNOWLEDGMENTS

A long trip towards the completion of the Ph.D. finally comes to an end. In the trip, I first met my supervisor, Prof. Thomas Reichler. I would like to thank him for his significant help, precious advice, and endless time. With his guidance, my days in Utah have been an exciting moment. I also would like to thank all my committee, Drs. John Horel, Larry Horowitz, Jan Paegle, and Zhaoxia Pu for their helpful feedback.

I would like to thank my friends for all the fun activities. In particular, Drs. Jae-Jin Kim, Jin-Soo Seo, Jun Kim, Chang-Yong Jang, and their families have made my life in Salt Lake City enjoyable. Dr. Hyun-Wung Kwon in Korea has continuously provided me with pleasant times here.

My parents have always taken care of and supported me, and I am most indebted to them for their never-ending love. I am also thankful for my sister and her family who have always encouraged me to pursue the Ph.D. and to complete this dissertation.

CHAPTER 1

INTRODUCTION

1.1 Background

The stratosphere forms about 15% of the atmospheric air mass and is more stable and less dense than the underlying troposphere. Until recently, the stratosphere has been considered a passive recipient of waves and energy from the troposphere. However, there is a growing body of evidence suggesting that the stratosphere is not just a passive layer located above the troposphere but that it affects tropospheric weather and climate in multiple ways. For example, the stratosphere can influence the entire high-latitude weather and climate system through the dynamical coupling between the stratosphere and the troposphere (Baldwin and Dunkerton, 2001). Weather and climate centers have underestimated the full potential of the stratosphere in improving predictions since their models did not include an adequate stratospheric component. Recently, weather centers such as the European Center for Medium-Range Weather Forecasts (ECMWF) attempt to emphasize the stratosphere as adding more stratospheric levels in their operational models and as moving the model lid from the tropopause to the stratopause. The stratospheric impact on surface climate also becomes evident through the Antarctic ozone depletion: ozone depletion related cooling of the stratosphere leads to a poleward shift of the midlatitude jets, corresponding to an increase of the southern annular mode (SAM)

index at the surface (Thompson *et al.*, 2000). Consequently, incorporating the effects of stratospheric ozone depletion may help make better predictions of future climate change (Son *et al.*, 2008b). Since ozone is expected to recover in the future, it is important to understand in which ways the recovery will affect the circulation.

The concept of the so-called annular mode (AM), which is a dominant pattern of the atmospheric variability, plays an important role for an understanding of stratospheric effects on the troposphere. The Arctic oscillation (AO) (Thompson and Wallace, 1998) pattern, which is another name of the AM over the Northern Hemisphere near the surface, is shown in Figure 1. The AO manifests itself by opposite patterns in sea level pressure (SLP) over middle and high latitudes. Variability in the AO generates significant impact on weather and climate (Hurrell, 1995). For example, the positive phase of the AO, which is defined as a period of lower than normal atmospheric pressure over the Arctic, strengthens the westerlies over the North Atlantic Ocean region, and produces warmer and wetter conditions than normal over the United States and northern Europe. The negative phase of the AO, on the other hand, leads to weaker westerlies over the Central Atlantic Ocean, frequent cold air outbreaks over the U.S. and northern Europe, and increased storminess over the Mediterranean region (Thompson and Wallace, 2001). During northern winter, the AO extends upward into the stratosphere (Thompson and Wallace, 1998; 2000), where it is strongly connected with the position and strength of the polar vortex (Norton, 2003). The vertical extension of the AO to other pressure levels is referred to as the northern annular mode (NAM) (Thompson and Wallace, 1998; Baldwin and Dunkerton, 2001). More precisely, the NAM is defined as the leading empirical orthogonal function (EOF) of hemispheric geopotential height at isobaric levels. With

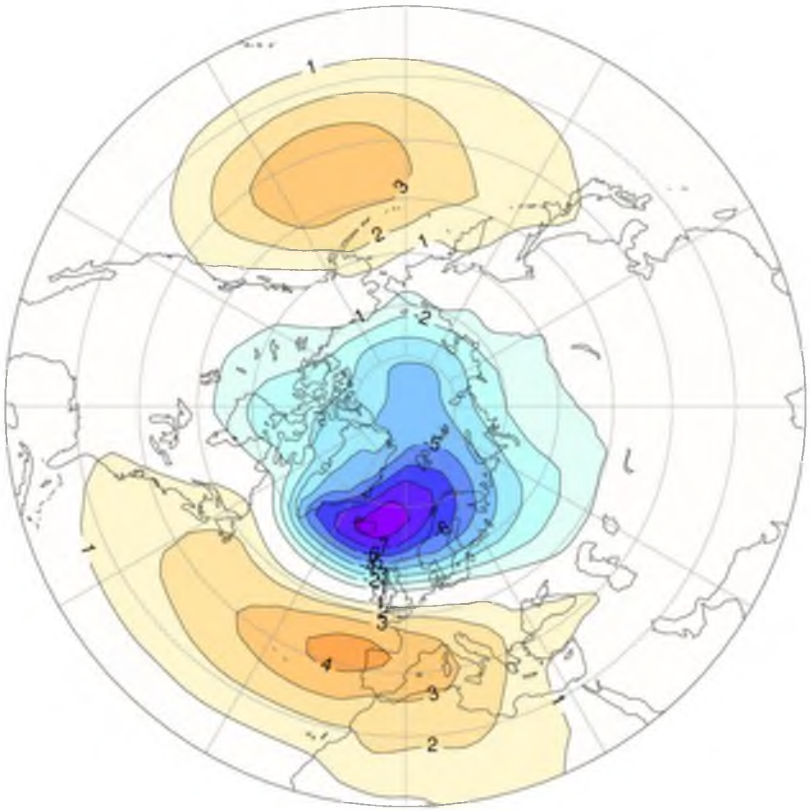

Figure 1 The Arctic oscillation pattern from sea level pressure during 1979-2000 using NCEP/NCAR reanalysis. During the northern winter, it extends upward into the stratosphere where it modulates the strength and position of the westerly polar vortex that encircles the Arctic polar cap region. The Arctic oscillation and the North Atlantic oscillation are different interpretations of the same phenomenon.

this definition, the AO is then simply the surface expression of the NAM.

Recent studies have shown that stratospheric circulation anomalies, which manifest themselves as variations in the structure and position of the polar vortex, often seem to propagate downward from the stratosphere to the surface with a relatively long time scale (10-60 days) (Baldwin and Dunkerton, 1999; Christiansen, 2001). This phenomenon of downward propagation can be easily seen by analyzing the state of the NAM index as a function of time and height.

Figure 2 shows the composite evolution of NAM variations in response to extreme

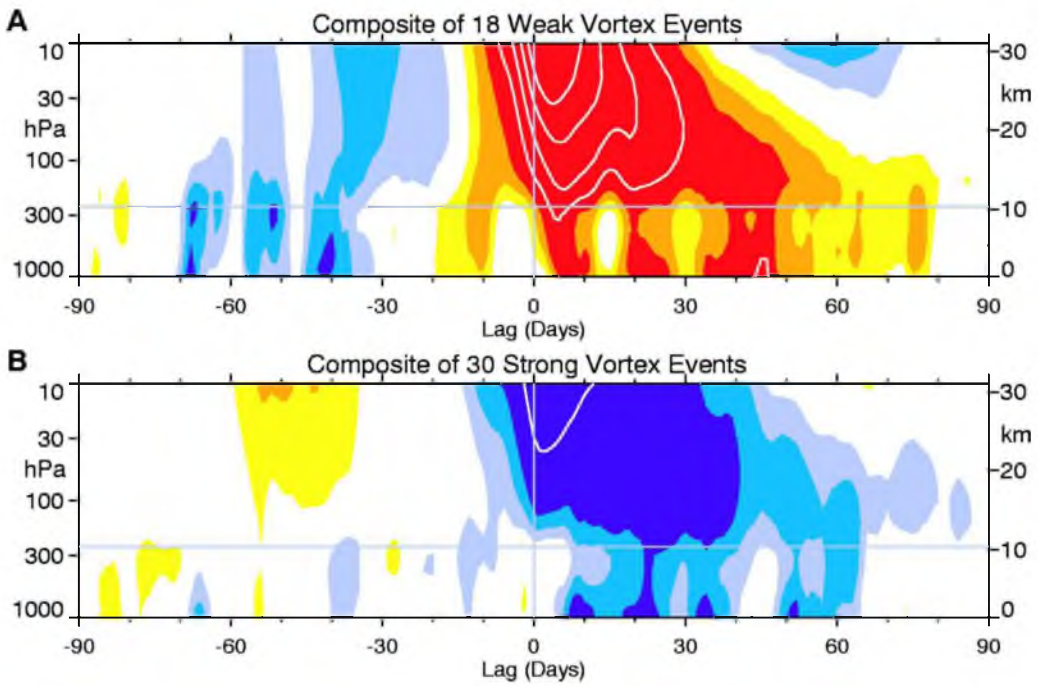

Figure 2 Observed composites of time-height development of the northern annular mode for (A) 18 weak vortex events and (B) 30 strong vortex events. The events are determined by the dates on which the 10 hPa annular mode values cross -3.0 and +1.5, respectively. The indices are nondimensional; the contour interval for the color shading is 0.25, and 0.5 for the white contours. Values between -0.25 and 0.25 are unshaded. The thin horizontal lines indicate the approximate boundary between the troposphere and the stratosphere. (From Baldwin, M. P. and T. J. Dunkerton, 2001, Stratospheric harbingers of anomalous weather regimes, *Science*, 244, 581-584. © American Association for the Advancement of Science. Used with permission: #3336740595153)

stratospheric events. On average, stratospheric annular mode variations appear to precede tropospheric variations of the same sign. The observed time lag between stratospheric and tropospheric NAM anomalies suggests that stratospheric anomalies may have a causal role in creating tropospheric anomalies.

1.2 Extreme events in the stratosphere

Stratospheric sudden warming (SSW) events happen only during winter, almost exclusively over northern high latitudes (only one SSW event happened over the

Southern Hemisphere in late September 2002 during more than 5 decades of observations, Baldwin et al. 2003a), and SSWs occur only once every other year or so. SSWs are abrupt warming events of the polar stratosphere: a rise of stratospheric temperature by several tens of degrees occurs within a few days, when the dominant westerly polar vortex slows down and eventually disappears. As the strength of the stratospheric polar vortex weakens, corresponding changes in the stratospheric circulation tend to propagate downward and into the underlying troposphere. This downward propagation occurs within a week or so and persists up to 2 months (Baldwin and Dunkerton 1999, 2001; Christiansen 2001).

The origin of these anomalies is planetary wave activity (i.e., Rossby waves) that emanates upward from the troposphere. These waves are usually excited when the westerly background flow in the troposphere is forced to pass topographic barriers or strong zonal temperature gradients. Planetary wave activity is more pronounced over the Northern Hemisphere than over the Southern Hemisphere due to the existence of a stronger land-sea contrast and high mountain ranges. Two major continents (Eurasia and North America), separated by two large ocean basins (the Pacific and the Atlantic), over the Northern Hemisphere frequently cause the excitation of planetary waves with wave number one or two (one or two wavelengths around a latitude circle). Only planetary waves of wave number one or two are long enough to penetrate through the tropopause up into the stratosphere (Charney and Drazin 1961). As the waves propagate upward, they are refracted latitudinally by the existing zonal wind distribution. Most waves are refracted towards the equator along a so-called equatorial wave guide, and absorbed at the zero wind line in subtropical latitudes (Dickinson 1968).

However, in contrast to the normal situation, sometimes these waves are refracted towards higher latitudes. As waves propagate upward, they increase their amplitudes with decreasing air density in order to maintain their energy. At some point, the waves become unstable and break, depositing their momentum to their environment (Holton 1980) and decelerating the polar vortex (Matsuno 1971). When this deceleration is intense and persistent, then the polar vortex eventually breaks down, the temperature over the pole increases, and in extreme cases an easterly appears over high latitudes due to a reversal of meridional temperature gradients.

As mentioned before, the circulation anomalies induced by SSW events often descend into the lowermost stratosphere and even to the surface of the Earth. The complex chains of events leading to upward propagating planetary waves and downward propagation of circulation anomalies are well illustrated in Figure 3. The downward propagation occurs within 10 days or so, and its influence can persist out to 60 days. This dissertation attempts to investigate the stratospheric influence on the tropospheric climate and the ocean. If a dynamical model would be able to capture these processes, the faithful representation of the stratospheric components in the model would likely lead to improved tropospheric prediction of weather and climate.

The ozone in the stratosphere is also important for changes in the tropospheric circulation (Son *et al.*, 2008b; Polvani *et al.*, 2011; Gillett and Thompson, 2003). The ozone is initially produced in the tropical stratosphere, and it moves into the polar areas through the Brewer-Dobson circulation (BDC) (Brewer, 1949; Dobson, 1956). The BDC is a simple model of the atmospheric circulation, which explains why the tropical air has less ozone than the polar air. The BDC is driven by the planetary waves generated in the

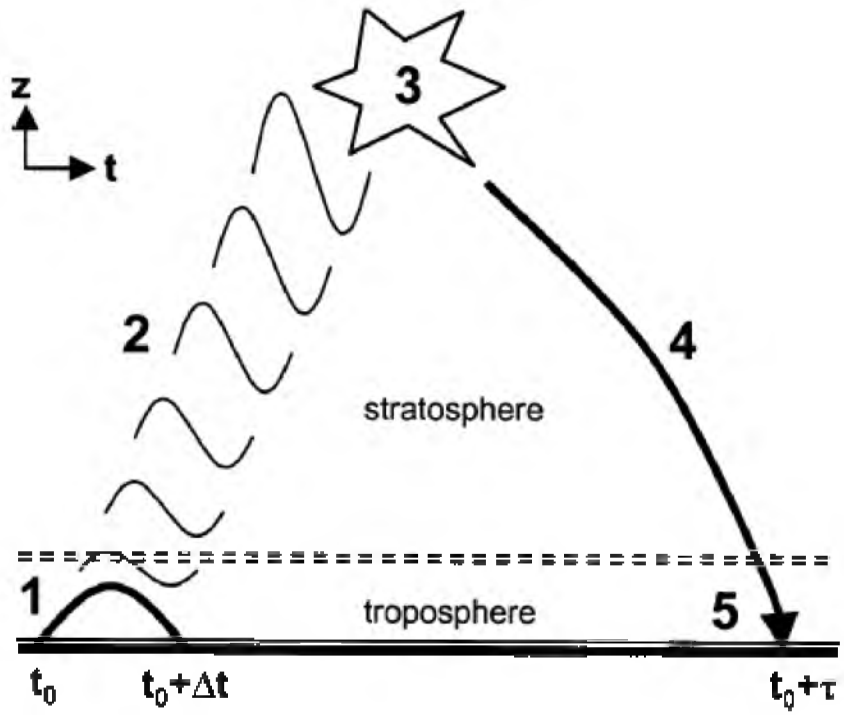

Figure 3 Schematic illustration of the individual events that lead to downward propagation. Planetary waves from the troposphere (stage 1) travel upward and refract into the stratospheric polar vortex (stage 2). The waves break and become absorbed, creating anomalies in the strength of the vortex (stage 3). Over the course of 1-2 weeks, those anomalies descend from the middle to the lower stratosphere, where they persist for up to 2 months (stage 4). This in turn induces anomalies in the surface AO (stage 5). (From Reichler, T., P. J. Kushner, and L. M. Polvani, 2005, The coupled stratosphere-troposphere response to impulsive forcing from the troposphere, *J. Atmos. Sci.*, 62, 3337-3352. © American Meteorological Society. Used with permission. doi:http://dx. doi.org/10.1175/JAS3527.1)

troposphere. Such waves are controlled by the strength of the polar vortex. For example, a strong vortex limits the propagation and breaking of the waves in the stratosphere (Charney and Drazin, 1961; Gerber, 2012). As a result, weaker BDC transports less ozone-rich air from the tropical upper stratosphere into the polar regions of the lower stratosphere (Holton *et al.*, 1995). The strong vortex by itself works as a barrier of the meridional circulation from the tropics to the extratropics (Haynes, 2005; Shepherd, 2007). It prohibits ozone from moving into high latitudes.

1.3 Research overview

Continuing previous studies, we will further investigate the stratospheric influences on the troposphere and on the ocean using climate models. Most works are based on annular modes, which are dominant patterns of climate variability. We have constructed three main chapters for the dissertation. The chapters are comprised of their own abstract, introduction, description of methods and data sets, interpretation of results, and summary and conclusion in order to make a clear understanding of their own subjects. The subjects are 1) the role of positive feedbacks between stratospheric ozone and the circulation on climate variability in the stratosphere and the troposphere, 2) the uncertainty of the annular mode time scales and the role of stratospheric time scales on the troposphere, and 3) the role of the stratosphere on the oceanic circulation.

The first part of this dissertation, described in Chapter 2, involves positive feedbacks between stratospheric ozone and the circulation and its role on the atmospheric variability. We hypothesize that the reciprocal interaction between chemical and dynamical changes reinforces each other and therefore create our hypothesized positive feedback. We use a coupled chemistry-climate model to validate the existence of the feedback. By intensifying or breaking the feedback chains, we attempt to understand the role of the feedback on the stratospheric and further tropospheric variability. We verify our results by investigating the outputs of the second chemistry-climate model validation activity (CCMVal-2) organized by the stratospheric processes and their role in climate (SPARC) and the 5th coupled model intercomparison project (CMIP5) models, in which the positive feedback acts to increase the atmospheric variability.

The second part of this dissertation, Chapter 3, quantifies the uncertainty of annular

mode (AM) time scales. It also depicts the role of stratospheric time scale on the tropospheric time scale. The proper simulation of the AM time scale is regarded as an important benchmark for the ability of climate models. Gerber *et al.* (2008b) found an overestimated AM time scale from climate models, implying that the model's climate circulation is overly sensitive to external forcing, as suggested by the fluctuation-dissipation theorem (Leith, 1975). They also argued that the AM time scale converges very slowly, thus necessitating relatively long simulations. Here we address the problem of stability of the AM time scale and investigate the robustness of a time scale derived from the 50-year historical reanalysis record. We employ a long simulation with the Geophysical Fluid Dynamics Laboratory (GFDL) climate model CM2.1 and investigate the AM time scale from individual 50-year segments. We conclude that if nature's AM time scale is similarly variable to this model, there is no guarantee that the 50-year historical reanalysis record is a fully representative target for model evaluation. We also find a robust relationship between the magnitude and the seasonal timing of the AM time scale in both troposphere and stratosphere, confirming and extending earlier results of a dynamical coupling between the stratosphere and the troposphere and of influences of stratospheric variability on variability in the troposphere.

The third part of this dissertation, Chapter 4, illustrates the stratospheric connection to oceanic circulation. We suggest an interdecadal covariability between changes in the stratospheric circulation and changes in the oceanic circulation over the North Atlantic Ocean. A stratospheric connection to the ocean appears in the North Atlantic Ocean. The North Atlantic oscillation (NAO), a large-scale pattern of near-surface circulation anomalies over the North Atlantic, is modulated by the polar vortex in the stratosphere.

The NAO in turn drives the Atlantic meridional overturning circulation (AMOC). Using climate models, we demonstrate that this similarity is consistent with the hypothesis that variations in the sequence of stratospheric circulation anomalies significantly affect the circulation in the North Atlantic Ocean. We generalize our results by investigating further simulations taken from the outputs of the CMIP5.

CHAPTER 2

A POSITIVE FEEDBACK BETWEEN STRATOSPHERIC OZONE AND THE CIRCULATION

2.1 Abstract

A possible influence of positive feedbacks between stratospheric ozone and the circulation on the atmospheric variability is investigated. We hypothesize that the ozone loss feeds back into the stratospheric circulation, producing more ozone deficit. Chemical ozone depletion and the associated polar cooling result in a stronger vortex. The enhanced vortex limits the propagation and breaking of planetary waves, reducing the Brewer-Dobson circulation, finally reducing poleward transport of ozone-rich air. The stronger vortex is also less penetrable for poleward transports, leading to less influx of ozone. A reciprocal interaction between chemical and dynamical changes may reinforce each other and therefore create our hypothesized positive feedback. The impact of the feedback is evident at interannual variations of ozone and its long-term trends.

We design three very long simulations using a coupled chemistry-climate model. By giving an initial change in stratospheric ozone over the polar stratosphere, we emphasize the hypothesized feedbacks. We find that the feedback by ozone loss produces an intensification of the stratospheric circulation until the late spring over the Southern Hemisphere. The intensification leads to the variable timing of the vortex breakdown and

thus it increases stratospheric variability. A fixed ozone simulation includes no influence of dynamics on the ozone chemistry so that it intends to break the suggested feedback loop. We find that the simulation has almost the same timing of vortex breakdown, producing a small stratospheric variability. These results are verified by the second chemistry-climate model validation activity (CCMVal-2) and the fifth coupled model intercomparison project (CMIP5) models, in which the feedback leads to an increase in variability, and the lack of the feedback produces a decrease in variability.

The feedback strength and thus the climate sensitivity can be measured by the persistence time scale of annular mode variability. The ozone depletion simulation is mostly characterized by increased persistence, attributed to positive feedbacks. The persistence is reduced in the fixed ozone simulation mainly due to the lack of such feedback.

In the presence of our suggested positive feedback between ozone and the circulation, a small external forcing can cause large changes in the annular mode. With understanding such feedback, we can faithfully predict changes in variability of the annular mode with the expected future recovery of ozone.

2.2 Introduction

Since the discovery of the Antarctic ozone hole by Farman *et al.* (1985), understanding sources and consequences of stratospheric ozone loss has been the subject of intense research. One fundamental question that is still largely unanswered is whether the ozone loss can feed back on other aspects of the physics, chemistry, or dynamics of the stratosphere to produce additional ozone deficit. For example, ozone depletion may be both a cause for and a consequence of stratospheric cooling: as shown in Figure 4,

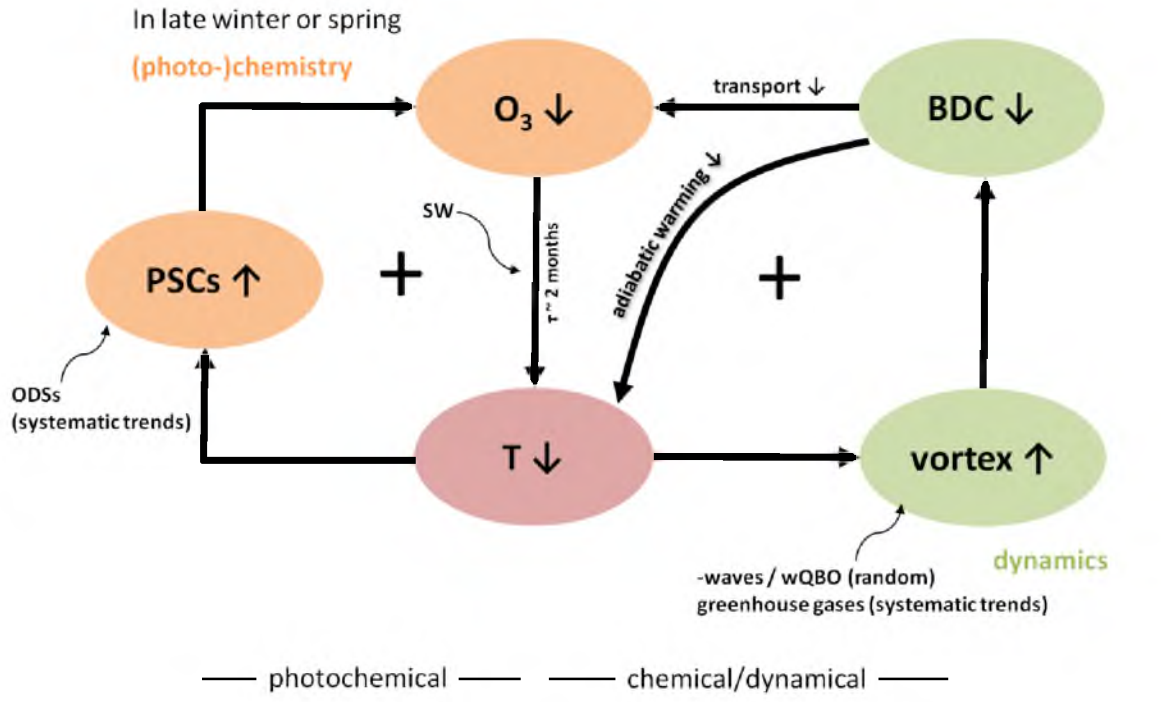

Figure 4 Schematic representation of hypothesized feedbacks.

cooling creates favorable conditions for the formation and persistence of polar stratospheric clouds (PSCs), triggering heterogeneous chemical processes associated with chlorine and bromine (Solomon, 1999). The ozone destruction and the related lack of radiative heating leads to additional cooling (Randel and Wu, 1999). Ozone depleting substances (ODSs) such as chlorine or volcanic aerosols during late winter or spring lead to positive feedbacks involving the photochemistry of the stratosphere (Shine, 1986). However, the radiative time scales in the polar stratosphere are very long and it would take about 1-2 months for ozone changes to produce temperature anomalies, rendering it somewhat unclear how effective this possible feedback is.

There is also the possibility for mutual interaction between ozone and the stratospheric circulation, creating what one might call a chemical/dynamical feedback. It

is well known that Antarctic ozone depletion and the associated cooling result in an intensification and poleward expansion of the polar vortex over the Southern Hemisphere (SH) (McLandress *et al.*, 2011; Polvani *et al.*, 2011; Thompson *et al.*, 2011). A stronger vortex may limit the propagation and breaking of tropospheric planetary waves in the stratosphere (Charney and Drazin, 1961; Albers and Nathan, 2013), reducing the Brewer-Dobson circulation (BDC) (Brewer, 1949; Dobson, 1956), transporting less ozone-rich air from the tropical upper stratosphere into the polar regions of the lower stratosphere (Holton *et al.*, 1995). A weakened BDC also reduces downwelling and adiabatic warming over the pole, hence causing additional cooling. Lastly, a stronger vortex is also less penetrable for meridional transports by diffusion and turbulent mixing, again leading to cooling and less influx of ozone from lower latitudes (Haynes, 2005; Shepherd, 2007). In other words, chemical and dynamical changes may reinforce each other and therefore create a second, chemical/dynamical feedback (Figure 4). As with the first feedback, this feedback would depend on sunlight and a polar vortex, and is therefore expected to exist only during late winter and spring. In contrast to the first, however, it does not require the existence of ODSs.

The two hypothesized feedbacks are both positive, and they should therefore have the potential to increase the variability and climate sensitivity of the stratosphere. Through the dynamical coupling between the stratosphere and the troposphere (Baldwin and Dunkerton, 2001), this may impact the entire high-latitude climate system (Hartmann *et al.*, 2000). The goal of this study is to investigate the validity of this hypothesis using a model based approach.

To motivate this study and to provide some initial evidence for the hypothesized

chemical/dynamical feedback and its effect on variability, we present the results from simulations of the Second Chemistry-Climate Model Validation (CCMVal-2) activity (Eyring *et al.*, 2010). The corresponding models have interactive chemistry and a well-resolved stratosphere; they should therefore capture the two feedbacks. Examining the model simulated seasonal cycle of interannual variability in the stratosphere separately for a period of strong ozone depletion and for one with relatively stable ozone conditions, we find a significant increase in annular mode (AM) variability during times of depleted ozone (Figure 5). This increase starts in August and is most notable during spring; it is absent in fall and midwinter. The increase in interannual variability during times of strong ozone depletion and also its seasonality agree well with our photochemical feedback hypothesis, which depends on the presence of ODSs and on sun light, and which perhaps acts in concert with the chemical/dynamical feedback to increase variability.

As shown in Figure 5, the interannual variability of the stratospheric circulation over the SH is largest during austral spring. This is probably accompanied by variations in Antarctic ozone, which in turn may be caused by changes in planetary wave activity (Salby *et al.*, 2012). The planetary wave breaking in the extratropics drives the BDC, which characterizes the residual circulation and thus the transport of ozone through the stratosphere: upwelling at low latitudes, poleward movement at midlatitudes, and downwelling at high latitudes.

Over the NH, interannual variations in the activity of planetary waves can also explain interannual variations of ozone (Salby, 2008; Hadjinicolaou *et al.*, 2002; Pyle *et al.*, 2005). For example, Salby (2008) showed that a low activity of planetary waves

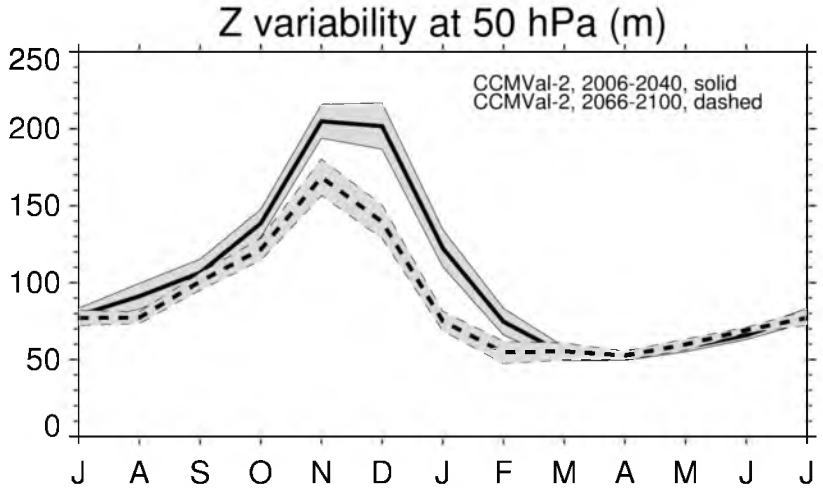

Figure 5 Interannual variability of polar cap averaged geopotential height (60°-90°S) at 50 hPa from CCMVal-2 models as a function of month. Solid line style is for 2006-2040, a period of strong ozone depletion, and dashed is for 2066-2100, a period of ozone recovery. Grey shading denotes plus and minus one standard error amongst the different models. A slowly varying trend is removed from a long time series of the year 1960-2100 at each month. The trend is derived using a low pass Lanczos filter with a 30-year window (Gerber *et al.*, 2010).

weakens the residual circulation and induces anomalously cold temperatures through reduced adiabatic warming. The cooling promotes the creation of PSCs, enhancing heterogeneous ozone depletion. Manzini *et al.* (2003) found from a chemistry-coupled climate model (CCCM) that ozone depletion leads to cooling and in turn to additional ozone depletion in the polar lower stratosphere, suggesting a positive feedback.

Hartmann *et al.* (2000) also suggested a dynamical feedback between mean wind structure and stratospheric ozone transport. Albers and Nathan (2013) used a CCCM to investigate feedbacks between chemistry and dynamics and found that radiative cooling from reduced ozone produces a meridional temperature gradient, a strengthened polar vortex, a decrease in upward planetary waves, and a decrease in polar downwelling, hence more ozone loss. Planetary wave activity, which controls downwelling over the

pole, is crucial for this chemical/dynamical feedback. Positive feedbacks between chemistry and planetary waves were also found from zonally asymmetric ozone (Albers *et al.*, 2013; Albers and Nathan, 2012) and from an ozone-modified refractive index (Nathan and Cordero, 2007). Braesicke and Pyle (2003) found that if ozone perturbations are prescribed in the midlatitudes they result in relatively small circulation change. In the present study we focus on ozone perturbations over the high latitudes and inside the polar vortex, where the response of the circulation is expected to be stronger.

The goal of the present study is to further examine the hypothesized ozone feedbacks. The questions we are trying to answer are: Can we detect positive feedbacks involving chemistry and dynamics of the stratosphere? During which seasons and over which regions do these feedbacks act? How important are the feedbacks relative to each other and relative to natural variability of large scale climate? How are these feedbacks represented in models? To this end, we investigate three simulations with a CCCM, in which parts of the two hypothesized feedback loops are allowed or broken (Figure 4).

This chapter is organized as follows: In section 2.3, we describe models and experimental design. Section 2.4 presents the methods. In section 2.5, we present our results: we first provide evidence that a simulation with fully interactive chemistry and ozone depletion leads to memory that cannot be explained from the persistence of either ozone or the circulation alone; we further demonstrate that ozone depletion leads to a statistically significant increase of variability in the stratosphere, which in turn also impacts the troposphere; our findings are confirmed by investigating simulations with the CCMVal-2 and CMIP5 models. Finally, in section 2.6, we offer a summary and interpretation of our results.

2.3 Models and experimental design

2.3.1 GFDL-Climate Model (CM3)

A climate model is a primary tool to investigate coupling processes between the stratosphere and troposphere due to short and poor observations of the stratosphere. Here, we use an advanced version of the coupled climate model (CM3), developed at the Geophysical Fluid Dynamics Laboratory (GFDL) (Griffies *et al.*, 2011; Donner *et al.*, 2011). The atmospheric model (AM3) includes most of the atmospheric components such as interactive stratospheric and tropospheric chemistry with a wide range of time scales from years to decades. It employs a finite-volume dynamical core with horizontal resolution of approximately 200 km. It has 48 vertical levels with the top level located at 0.01 hPa (~80 km). The ocean and sea ice models in CM3 are the same as in previous versions of this model (CM2.1). The ocean model is run at a horizontal resolution of 1 degree in zonal direction and increasing in the meridional direction from 1/3 degree at the equator to 1 degree at the pole. The vertical resolution is 50 levels with 22 levels of 10 m thickness each in the top 220 m. The sea ice model has the same horizontal grid of the ocean model with three vertical layers: one for snow and two for ice. The CM3 used in this study is identical to the climate model (GFDL-CM3) used for the CMIP5.

2.3.2 Design of experiments

We use both chemistry and nonchemistry version of the CM3 in order to investigate the interaction between stratospheric chemistry and circulation from interannual to interdecadal time scales. The model configurations are the same except for the chemistry scheme. The chemistry version is named as the CTRL, and its analysis is based on 2000 years. We add an experiment of ozone depletion with the chemistry version, and generate

500-year simulations (DEPLO3) in order to examine the interaction between depleted ozone and corresponding variations in the stratospheric circulation. In the nonchemistry version, the ozone concentration is prescribed rather than calculated interactively. This simulation is FIXO3, and it contains 500 years. The ozone concentrations in FIXO3 are from a 10-year monthly mean climatology produced from the AM3. These climatological values are reused each year of the coupled run. As we will show later, the FIXO3 ozone is almost the same as the CTRL through all latitudes. Since the fundamental difference between FIXO3 and CTRL is the existence of the chemical module, the small differences in ozone provide an ideal environment to compare the nonchemistry model with its chemistry version. The atmospheric model (and atmospheric chemistry) in the AM3 is the same as in the coupled model, and all forcings are the same between the atmospheric model and coupled control runs. A summary of our simulations is found in Table 1.

2.3.3 CMIP5

The World Climate Research Programme (WCRP) has promoted a new set of coupled climate model experiments. These experiments comprise the 5th phase of the Coupled Model Intercomparison Project (CMIP5) (Taylor *et al.*, 2012). We employ the CMIP5 models to obtain the confidence on the results from our CM3 simulations. We only select models which provide simulations from both chemistry and nonchemistry versions. The Center for Climate System Research (CCSR) from the University of Tokyo provides the Model for Interdisciplinary Research on Climate (MIROC) (Watanabe *et al.*, 2011). The nonchemistry model is the MIROC-ESM, and its chemistry version is the MIROC-ESM-CHEM. The National Center for Atmospheric Research (NCAR) also provides the Community Earth System Model (CESM) (http://www.cesm.ucar.edu/

Table 1 Models used in this study. Numbers in parenthesis from model name show number of ensemble runs used in this study.

	Model	Version	Experiment	Length (years)
Our Simulations	GFDL-CM3 (1)	Chemistry	CTRL	2000
			DEPLO3	500
		Nonchemistry	FIXO3	500
CMIP5	GFDL-CM3 (1)	Chemistry	piControl	500
			rcp45	35: 2006-2040 35: 2066-2100
	MIROC-ESM-CHEM (1)		piControl	255
			rcp45	35: 2006-2040 35: 2066-2100
	CESM1-FASTCHEM (1)		piControl	222
			rcp45	Not Available
	MIROC-ESM (1)	Nonchemistry	piControl	531
	CCSM4 (1)		piControl	501
CCMVal-2	CCSRNIES (1)	Chemistry	REF-B2 SCN-B2b SCN-B2c	161: 1960-2100
	CMAM (3)			
	MRI (1)			
	SOCOL (1)			
	UMSLIMCAT (1)			

experiments/cesm1.0/). The chemistry version of the CESM is the CESM1-FASTCHEM and its nonchemistry version is the CCSM4. The details about these models are found in Eyring *et al.* (2013). For brevity, both chemistry and nonchemistry models are run with identical model configurations. The main difference between the chemistry and nonchemistry versions is that stratospheric ozone chemistry is interactively coupled with dynamics in chemistry versions, but ozone concentrations are prescribed in their nonchemistry versions. Detailed information of the CMIP5 models used in this study is also found in Table 1.

2.3.4 CCMVal-2

The stratospheric processes and their role in climate (SPARC) has established the chemistry-climate model validation activity (CCMVal) for coupled chemistry-climate models (Eyring *et al.*, 2008). The CCMVal intends to achieve better understanding of an interaction between chemistry and climate (Eyring *et al.*, 2010). For this study, we use three types of CCMVal simulations. We first use REF-B2 reference simulation, which includes present and future projections (Eyring *et al.*, 2008). In order to compare the differences in variability during ozone depleted periods with that during normal ozone periods, we next select SCN-B2b (aka fixed ODSs) sensitivity simulation. We finally include SCN-B2c (aka fixed greenhouse gases) simulation to separate the effects of greenhouse gases from those of ozone depletion. We employ all available ensembles from each model. Each model is given by equal weighting regardless of its ensemble size in order to make a multimodel mean. Monthly outputs of geopotential height are obtained from five models of the CCMVal-2. We use all available years from 1960 to 2100. A list of the CCMVal-2 models is found in Table 1.

2.3.5 ERA-INTERIM Reanalysis

We use the total ozone and temperature at stratospheric levels for 34 years from 1979 to 2012 from the ERA-INTERIM reanalysis (Dee *et al.*, 2011). The reanalysis is referred to as the ERA hereafter. We compare the outcome from the ERA with that from climate model in order to understand how well the models reflect the impact of the dynamics on the chemistry of the stratosphere.

2.4 Methods

Most of our results are based on the area weighted average of a variable poleward of 60 degree in the SH. In order to express the polar cap average, we define a notation as (60°-90°S) after a variable name. For example, total ozone (60°-90°S) indicates the area weighted polar average of total column ozone over 60°-90°S latitudes.

We use monthly geopotential height (60°-90°S) from the CM3, CCMVal-2, and CMIP5 models in order to calculate the atmospheric variability. We first remove seasonally changing climatology using 150-year Lanczos filter at each month of year (Duchon, 1979). By doing this, we can successfully ignore a drift that a climate model may contain. We also remove a slowly varying trend mainly caused by actual ozone variations from geopotential height fields of the ERA, CCMVal-2, and the concatenated time series of historical and rcp45 from the CMIP5. In order to compute the trends, we first calculate a time varying climatology of geopotential height using a low pass Lanczos filter with a 30-year window. This climatology is then subtracted from the field of geopotential height to compute anomalies. This technique is similar to that described by Gerber *et al.* (2010).

Interannual variability of geopotential height is simply defined as the standard deviation of geopotential height at all levels in each month of year. The daily variability is defined as the standard deviation of the daily geopotential height (60°-90°S) following Figure 7 of Gerber *et al.* (2010).

The World Meteorological Organization (WMO) provides a standard definition of the stratospheric sudden warmings (SSWs): when zonal mean zonal winds at 60°N and at 10 hPa become from westerly to easterly at any one date from November to March. We

do not consider the final warmings, but midwinter warmings.

We quantify the persistence of AM variability by removing or retaining the effects of interannual variability (Keeley *et al.*, 2009). The persistence is given by the time for the auto-correlation function of the SAM index to cross a value of 1/e. Short- and long-time scales indicate fast and slow decay rates of AM anomalies, respectively (Gerber *et al.*, 2010). For persistence that includes the effects of interannual variability, the auto-correlation function is derived from daily AM anomalies that are calculated from simply removing long-term climatological means from the original data. For persistence that excludes effects of interannual variability, we subtract for a given year from the original daily AM data the corresponding seasonal mean from that year.

2.5 Results

2.5.1 Climatological differences

We start with a brief description of the climatological features of our simulations. The total ozone climatology derived from CTRL is contoured as a function of month and latitude in Figure 6a. Ozone is primarily produced in the tropical stratosphere by the UV photolysis of oxygen and from there it is transported to the high latitude winter stratosphere by the Brew-Dobson circulation (BDC) (Brewer, 1949; Dobson, 1956). The largest amount of ozone in the polar stratosphere is found during spring of each hemisphere. The zonal wind climatology at 10 hPa from CTRL is illustrated in Figure 6c. The stratospheric circulation during winter is dominated by strong westerlies that maximize at 60° latitudes. This high-latitude wind maximum forms the so-called polar vortex, which is the result of thermal wind balance: the vertical wind shear is proportional to the equator-to-pole temperature gradient, and the extremely cold

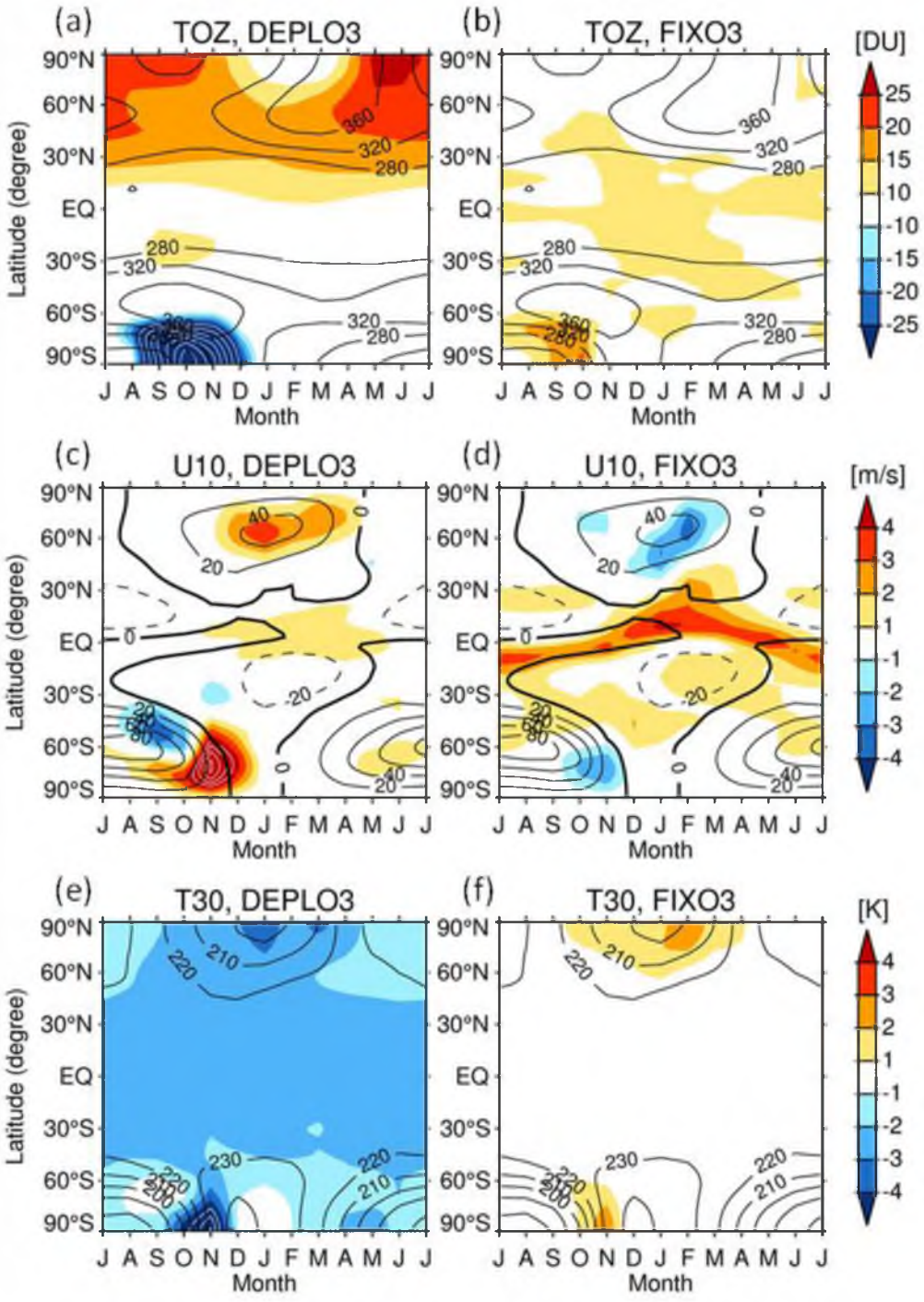

Figure 6 Zonal mean climatology of (a, b) total ozone (DU), (c, d) zonal wind at 10 hPa (m/s), and (e, f) temperature at 30 hPa (K) for (a, c, e) DEPLO3 and (b, d, f) FIXO3 as a function of month and latitude. Shown are (shading) anomalies with respect to CTRL and (contours) CTRL climatology. Total ozone, zonal wind, and temperature greater than or equal 30 DU, 5 m/s, and 5 K are contoured in white at intervals of 10 DU, 1 m/s, and 1 K intervals, respectively.

temperatures over high latitudes during polar nights (Figure 6e) lead to the formation of the vortex.

We next investigate the differences in ozone, temperature, and zonal wind between the simulations. As expected, DEPLO3 exhibits large ozone depletion over the SH from September to November (Figure 6a). The maximum ozone reduction (~90 DU) occurs at the South Pole during October. Therefore, DEPLO3 exhibits a colder and stronger vortex than CTRL (Figure 6c, e). At the same time, the vortex is shifted somewhat poleward (Figure 6c). Interestingly, DEPLO3 shows little difference in total ozone at low latitudes over the SH, and it has more ozone than CTRL over the NH. The largest increase in total ozone occurs at the North Pole from late spring to summer. The question to ask is why DEPLO3 has more ozone than CTRL over the NH during boreal summer. One possible answer is changes in vertically propagating planetary waves that control the BDC (Holton *et al.*, 1995). During winter and spring, the polar vortex in the NH stratosphere is stronger in DEPLO3 than in CTRL, as indicated in Figure 6c from enhanced zonal winds at 10 hPa. The stratospheric winds control the way planetary waves behave by raising the breaking level of the waves and deepening the circulation, which is suggested by Gerber (2012). If the polar vortex is weak, upward propagation of planetary waves are blocked in the lower stratosphere. The bottom part of the BDC becomes strong, but the top part becomes weak. If the vortex is strong, planetary waves can propagate upward into the stratosphere, so the top part of the BDC becomes strong. Since the polar vortex in DEPLO3 is much stronger than that in CTRL over the NH above the middle stratosphere (Figure 6c), the BDC strengthens. The strengthened BDC leads to increased transports of ozone from the tropics to the pole. The resulting positive ozone anomalies persist until

summer, as indicated by the gradual increase in total ozone from spring to summer.

In contrast, FIXO3 exhibits small differences in total ozone relative to the CTRL over all latitudes and throughout the year. Since the fundamental difference between FIXO3 and CTRL is the existence of the chemical module, small differences in ozone provide an ideal environment to compare the nonchemistry model with its chemistry version. In particular, the intensifying mechanism by the reciprocal interaction between chemistry and dynamics will be the main issue in this study. The comparison between chemistry and nonchemistry shows that the greatest difference of total ozone occurs at the South Pole in October (Figure 6b). The structure of zonal wind and temperature during austral spring becomes opposite to that from DEPLO3. FIXO3 shows a warming over the polar area (Figure 6f) and a weak polar vortex by the thermal wind (Figure 6d).

2.5.2 Ozone feedback: chemistry vs. transport

We hypothesize that changes in the stratospheric circulation by chemical ozone depletion reinforce the ozone loss during late winter and spring. With the chemically depleted ozone in late winter and spring, the stratosphere becomes colder due to less solar absorption by the reduced ozone. The strongest cooling occurs over the South Pole due to the most diminished ozone there (Figure 6a, e). An enhanced polar vortex is generated by the thermal wind, and it, in turn, leads to the ozone deficit by blocking the poleward transport of ozone in the lower stratosphere (Shepherd, 2007). The way the chemically reduced ozone produces more deficit by less transport is a positive chemical/dynamical ozone feedback. The feedback begins with a stratospheric cooling, and it recursively produces more cooling. For evidence in support of our hypothesis about the feedback, we compared the chemical ozone loss with dynamical ozone loss (Braesicke and Pyle, 2003).

First, the chemical ozone loss is primarily represented by climatological differences in total ozone between DEPLO3 and CTRL (black line in Figure 7). Second, the dynamical change is explained by the poleward transport of ozone through the BDC. An easy way to quantify the dynamical change of ozone is to calculate the difference in total ozone between strong and weak vortex events for CTRL (red curve in Figure 7). As previously mentioned, the polar vortex acts as a dynamical barrier of the meridional circulation (Shepherd, 2007; Brasseur and Solomon, 2005). If the polar vortex is strong, the dynamical transport of ozone from low to high latitudes becomes weak. If the vortex is weak, the transport becomes strong. Thus, the difference between strong and weak vortex represents the dynamical ozone loss by the transport. We define strong and weak vortex events as years in which the zonal wind at 10 hPa and 60°S crosses the climatological mean plus and minus one standard deviation (Braesicke and Pyle, 2003). Transport related ozone changes due to strong and weak vortex events (red curve) are very similar to the chemical ozone change. We further look into the ozone change within DEPLO3 using the same definition of the strong and weak vortex. The ozone change includes influences from both chemical and dynamical ozone losses. DEPLO3 exhibits even larger (almost twice) ozone deficit between strong and weak events (orange line in Figure 7), suggesting that there is a chemical/dynamical mechanism enhancing the ozone deficit. The interaction between ozone variations and vortex change hints at the possibility for the existence of the positive ozone feedback.

We now revisit the climatological differences in the stratospheric circulation between DEPLO3 and CTRL (Figure 6). Over the SH, the polar vortex is still strong during late winter and its maximum is located at about 60°S (Figure 6c). The stratosphere

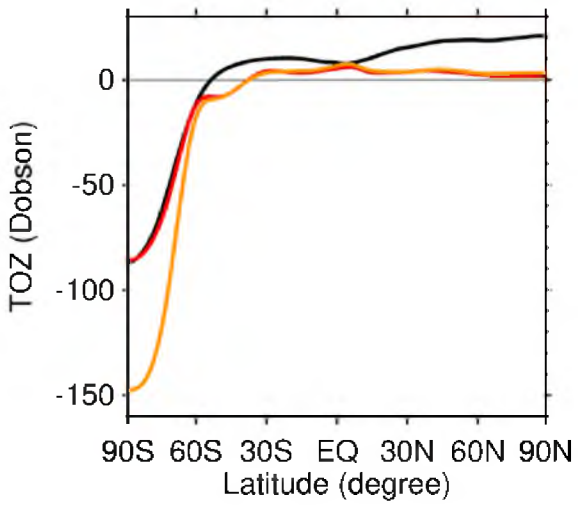

Figure 7 Difference in total ozone during October and November. (black) Climatological difference between DEPLO3 and CTRL. Difference between strong and weak vortex events (red) in CTRL and (orange) in DEPLO3. Strong and weak vortex events are defined when zonal wind at 10 hPa at 60°S exceeds plus and minus its interannual standard deviation, respectively.

is still cold (Figure 6e). The sunlight first enters the stratosphere. In DEPLO3, chemical ozone depletion begins in late August (Figure 6a) and the polar vortex moves poleward (Figure 6c). This result is broadly similar to the response of stratospheric zonal winds to ozone changes seen in Son *et al.* (2010) and Karpechko *et al.* (2010). We also find that the winds over the polar region continuously grow, and the poleward movement of the winds due to ozone depletion disappears in November. The strong winds become dominant over the entire mid- and high latitudes, and persist up to January. The enhanced winds reduce the BDC because the polar vortex itself is a dynamical barrier against meridional circulation. Thus, DEPLO3 exhibits more reduced poleward transport of ozone than CTRL. The reduced ozone again leads to the enhanced acceleration of the winds at the poleward side of the vortex center, indicating the positive ozone feedback. If there is no positive feedback, changes in ozone and zonal winds will be constant with

time. Positive wind anomalies in DEPLO3 appear in the entire lower stratosphere (not shown). Thus, the acceleration of zonal winds is a general response of stratospheric circulation to the ozone reduction (Son *et al.*, 2008b; Karpechko *et al.*, 2010).

Comparing the anomalies from DEPLO3 with those from FIXO3 also gives some insight into a possible ozone feedback. FIXO3 is driven by a somewhat positive ozone anomaly in the SH polar lower stratosphere during austral spring. This develops positive temperature anomalies, and zonal winds that are weakened and shifted equatorward. Conversely speaking, those changes in the dynamical fields come from interaction between chemistry and dynamics in CTRL because ozone is prescribed in FIXO3. There probably exists very weak ozone depletion over the polar stratosphere in austral spring in CTRL (Figure 6b). Apparent are small changes in thermally driven winds between FIXO3 and CTRL. The magnitude of the weakened winds in FIXO3 is much smaller than that of strengthened winds in DEPLO3. The strengthened winds in DEPLO3 result from an amplifying mechanism due to the ozone depletion there.

2.5.3 Interaction between ozone and circulation on various time scales

The scatter plot in Figure 8 shows interannual variations of 50 hPa temperature (60°-90°S) and total ozone (60°-90°S), each averaged for October and November, for each available year from ERA, DEPLO3, and CTRL. Temperatures from ERA range between 200 and 230 K, and so do the temperatures from DEPLO3 and CTRL. The variations in temperature and ozone show a good linear relationship as indicated by the thin lines, even when stratospheric temperatures are not cold enough to form polar stratospheric clouds (PSCs). We believe that this relationship is indicative for the mechanism outlined in Figure 4: interannual variations in the activity of tropospheric planetary waves lead to

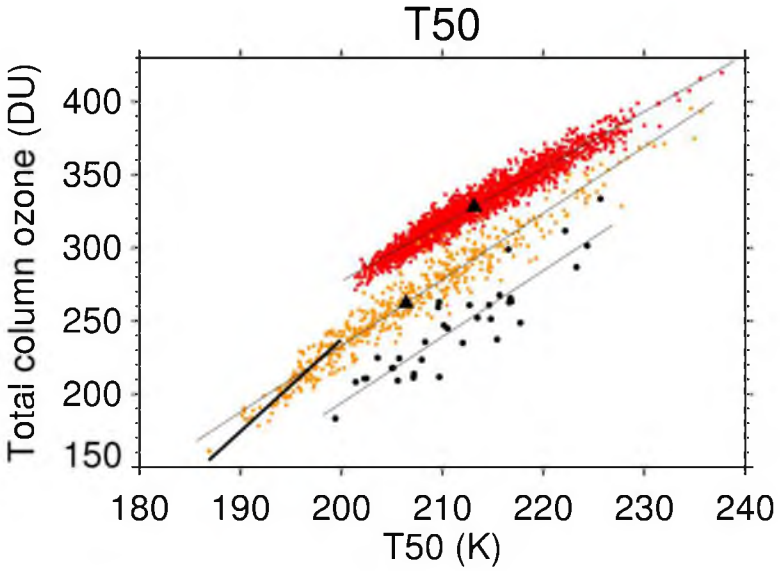

Figure 8 Scatter plot of 50 hPa temperature and total ozone (60°-90°S) averaged for October and November from (red) CTRL (2000 years), (orange) DEPLO3 (500 years), and (black) ERA reanalysis (34 years, 1979-2012). A slowly varying trend for ERA reanalysis is derived using a low pass Lanczos filter with a 30-year window. Triangles denote climatological averages from CTRL and DEPLO3. Thin lines are least square fit regression lines. Thick regression line is for DEPLO3, computed from temperature data of less than 200 K.

consistent changes in both stratospheric ozone and temperature. (Salby, 2008; Salby *et al.*, 2012).

We now investigate the interannual relationship between stratospheric ozone and temperature in more detail. In ERA, the average regression slope between total ozone and temperature is 4.5 DU/K: a temperature change of 1 Kelvin is associated with an ozone change of 4.5 DU. Interestingly, the regression slope from DEPLO3 is identical to that from ERA. The regression slope from CTRL amounts to 3.9 DU/K, and its smaller regression slope is expected, because CTRL lacks very cold stratospheric conditions, which are, by themselves, a suggestive feature of strong ozone depletion through planetary wave activities (Salby *et al.*, 2012). A list of interannual regression slopes is

summarized in Table 2.

To make this statement clear, we further investigate the years of less than 200 K from DEPLO3. DEPLO3 exhibits many years of temperatures lower than 200 K and this behavior does not appear in CTRL (Figure 8). Temperatures less than 196 K, on the basis of daily stratospheric minimum temperature, are indicative of photochemical ozone destruction and provide a good environment for PSCs to form (Solomon, 1999). Since we are dealing with a monthly temperature over the polar area, a moderate threshold of 200 K is perhaps acceptable to study the interaction between ozone chemistry and dynamics here. Heterogeneous reactions on PSC surfaces activate reservoir forms of chlorine. When the sunlight enters during late winter and spring, the active chlorine starts chlorine-catalyzed reaction with ozone so that ozone destruction begins (Solomon *et al.*, 1986; Crutzen and Arnold, 1986). The cold stratospheric temperature also indicates the strong polar vortex, suggesting less transport of ozone-rich air from tropics to poles. Thus, the chemical ozone depletion under the condition of cold stratosphere is added to the ozone loss by the transport, and it intensifies the ozone depletion. Such process is easily confirmed by the much steeper slope which is correspondent to 6.3 DU/K (thick line in Figure 8). Overall, the interannual slopes indicate the impact of the dynamics to the chemistry, which is one leg of our suggested chemical/dynamical feedback loop.

Many researchers have already explained the impact of ozone depletion and recovery on change in atmospheric circulation (Son *et al.*, 2008b; Son *et al.*, 2009; Polvani *et al.*, 2011; Gillett and Thompson, 2003; Perlwitz *et al.*, 2008). Their work is based on the analysis of trend over many years or model sensitivity. Such trends are indicative for the chemistry driving temperature change, which is the second leg of our suggested feedback

Table 2 Regression slope (DU/K) between total ozone vs. 50 hPa temperature.

Slope (DU/K)	CTRL	DEPLO3	DEPLO3 (<200K)	DEPLO3 vs. CTRL	ERA
Interannual	3.9	4.5	6.3	-	4.5
Trends	-	-	-	9.8	16.7

loop. As we already described before, the ozone depletion leads to a stronger vortex and resulting reduced poleward transport of ozone. In this sense, the slope is expressed as $\partial T/\partial O_3$. In ERA, the trend is about 0.06 (=1/16.7) K/DU. We compare the ERA trend with the mean change in CM3. Climatological averages from DEPLO3 and CTRL are shown with filled triangles in Figure 8. The mean response of stratospheric temperature to ozone between the two simulations amounts to about 0.1 (=1/9.8) K/DU. CM3 is, thus, about 1.7 times more sensitive than ERA.

One needs to take the inverse form of trends in order to make the direct comparison of trends with interannual slopes. The corresponding trends for ERA and CM3 are 16.7 and 9.8 DU/K, respectively. One needs to have a 9.8-16.7 DU ozone change to cool the vortex by 1 K. However, the impact of dynamics on chemistry represented from interannual slopes suggests that the same 1 K cooling of the vortex, the associated strengthening of the vortex, and reduction of transports lead to ozone decrease of 4.5 DU. It seems that the impact of dynamics on chemistry leads to a much faster relationship than the impact of chemistry to dynamics. For the small regression slope of interannual variations, one might argue that the influence of ozone on the vortex is weaker than the impact of the vortex to the ozone.

Weber *et al.* (2011) reported that the interannual variability in the BDC strength in the boreal winter would be a factor of about three times to the mean change in

observations and their models. Since changes in the lower stratospheric temperature are strongly affected by the variations in the BDC, our results, which show that the trends are more than twice the interannual slopes, agree well with their work.

In summary, we have found two kinds of impact so far. One is from interannual variations, in which stratospheric circulations affect the ozone, $\partial O_3/\partial T$. The other is from trends or low frequency features, which explain ozone impact on the circulations, $\partial T/\partial O_3$. The regression values should be the reciprocals, i.e., how much change in stratospheric temperature we get for a certain change in ozone, and the ozone change also affects the circulation.

2.5.4 Memory of ozone and geopotential height

Auto-correlation functions have been frequently used to investigate atmospheric persistence and memory (Gerber *et al.*, 2008b; Baldwin *et al.*, 2003b; Ambaum and Hoskins, 2002). We therefore investigate the persistence of ozone over the SH. The persistence time scale is given by the time for the auto-correlation function of the ozone time series to continuously drop from 1 at 0 lag and to cross a value of 1/e. Figure 9a shows the time scale of ozone as a function of the month of the year. From CTRL (red line), Antarctic ozone generally exhibits the longest persistence or "memory" from austral autumn to winter. In other words, an ozone anomaly that develops before winter tends to persist until spring. This result is consistent with the results of Fioletov and Shepherd (2003) who also found that winter ozone anomalies remain until the following summer in both hemispheres. The long ozone memory starts to decrease in September. It completely disappears in November, when the SH polar vortex generally breaks down. The orange line in Figure 9a shows the time scale of ozone from DEPLO3. DEPLO3

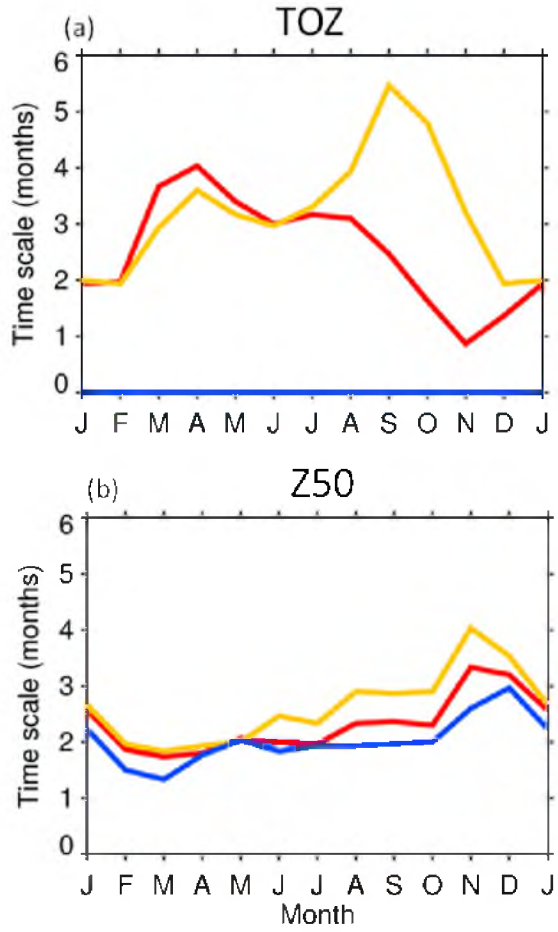

Figure 9 Time scale of (a) total ozone (60°-90°S) and (b) geopotential height at 50 hPa as a function of month. The time scale is given by the time for the auto-correlation function of the monthly mean ozone time series to continuously drop from 1 at 0 lag and to cross a value of 1/e.

suggests considerably longer memory than CTRL in austral spring, while no significant differences are found in the other seasons. This finding is consistent with the prolonged vortex in DEPLO3 that lasts up to December (Figure 6a), so that ozone anomalies persist longer than in CTRL. Similarly, Kuroda and Kodera (2005) demonstrated that the ozone memory increases under ozone depleted conditions.

We next examine the persistence time scale of geopotential height at 50 hPa from CTRL (red line in Figure 9b). Geopotential height has, in general, shorter persistence

time scales than ozone. More importantly, DEPLO3 (orange line in Figure 9a) exhibits increased memory in the winter as compared to CTRL, which is similar in structure to that of ozone (Figure 9a). In particular, in both ozone and geopotential height, the largest increase occurs at the time of maximum ozone depletion in the spring. The increase in persistence seen in ozone and geopotential height during austral spring suggests a close connection between the two quantities.

In FIXO3 there is an interesting increase in the time scale of geopotential height in December. The increase corresponds to about 3 months. This means that geopotential height in December is less correlated with the previous few months when interactive chemistry is used. This behavior is probably related to the earlier break down of the vortex in FIXO3 as compared to CTRL (Figure 6b). In FIXO3 the zonal wind turns earlier into easterlies with easterlies persisting from late November up to January. The longer period of easterly winds seems to be related to the increased persistence during January with the preceding months.

2.5.5 Interaction between ozone and stratospheric circulation

Perhaps the most straightforward way to diagnose the relationship between ozone and geopotential height is the cross-correlation between the two variables for specific monthly lags. The month-to-month lagged cross-correlation may be used to study cause and effect between the two on intraseasonal time scales. We first investigate the lagged correlation between total ozone (60°-90°S) and geopotential height (60°-90°S) from monthly anomaly data, and find that ozone and stratospheric circulation are two-way coupled (Figure 10). After the impact of ozone on the circulation becomes dominant in the stratosphere, its impact penetrates lower into the troposphere with time. It takes 1 to 2

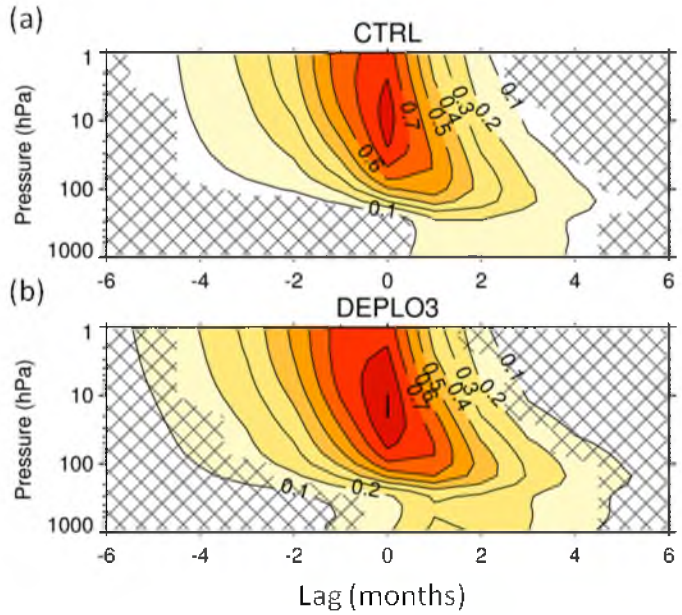

Figure 10 Lagged correlation between total ozone (60°-90°S) and geopotential height at various levels, using all months of the year from (a) CTRL and (b) DEPLO3 simulations. Positive (negative) lags indicate that ozone leads (lags) geopotential height. Hatching indicates correlations that are not significantly different from zero at the 5% error level according to a 2-tailed Student's t-test.

months for the ozone impact to reach the surface. We note that the downward descent of the relationship between ozone and geopotential height closely resembles the downward propagation of the southern annular mode (e.g., Thompson *et al.*, 2005).

We further investigate the relationship between stratospheric ozone and the circulation in order to understand in which season the interaction between the two becomes strongest. We use geopotential height anomalies averaged over the polar cap as a simple surrogate for change in the stratospheric circulation. The red curve in Figure 11a illustrates the cross-correlation between September total ozone and 10 hPa geopotential height at various lags. Values at +1 (-1) month lag indicate correlations between September total ozone and October (August) geopotential height. The highest correlation between ozone and geopotential height occurs at zero lag, indicating that the two fields

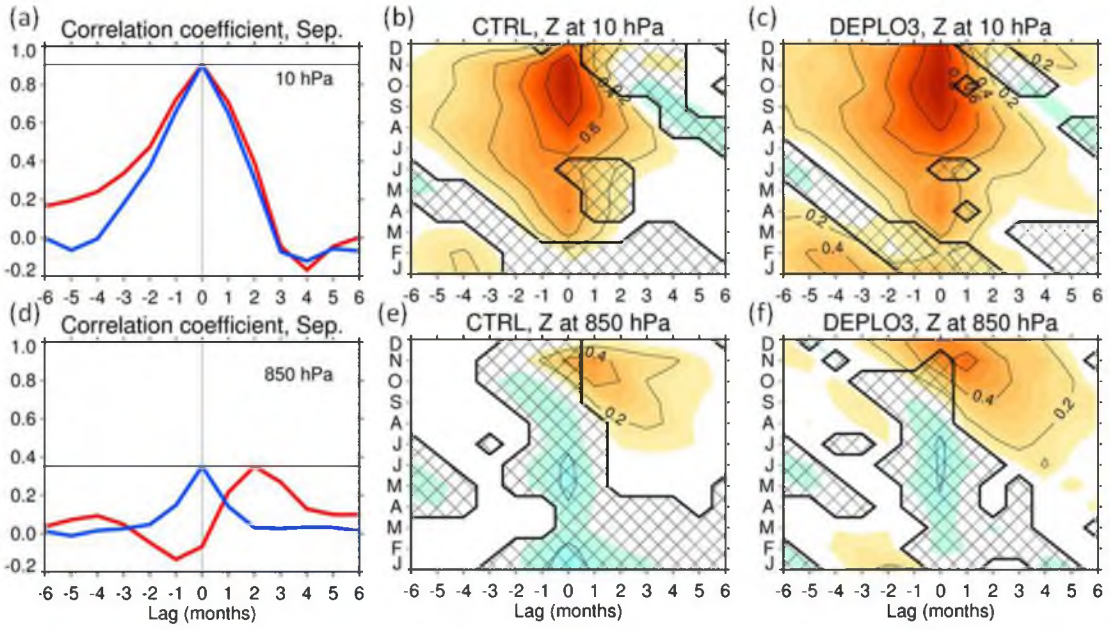

Figure 11 Lagged correlation for CTRL and DEPLO3 simulations. (red) Lagged correlation between total ozone (60°-90°S) in September and geopotential height at (a) 10 hPa and (d) 850 hPa in other months from CTRL. (blue) Scaled auto-correlation of geopotential height in September and in other months from FIXO3. Positive (negative) lags indicate that ozone leads (lags) geopotential height; for example, values at +1 (-1) month is a correlation between September ozone and October (August) heights. Horizontal line indicates scale factor given by the maximum in lagged correlation. (b, c, e, f) Lagged correlation for all months as in a, d panels for (b, e) CTRL and (c, f) DEPLO3. Hatching indicates that lagged correlations are smaller than scaled auto-correlation of geopotential height. See text for details.

are either influenced by another common factor or that one field influences the other in relatively short submonthly time scales. One such common factor could be planetary waves that propagate upward from the troposphere into the stratosphere and break there. Following Salby *et al.* (2012), changes in both ozone and stratospheric circulation are largely driven by such waves. Relatively large correlations at positive lags indicate that ozone anomalies in September are related to anomalies in geopotential height during subsequent months. The cross-correlations at negative lags are generally larger than that at positive lags, suggesting that on subseasonal time scales the influence of the circulation

on ozone is stronger than the impact of ozone on the circulation. This relatively large correlation between ozone and geopotential height is also discussed in observations by Son *et al.* (2013) who find that the high correlation between the southern annular mode and Antarctic ozone during spring is largely due to the interannual variability of the ozone hole. Comparably large magnitude of correlations in the stratosphere at positive and negative month lags suggests that there might be some connections between the two variables. The connections are further linked to a positive feedback as we will show in the next paragraph. As we have already seen in Figure 10, the ozone and geopotential height are coupled in the stratosphere, and ozone impact on the stratospheric circulation becomes dominant. Its impact propagates downward through the stratosphere-troposphere coupling (Thompson *et al.*, 2005), perhaps even leading to an impact of ozone anomalies on the circulation at tropospheric levels (Son *et al.*, 2013; Gillett and Thompson, 2003; Thompson *et al.*, 2011).

In order to estimate the persistence of geopotential heights in the absence of a potential chemical/dynamical feedback, we use simulation FIXO3 to determine the lagged auto-correlation of September geopotential height at 10 hPa (blue curve in Figure 11a) and compare it with the cross-correlation between ozone and geopotential height derived from CTRL (red curve). The auto-correlation from FIXO3 is scaled by the maximum cross-correlation between total ozone and geopotential height from CTRL. A cross-correlation larger than the auto-correlation for the same lag indicates a relationship that exceeds simple persistence of geopotential, which, in other words, may be due to the existence of a positive, reinforcing feedback between the ozone and geopotential height. As expected, Figure 11a shows that at negative lags cross-correlations are considerably

larger than auto-correlations. This can be interpreted that geopotential height anomalies in summer lead to the same signed ozone anomalies a few months later. At positive lags, cross-correlations also exceed the auto-correlations, but only by small amounts, making a subtle impact of ozone anomalies on geopotential heights. It will thus affect the change of the circulation.

We now expand our previous analysis, that was performed for September only, to all months of the year. Simulation CTRL (Figure 11b) exhibits positive cross-correlations in broad ranges from winter to spring at both positive and negative lags, with the highest cross-correlations occurring during October and November. The nonhatching areas denote that the auto-correlations are smaller than cross-correlations of the geopotential height, indicating that the persistence of geopotential height can be increased by the intensifying feedback with the ozone. It is interesting that the persistence increase occurs from austral autumn to spring (Figure 11b). The persistence increase in autumn and winter seems to be related to the growth of the polar vortex. The polar vortex starts to grow in the austral autumn (Figure 6c). It is still too weak to maintain the persistence. The weak persistence in this season is evident from the short length of nonhatching areas near 0 lags. Moreover, a long persistence during winter is maybe the outcome of the strongest polar vortex being there. However, there is still quite a long persistence in spring, when the polar vortex breaks down (Thompson *et al.*, 2005). What causes this long persistence? In part, it results from the intensifying interaction between ozone and geopotential height. As we discussed in Figure 11a, the positive cross-correlations at negative lags indicate geopotential height anomalies lead to the same signed ozone anomalies a few months later. At the same time, the positive cross-correlations at positive

lags are the impact of the ozone on the geopotential height. Although the impact of ozone on the circulation is a few months shorter than the influence of the circulation to the ozone, they covary with each other.

Cross-correlations from DEPLO3 are even stronger and cover larger areas (Figure 11c). These results suggest that ozone and the circulation indeed covary with each other in a model with interactive chemistry and that the strength of this covariability is tighter when ODSs are present and the possibility of ozone depletion is given. With ozone depletion, the persistence of geopotential height anomalies is even stronger. The persistence by the impact of ozone on the circulation is comparable to that by the influence of the circulation on the ozone. The reinforcing mechanism between ozone and the circulation becomes apparent in DEPLO3.

We also investigate the relationship between total ozone and geopotential heights in the troposphere (Figure 11d). There is a positive cross-correlation between ozone and heights at positive lags of about 2 months, which cannot be explained from persistence alone. In other words, September ozone anomalies are positively correlated with November tropospheric geopotential height. This delayed influence of variations of stratospheric ozone on the tropospheric circulation is reminiscent of the work by Son *et al.* (2013), who reported a significant impact of early spring ozone on midspring geopotential height over the SH, resulting in systematic variations in the hydrological and dynamical systems. This effect on the tropospheric circulation is probably related to the dynamical coupling from the stratosphere to the troposphere (Baldwin and Dunkerton, 2001). Similar sensitivities of the tropospheric circulation to ozone changes have been reported by Son *et al.* (2010, 2008b), Polvani *et al.* (2011), McLandress *et al.* (2011), and

Perlwitz *et al.* (2008).

2.5.6 Variability of the stratospheric circulation

We now investigate in detail the climatology of the SH polar vortex, with an emphasis on the transition period of the vortex from its well-developed state in mid-winter to its breakdown during austral spring. Overlapping time series of 10 hPa zonal winds at 60°S from the first 100 years of each simulation are shown in Figure 12. The selected time period covers the decay or 'breakdown' phase of the polar vortex, ranging from its mature stage with its westerly wind maximum during the end of winter (August), to the slow transition to zero wind during the end of spring (November) and the short period of wind reversal in summer (December). From inspecting individual annual time series one can see a clear contrast in the interannual variability of the winds: variability is small in midwinter and also in midsummer, and it is rather large during the spring breakdown period. Comparing the outcomes from the three simulations it also becomes clear that winds in DEPLO3 are more variable than in the other two simulations. This becomes even clearer in Figure 13, focusing on the mean winds and their interannual standard deviations among the three simulations. During the mature stage of the vortex the winds among the three simulations are almost exactly the same (Figure 13a, b). However, during spring when ozone depletion starts to occur, the vortex in DEPLO3 becomes colder (Figure 6e) and more persistent than in CTRL or FIXO3. The result is that in DEPLO3 the final breakdown of the vortex is delayed by about 2 weeks (Figure 13a, b). The vortex in DEPLO3 during spring is also more variable (Figure 13c, d). Both the increased persistence and the larger variability are consistent with our assumption of a positive photochemical feedback, which helps to sustain any existing anomaly. In

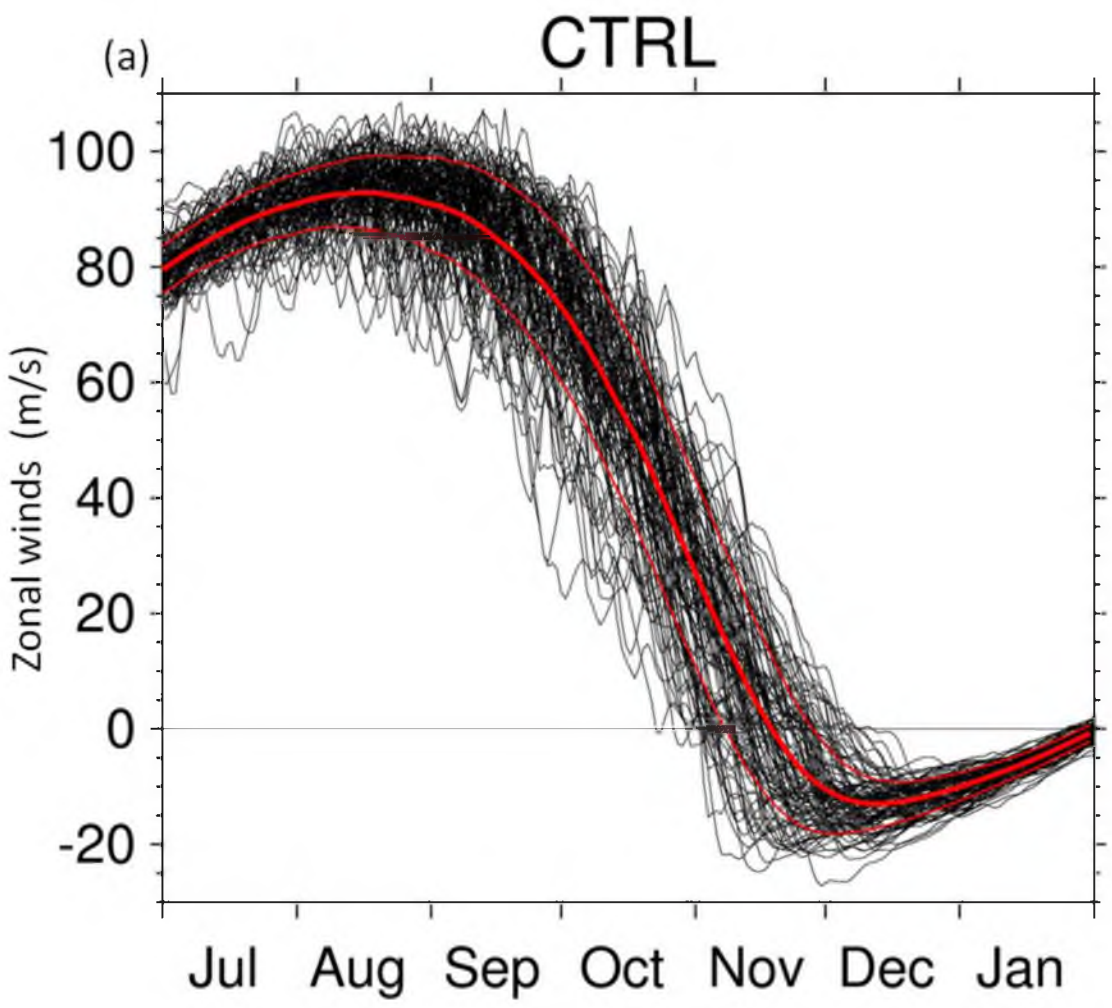

Figure 12 Time series of zonal winds (m/s) at 10 hPa and at 60°S taken from the first 100 years from each of the three simulations: (a) CTRL, (b) DEPLO3, and (c) FIXO3. Colored bold lines indicate climatological means over all years; colored thin lines show plus and minus one standard deviation around the means.

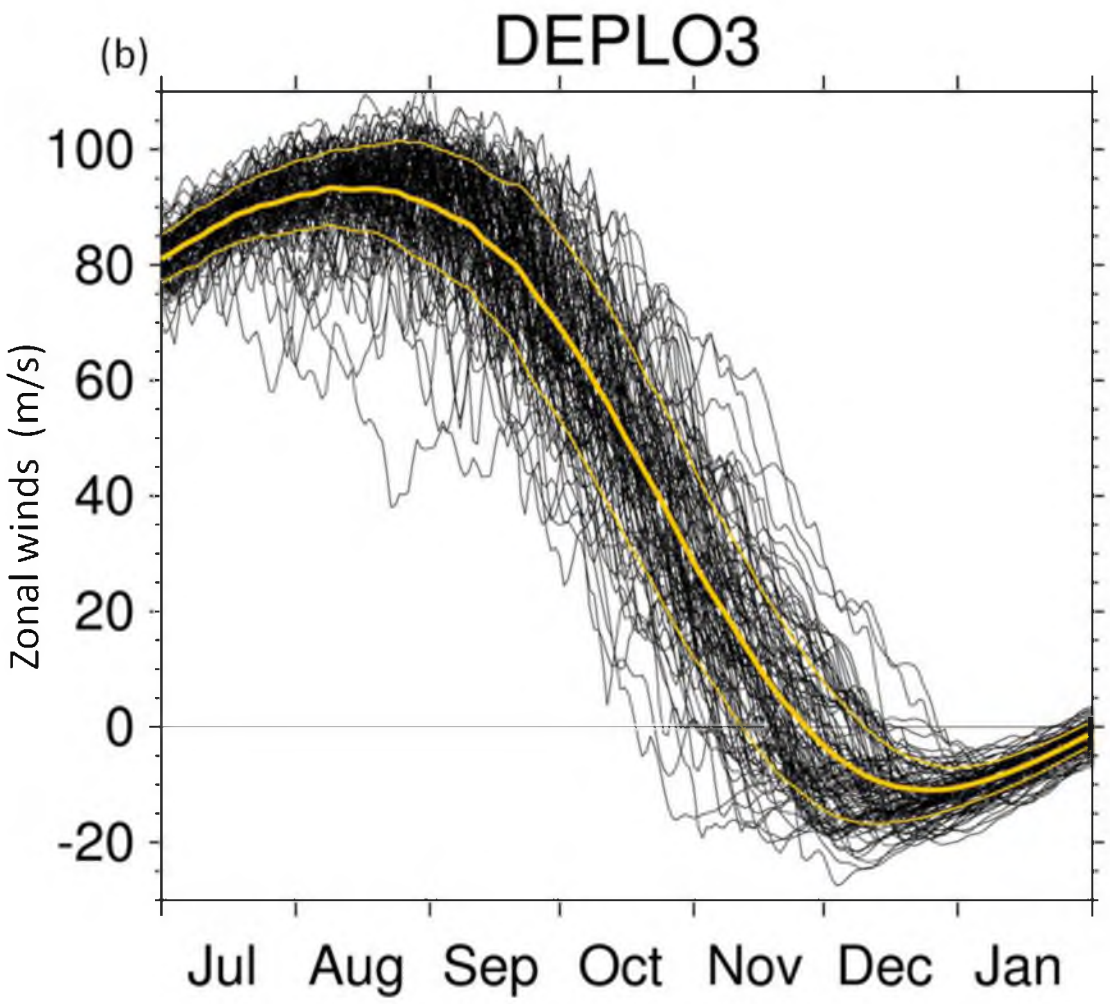

Figure 12 Continued.

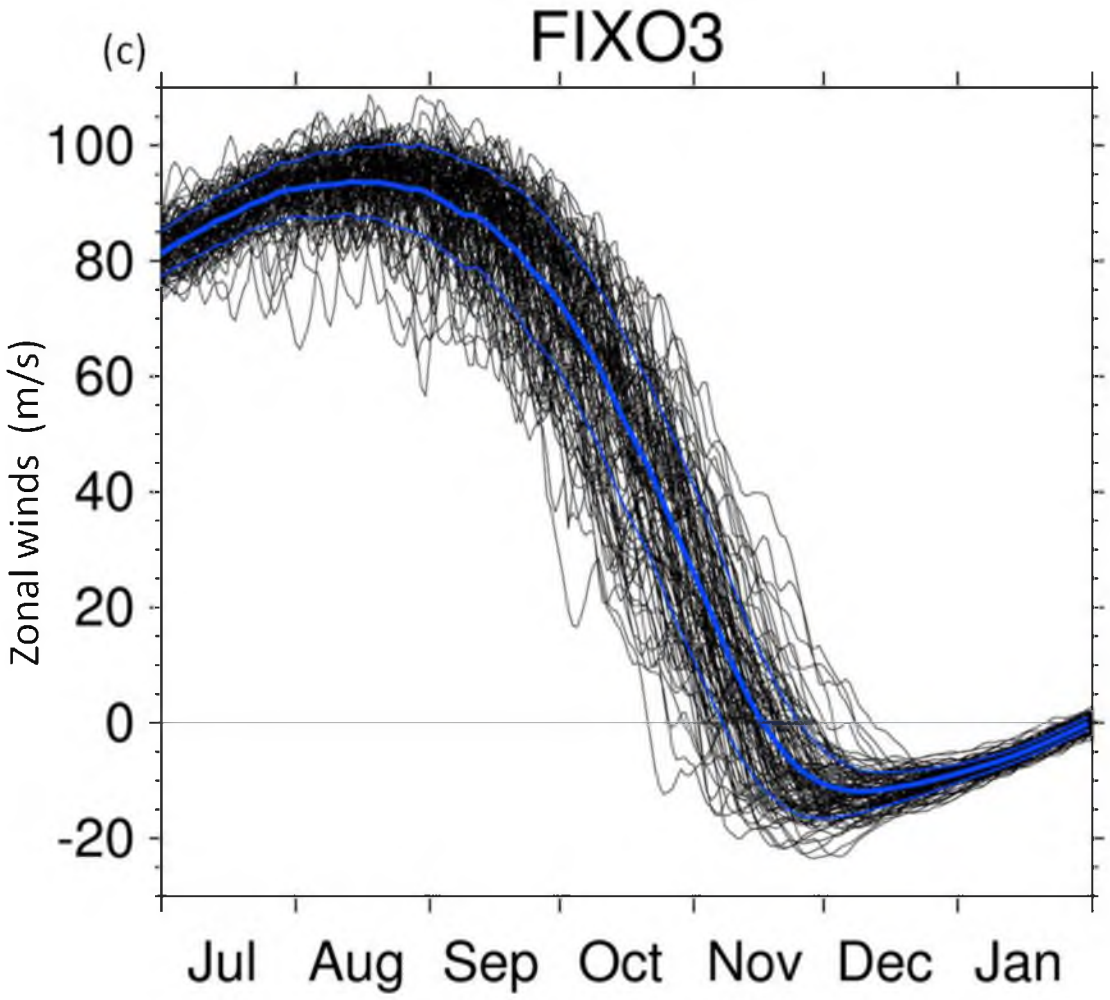

Figure 12 Continued.

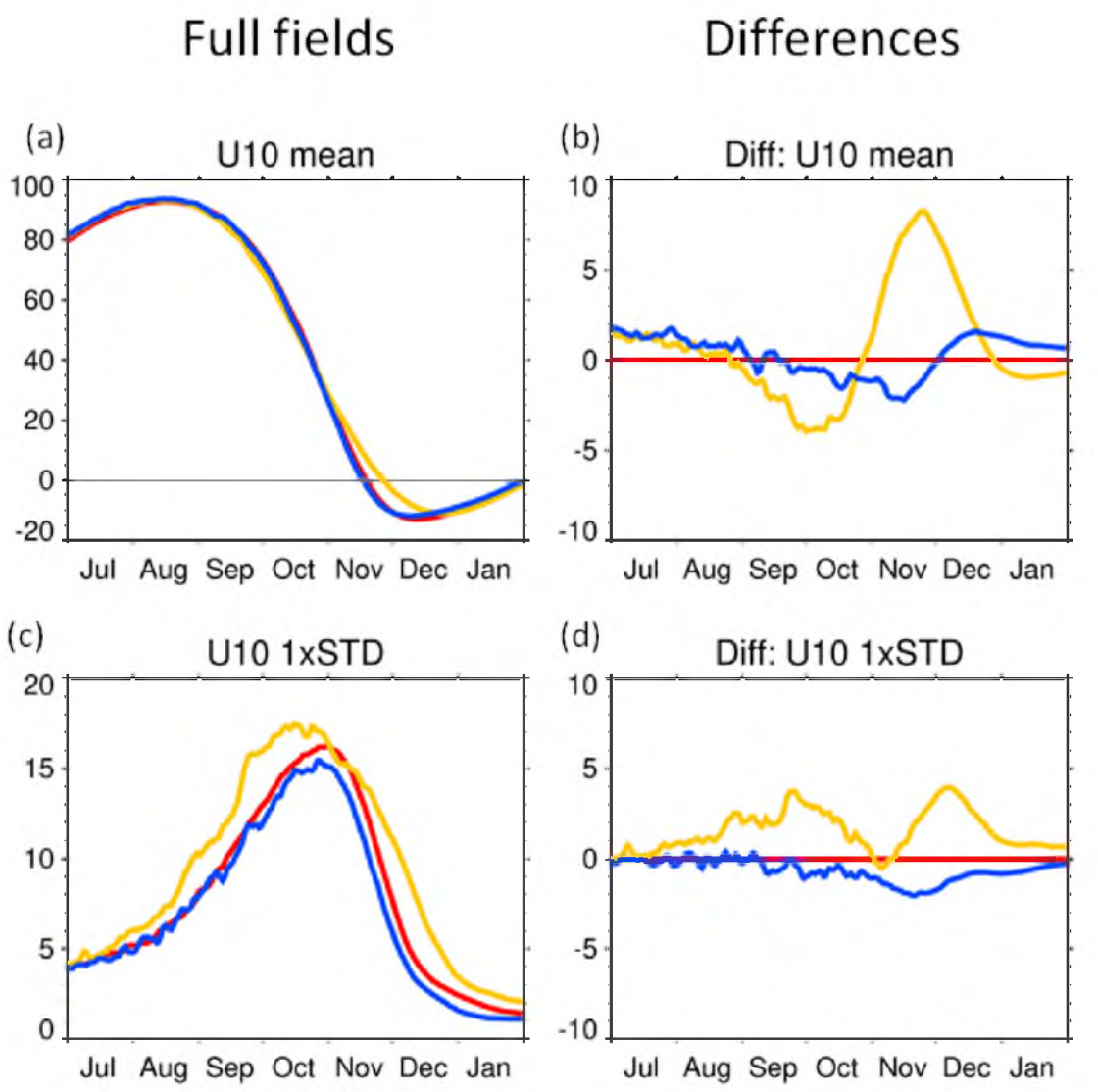

Figure 13 Zonal winds (m/s) at 10 hPa and at 60°S taken from the first 100 years from each of the three simulations. (a) Composite averages of zonal winds (m/s) at 10 hPa and at 60°S for (red) CTRL, (orange) DEPLO3, and (blue) FIXO3. (b) Differences in averages of the zonal winds against CTRL. (c) Standard deviation of 10 hPa winds at 60°S. (d) Differences of standard deviations against CTRL.

contrast to DEPLO3, FIXO3 exhibits the weakest variability, which is perhaps due to lack of the chemical/dynamical positive feedback.

We also examine geopotential height (60°-90°S) anomalies during the transition period of the vortex (Figure 14). The positive and negative values in the anomalies are the weak and strong vortex, respectively. Colored lines are averages for each vortex from all years. Again, strong and persistent vortex events happen most frequently in DEPLO3. Following Keeley *et al.* (2007), the response of stratospheric dynamics to ozone depletion acts to cool the Antarctic lower stratosphere during the transition period of the vortex. This cooling subsequently leads to a delay of final warmings over the SH (Waugh *et al.*, 1999). A positive feedback causes any time rate of change to become slower. Such indications for the long timescale can be seen from November to December in Figure 15: the decay rate in DEPLO3 is slower, i.e., the decline slope is smaller. In contrast to DEPLO3, a short-lived vortex is apparent in FIXO3. With uncoupled ozone chemistry, the vortex grows weaker than CTRL or DEPLO3. It also declines faster owing to the lack of a positive feedback between ozone and the circulation (Figure 15).

2.5.7 Change in atmospheric variability

We hypothesize that the ozone loss over the polar stratosphere feeds back into the stratospheric circulation, producing more ozone deficit (Figure 4). The suggested positive feedback between ozone and the circulation should thus act to intensify the circulation, which should be reflected in an increase of atmospheric variability in the extratropics represented by the annular modes (Thompson and Wallace, 2000). Previously in section 4.3, we discussed the reciprocal relationship between ozone and the circulation on various time scales. On one hand, on very long climate and interdecadal time scales,

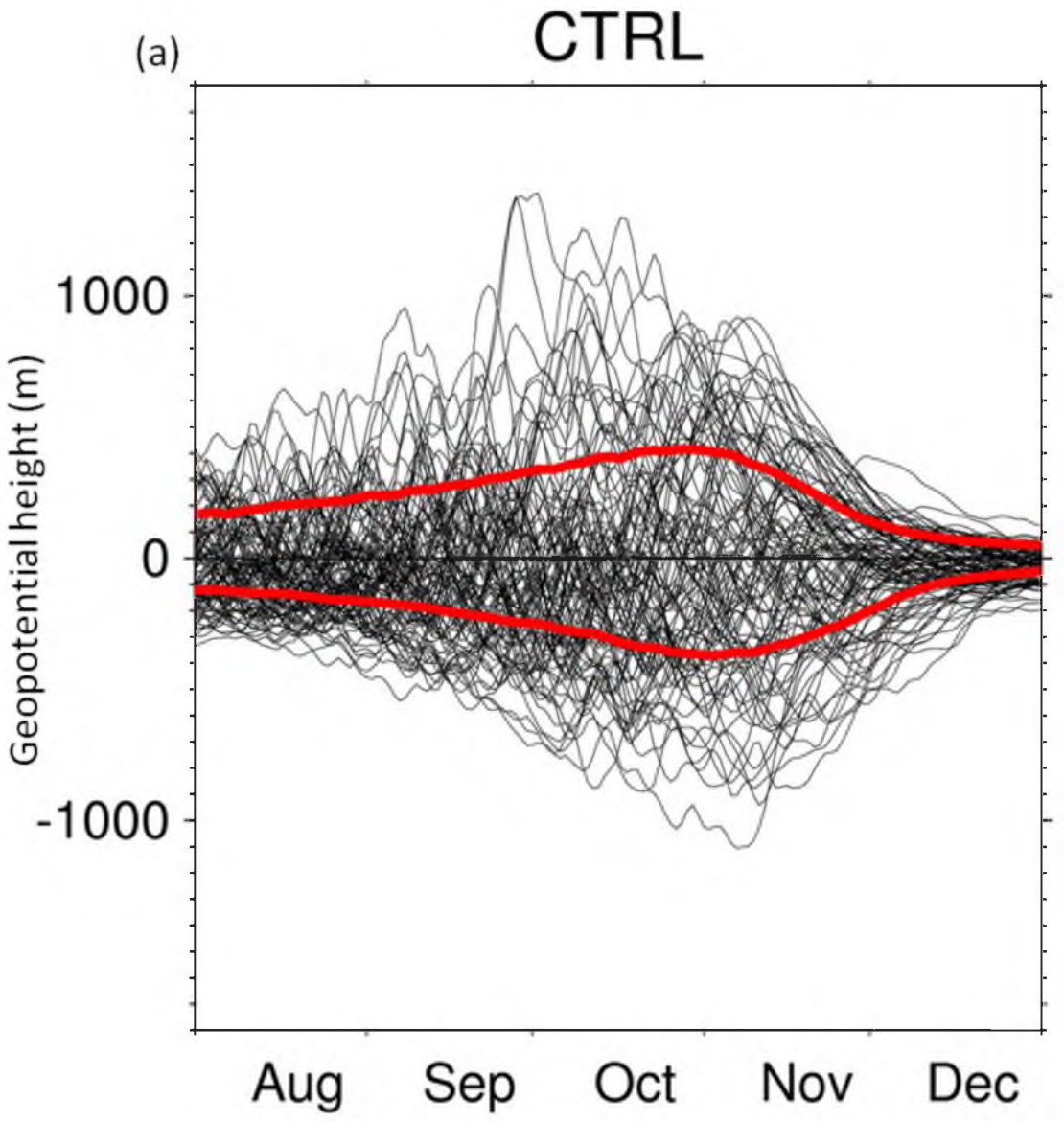

Figure 14 Time series of geopotential height (60°-90°S) at 10 hPa taken from the first 100 years from each of the three simulations: (a) CTRL, (b) DEPLO3, and (c) FIXO3. Colored lines indicate climatological means of strong and weak events over all years.

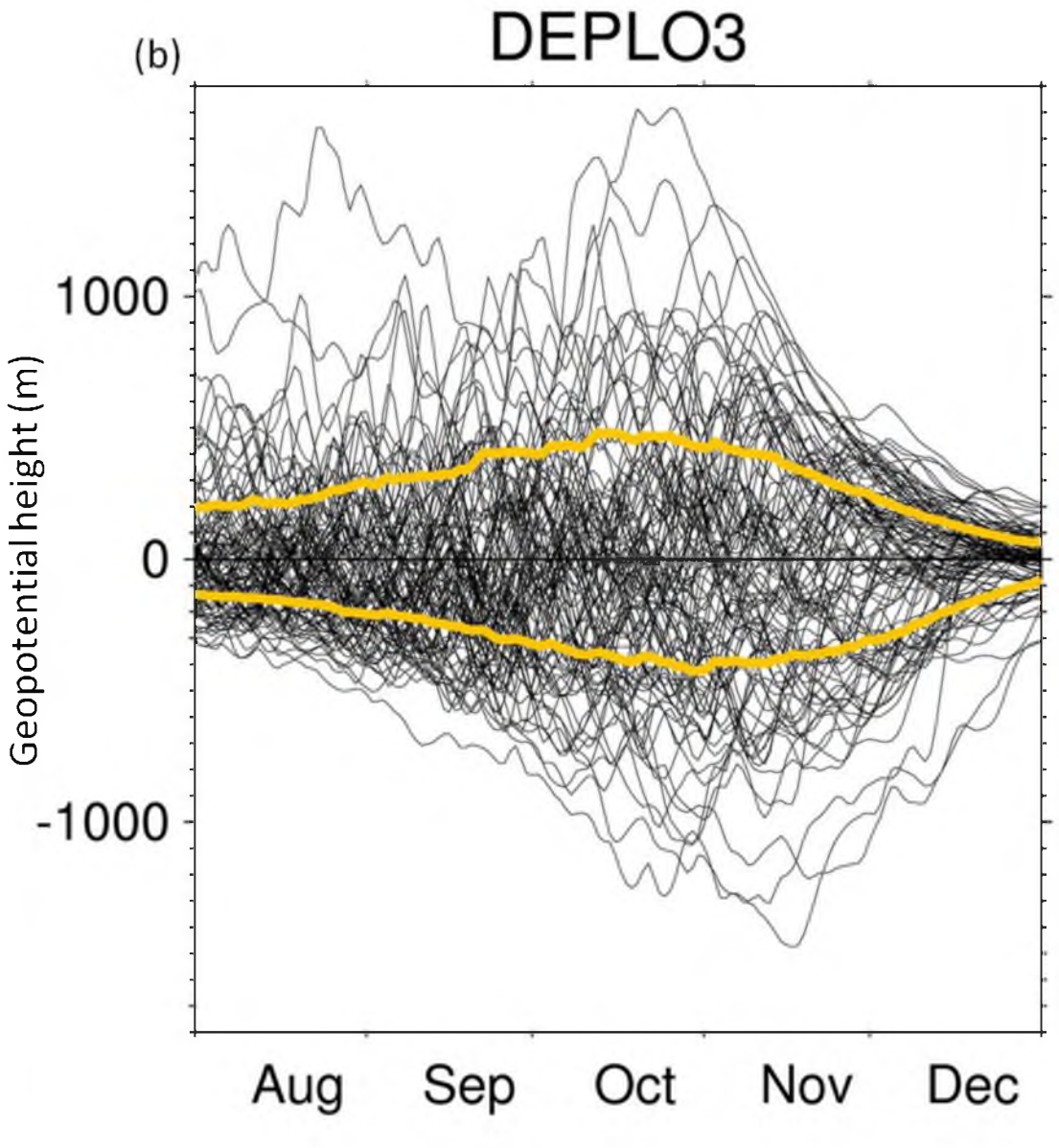

Figure 14 Continued.

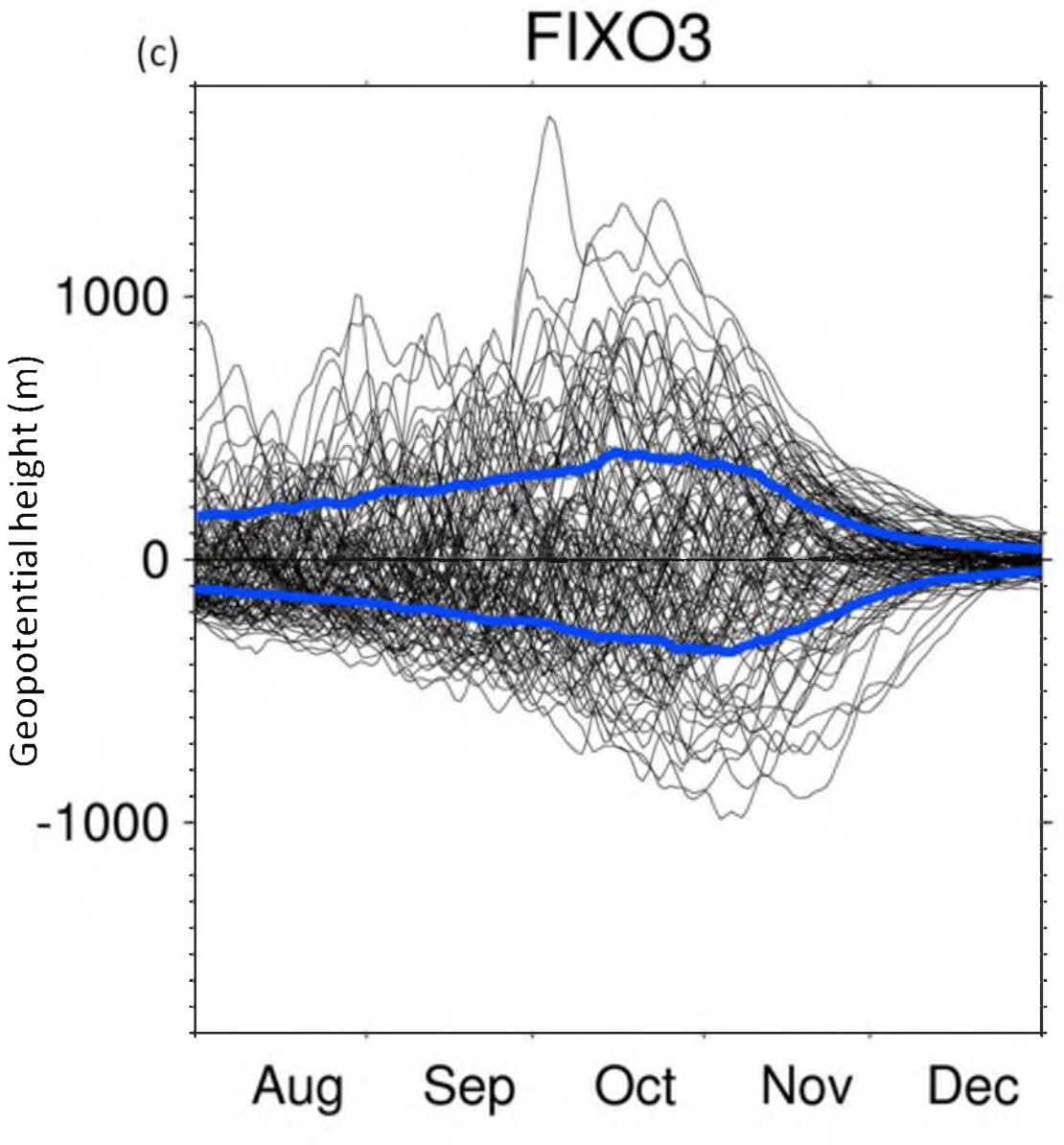

Figure 14 Continued.

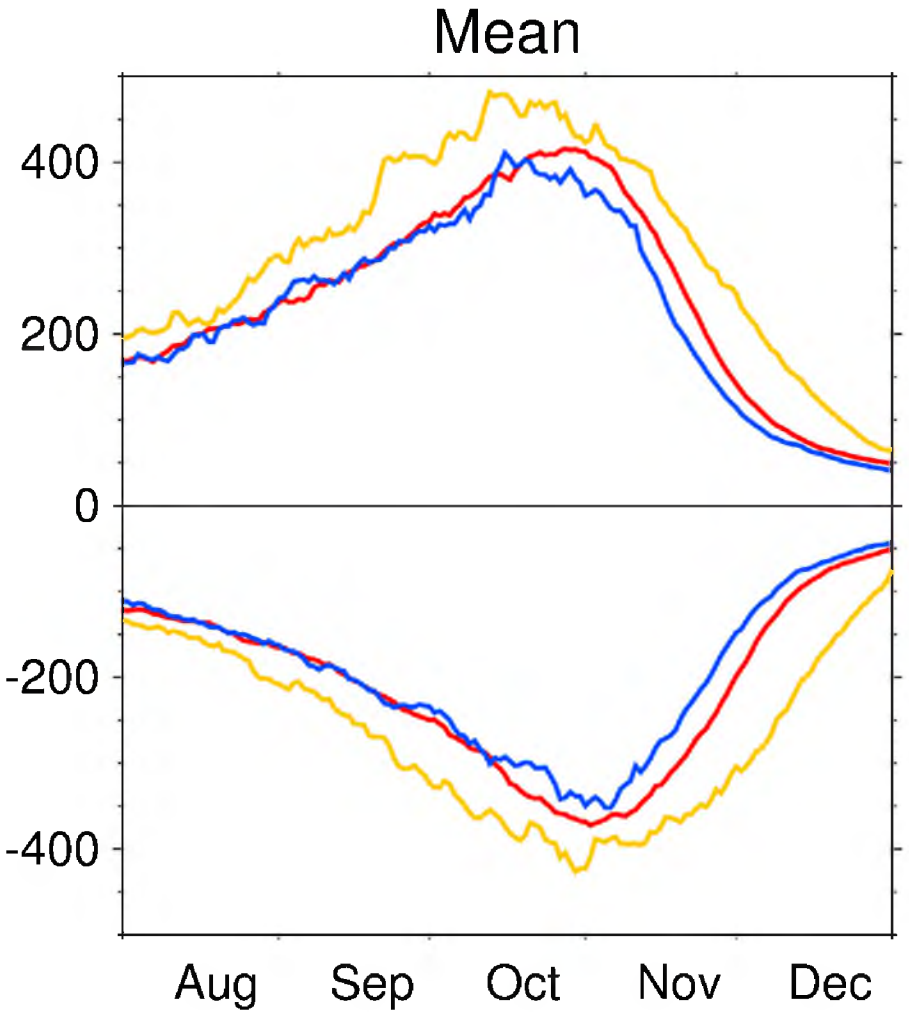

Figure 15 Composite averages of 10 hPa geopotential height (60°-90°S) for (red) CTRL, (orange) DEPLO3, and (blue) FIXO3.

ozone depletion is expected to influence circulation (e.g., Son *et al.*, 2008b). On the other hand, on interannual and shorter time scales, circulation changes are expected to influence ozone (e.g., Salby *et al.*, 2012). In order to cover the entire range of expected influences we examine in the following both the interannual and daily time scales. Figure 16 compares the variability of SH polar cap averaged geopotential height among our three simulations. Polar cap averaged geopotential heights are used because they represent a simple but good measure for the annular modes (Baldwin and Thompson, 2009; Cohen *et al.*, 2002), the primary modes of extratropical circulation variability. For simplicity, we only show variability from CTRL (Figure 16a, b) and percent change in variability of DEPLO3 (Figure 16c, d) and FIXO3 (Figure 16e, f) with respect to CTRL. The results are depicted as a function of month and height, and we focus on daily and interannual time scales. The interannual variability maximizes at 1 hPa in October (Figure 16a) and precedes the tropospheric peak in December by about 2 months, implying that stratospheric variability may affect tropospheric variability (Baldwin *et al.*, 2003b). Figure 16 also includes daily variability, because it is not entirely clear on which time scales the expected chemical/dynamical feedback acts, and any change in variability will help the interpretation of our results. For example, the breakdown of the polar vortex during late spring is associated with an increase in daily variability (Figure 16b, Gerber *et al.*, 2010), and changes in the timing of the breakdown may influence variability on all time scales. This means that changes in variability can occur because of at least two reasons: due to the hypothesized positive feedbacks, but also due to changes in the climatological timing of the vortex breakdown during late spring.

DEPLO3 exhibits substantial increases in stratospheric AM variability with respect

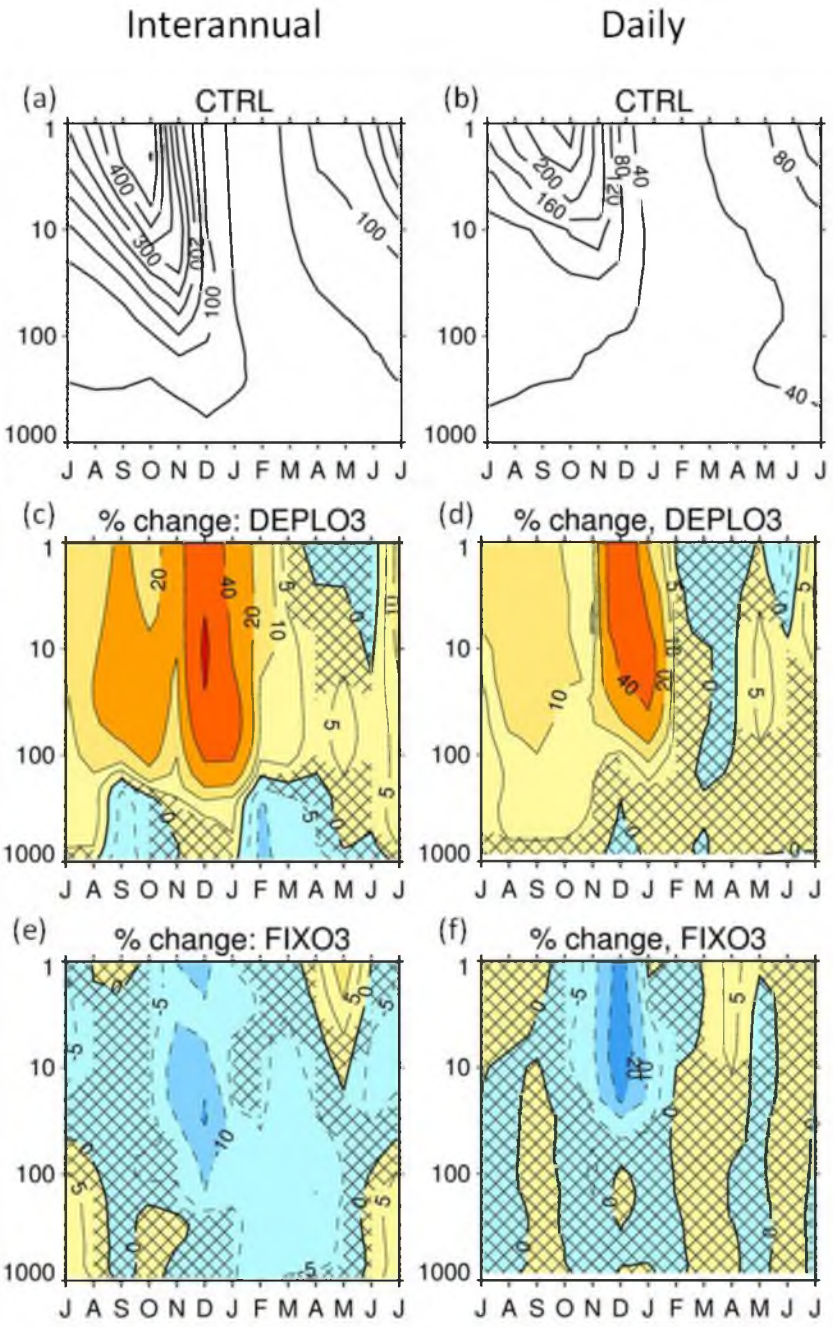

Figure 16 Variability of geopotential height (60°-90°S) from CTRL on (a) interannual and (b) daily time scales. (c-f) Geopotential height (60°-90°S) variability difference (%) between shown simulation and CTRL. Variability difference is calculated as (σ_{EXP} / σ_{CTRL} − 1) x 100%, where EXP is either (c, d) DEPLO3 or (e, f) FIXO3, and σ is interannual and daily standard deviation (see Methods section for details). A slowly varying trend is removed from all data by applying a 150-year low pass Lanzcos filter. Hatching shows insignificant (95%) results after F-test.

to CTRL. The maximum increase amounts to +80% at 10 hPa in December (Figure 16c, d). The December peak is related to the delayed breakdown of the colder and stronger polar vortex. At the same time, FIXO3 exhibits broad decreases in variability (Figure 16e), which also peak in December. Similarly as before, the December peak is related to the now somewhat earlier breakdown of the polar vortex, reducing somewhat the duration of the time period with high variability in spring.

In CTRL, zonal winds at 10 hPa and 60°S reach zero m/s in mid-November (Figure 6c), indicating the final breakdown of the vortex. In contrast to CTRL, DEPLO3 has a stronger and thus prolonged vortex (Figure 6c), which on average breaks down during late November, i.e., about 2 weeks later than in CTRL. At the same time, there are robust increases in variability over the SH from August to February in DEPLO3 with respect to CTRL (Figure 16c). The maximum increase amounts to +80% at 10 hPa in December. Following Salby (2008), the influence of anomalously large ozone on the anomalous temperature will be delayed by a few months due to the long radiative relaxation time scales in the stratosphere (Brasseur and Solomon, 2005). DEPLO3 exhibits the strongest ozone loss in October (Figure 6a). The maximum increase in the variability in December may represent the radiative impact of October ozone depletion on the enhanced cooling in December. The increase in the variability means that the timing of the vortex breakdown is more variable in DEPLO3 due to both photochemical and chemical/dynamical feedbacks within this simulation. This increase in interannual variability appears first in the upper stratosphere, from where it descends with some delay into the lower stratosphere. During January there are ca. 5% variability increases in the troposphere. The increase in the tropospheric variability becomes even stronger on

interdecadal time scales, which amounts to about 10% (not shown). The change in variability from FIXO3 (Figure 16e, f) shows a somewhat similar structure to that of DEPLO3 but with opposite sign. Now, there is 10-20% decrease in variability, which starts in November in the upper stratosphere and descending into the lower stratosphere in December. In FIXO3, the polar vortex breaks down at the same time because of no ozone forcing. It will produce a small stratospheric variability. However, the timing of vortex breakdown is more variable due to the chemical/dynamical feedback in CTRL. Together, these facts lead to the above mentioned decrease in variability.

We now discuss change in variability that occurs well before December, which, because of their timing, are not related to the vortex breakdown. Rather, they may be related to the hypothesized feedback between ozone and the circulation. In September and October, when ozone depletion becomes strong, DEPLO3 also exhibits an increase in stratospheric variability. During this time the polar vortex is strong and stable (Figure 6c, Thompson *et al.*, 2005), constraining the upward propagation of tropospheric planetary waves (Charney and Drazin, 1961; Gerber, 2012). The long polar night combined with weak tropospheric wave driving leads to strong cooling. PSCs can form under such cold conditions, which in turn may trigger heterogeneous chemical process and ozone destruction when sunlight is present (Solomon *et al.*, 1986; Solomon, 1999). The ozone destruction leads to additional cooling. In other words, under the influence of ODSs there may be a positive feedback involving the chemistry and dynamics of the stratosphere. It results in a strong polar vortex. In some other years, perhaps due to stronger wave driving, stratospheric temperatures are not cold enough to form enough PSCs, leading to a weak and relatively warm polar vortex. These processes may explain the broad increase in

variability during spring in DEPLO3 (Figure 16c, d).

Simulation FIXO3 (Figure 16e, f) exhibits only small changes in variability, except for the above discussed period in November and December that is due to a weaker vortex and its earlier breakdown. Nevertheless, during the remainder of the year the variability changes are consistently negative, they amount to about minus 5%, and they appear in most of the stratosphere and during most of the year (Figure 16e). This may be a sign for the hypothesized chemical/dynamical feedback. The only slight decrease in variability suggests that this feedback in isolation is relatively weak, and that it perhaps relies on the combination with the photochemical feedback to become more important.

Over the NH, the final breakdown of the polar vortex is in April (Figure 6d). However, the maximum stratospheric variability is in February (Figure 17a, b), which is related to variations in tropospheric wave driving. Strong wave driving may result in stratospheric sudden warmings (SSWs) (Matsuno, 1971), which are episodic high-impact events. Variations in the climatological number of SSWs are therefore important for the interpretation of NH variability differences in our simulations. As shown in Table 3, the average number of SSWs per year in our simulations ranges between 30 and 40%, which is considerably smaller than the about 60% seen in the observations (Charlton and Polvani, 2007). The reduced number of SSWs in climate models is a well-known feature, related to the lack of meridional heat fluxes (Charlton *et al.*, 2007). The number in DEPLO3 (35% in Table 3) is about the same as in CTRL (36%), but it is considerably higher in FIXO3 (46%). This increased number of SSWs in FIXO3 is consistent with the weaker and warmer vortex during midwinter (Figure 6d, f) and the relatively broad variability increase, which is most pronounced in November (Figure 17e).

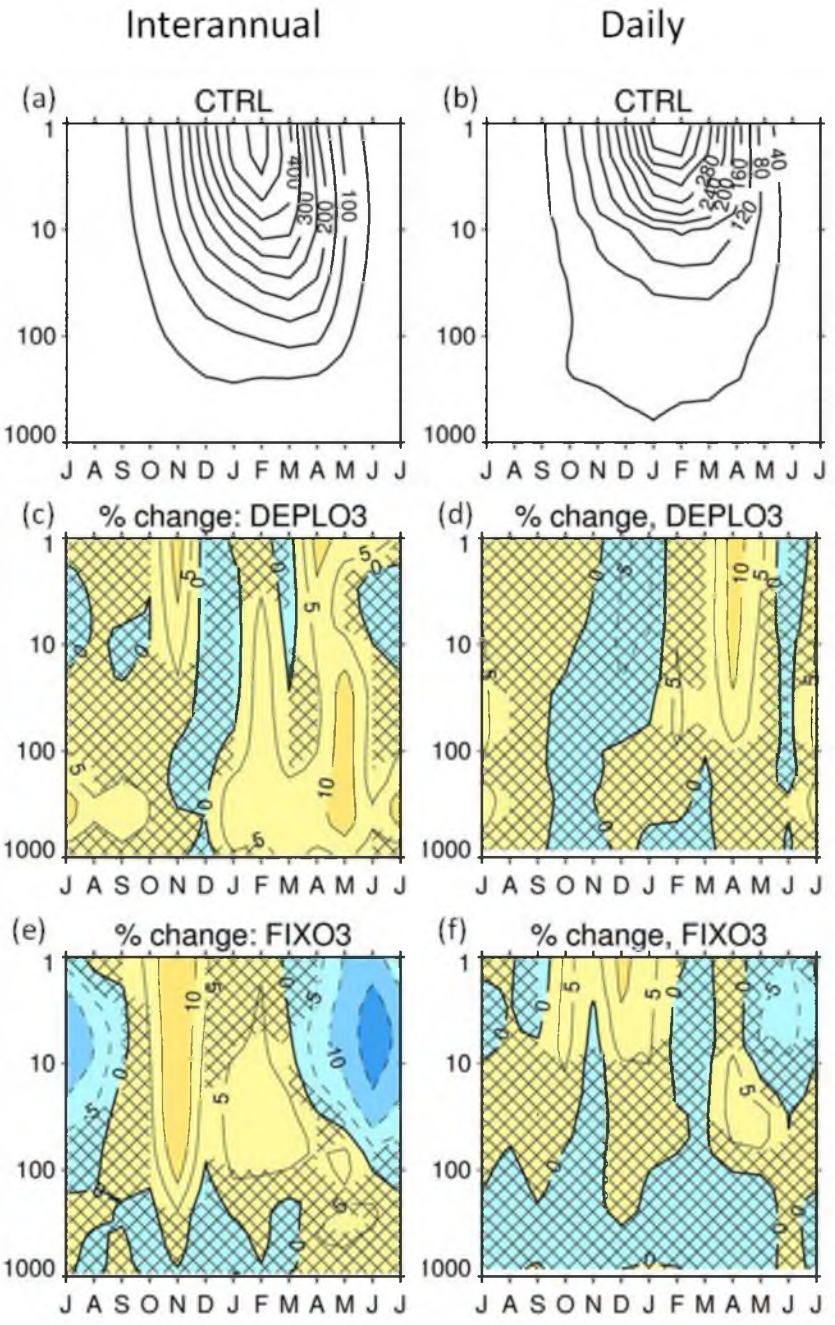

Figure 17 Variability of geopotential height (60°-90°N) from CTRL on (a) interannual and (b) daily time scales. (c-f) Geopotential height (60°-90°N) variability difference (%) between shown simulation and CTRL. Variability difference is calculated as (σ_{EXP} / σ_{CTRL} − 1) x 100%, where EXP is either (c, d) DEPLO3 or (e, f) FIXO3, and σ is interannual and daily standard deviation (see Methods section for details). A slowly varying trend is removed from all data by applying a 150-year low pass Lanzcos filter. Hatching shows insignificant (95%) results after F-test.

Table 3 SSW frequency (events per year x 100) over the NH

	CTRL	DEPLO3	FIXO3
SSWs	36%	35%	46%

From Figure 17 it becomes clear that over the NH it is difficult to detect clear impacts on annular mode variability from coupled chemistry. This is in part related to the fact that over the NH there is no anthropogenic ozone depletion in DEPLO3, leading to relatively small differences between CTRL and DEPLO3. Our difficulty is also that changes in variability are strongly affected by the varying number of SSW events amongst the simulations. The SSWs are coincident with the seasons of the positive feedback between ozone and the stratospheric circulation. The fact that both the SSWs and the positive feedback act to produce an increase in the variability makes it difficult to cleanly separate the effects of the feedback from the SSWs. Nevertheless, DEPLO3 exhibits modest (5-10%) increases in stratospheric variability during April and May, a time when the chemical/dynamical feedback is expected to be most important. Similarly, there are even stronger (5-20%) decreases in variability in FIXO3 from April to June. However, we are unable to determine with certainty whether these changes are indeed related to the hypothesized feedbacks or not.

Over the NH it is also difficult to detect the expected chemical/dynamical feedback from FIXO3 because the circulation is dominated by SSW related variability and the different SSW climatology amongst the different simulations.

2.5.8 Time scale of the annular mode

As we have shown earlier, changes in extratropical variability over the SH indicate the existence of amplifying positive feedbacks between ozone and the stratospheric circulation. One measure of the feedback strength may be given by the time scale of natural southern annular mode (SAM) variability, since this time scale is also related to climate sensitivity (Gerber *et al.*, 2008b; Ring and Plumb, 2008; Chen and Plumb, 2009), as suggested by the fluctuation-dissipation theorem (Leith, 1975). It is therefore useful to study changes in this time scale.

Keeley *et al.* (2009) suggested a way to quantify the persistence of AM variability by either removing or retaining the effects of interannual variability. The persistence calculation is based on the auto-correlation function of the AM time series (see Methods section for more details). Keeley *et al.* (2009) and Athanasiadis and Ambaum (2009) suggested that, on interannual time scales, the AM is primarily affected by external factors such as teleconnection patterns. In our simulations, which include such external factors, the interannual variability may be amplified by positive feedbacks between ozone and the circulation.

The a, c, and e panels in Figure 18 present the time scale (or persistence) of the SAM when effects from interannual variability are included. The longest SAM persistence occurs in the middle stratosphere in July, and the maximum seems to descend to the lower stratosphere and troposphere in subsequent months (Figure 18a). This is consistent with the findings of Baldwin *et al.* (2003b) for observations and Gerber *et al.* (2010) for chemistry climate models. The apparent drop in persistence after the persistence peak is probably the result from the little memory of the winter vortex after it turns to easterlies

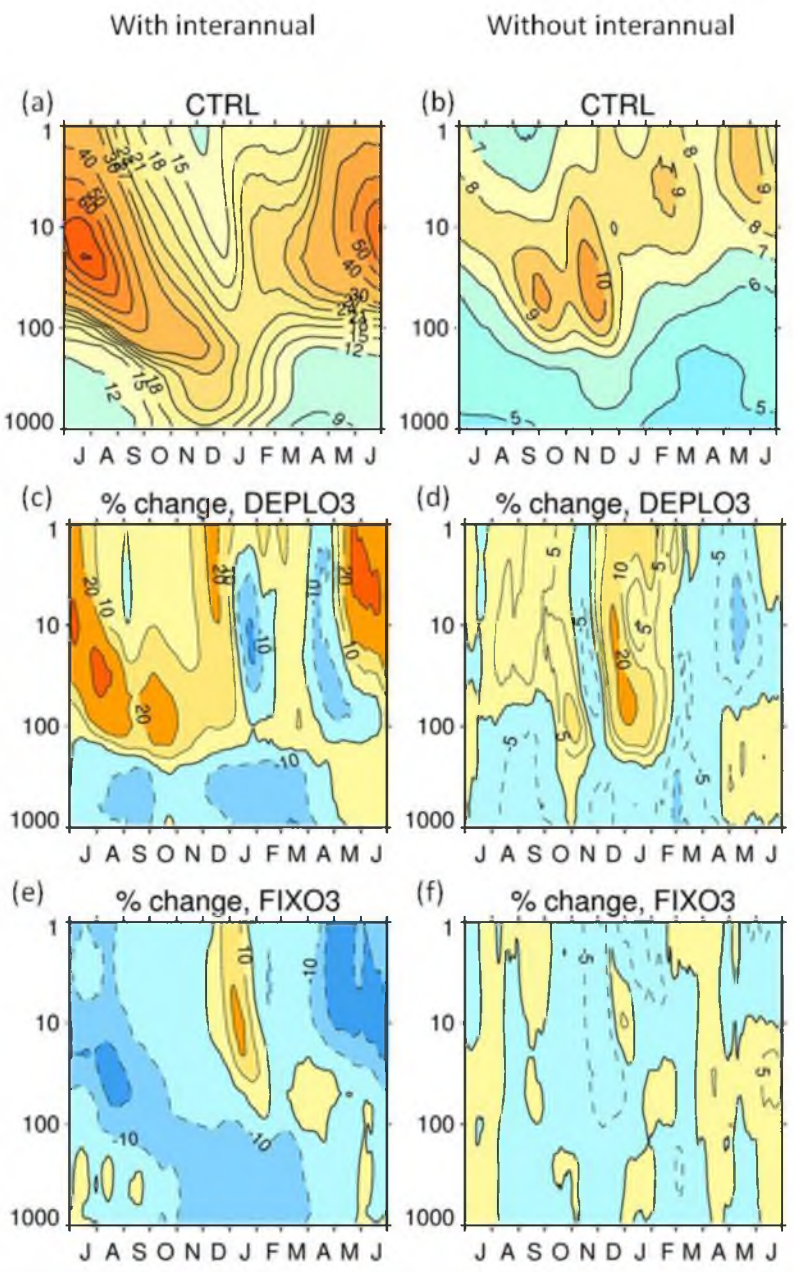

Figure 18 Time scales (days) of the southern annular mode (a) with and (b) without interannual variability. Time scale difference (%) of (c, d) DEPLO3 and (e, f) FIXO3 with respect to CTRL. Differences are calculated in analogy to those in Figure 16. The time scale is given by the time for the auto-correlation function of the SAM index to cross a value of 1/e. Shown are time scales (a, c, e) with interannual variability and (b, d, f) without interannual variability. For time scales with interannual variability, the auto-correlation function is derived from daily AM anomalies that are calculated from simply removing long-term climatological means from the original data. For time scales without interannual variability, we subtract for a given year from the original daily AM data the corresponding seasonal mean from that year. See Keeley *et al.* (2009) for details.

(Gerber *et al.*, 2010).

The times scales including interannual effects derived from DEPLO3 and FIXO3 show roughly opposing patterns: DEPLO3 is characterized by increased (Figure 18c) and FIXO3 by decreased persistence (Figure 18e). The increase in DEPLO3 coincides with a similar increase in variability (Figure 16c, d), and both effects are a likely consequence of the positive ozone feedback between ozone and the circulation. In contrast to DEPLO3, FIXO3 exhibits shorter time scales than CTRL (Figure 18e), ascribed to the lack of such feedback.

SAM persistence after filtering out effects from interannual variability is shown in the right panels of Figure 18. In general, the patterns discussed before when interannual variability is included can also be found here. For example, relatively long persistence generally occurs in the lower to middle stratosphere during austral spring, from where it tends to descend into the troposphere (Figure 18b). The dipole pattern in the lower stratosphere from November to January in DEPLO3 is perhaps again related to the delayed breakdown of the polar vortex (Figure 18d).

2.5.9 Atmospheric variability in CCMVal-2 models

We now extend our analysis and investigate additional model simulations taken from the CCMVal-2 project archive. For each model, we analyze the change in interannual variability of the two annular modes between a simulation with ozone depleted conditions and a simulation that was run under normal (i.e., nondepleted) ozone conditions. The simulation data for normal ozone conditions are derived from the SCN-B2b (aka, fixed ODSs) experiment of CCMVal-2, in which the concentrations of ODSs were held constant at pre-1960 levels and only GHGs and SSTs were allowed to build up (Eyring *et*

al., 2010). The ozone depletion simulations are taken from the REF-B2 experiment, when a significant amount of ODSs is present. Since the only difference between the two experiments is the presence of ODSs, changes in variability between the two experiments are under the assumption of linearity caused by the ozone depletion and its interaction with the dynamics. The REF-B2 experiment includes increasing greenhouse gas (GHG) concentrations and varying amounts of ODSs so that we need to separate their effects from those from ODSs. We thus also show the outcome from SCN-B2c, a sensitivity experiment that was run with fixed GHG concentrations. This allows understanding the effects of GHG increases on circulation variability. For each of the three experiments, we use all available years from 1960 to 2100. For our analysis we only select the five models that were common to all three experiments (Table 1), and only show multimodel means. The CCMVal-2 models and their periods used are summarized in Table 1. Prior to our analysis we remove from all simulation data slowly varying trends related to variations in external forcings. This is accomplished using a low pass Lanczos filter with a 30-year window (Gerber *et al.*, 2010).

Figure 19 shows an interannual variability and its percentage changes in polar cap averaged (60°-90°) interannual geopotential height variability between experiments REF-B2 (ODS and GHGs vary) and SCN-B2b (only GHGs vary). The analysis is very similar to that shown in Figure 16 and 17 before, with the idea that the photochemical feedback under ozone depleted conditions should lead to an increase in variability. The variability structure over the SH (Figure 19c) is quite similar to that of DEPLO3 (Figure 16c), presumably related to the existence of the photochemical feedback. In particular, there is a strong increase in variability from December to January in the stratosphere, which is

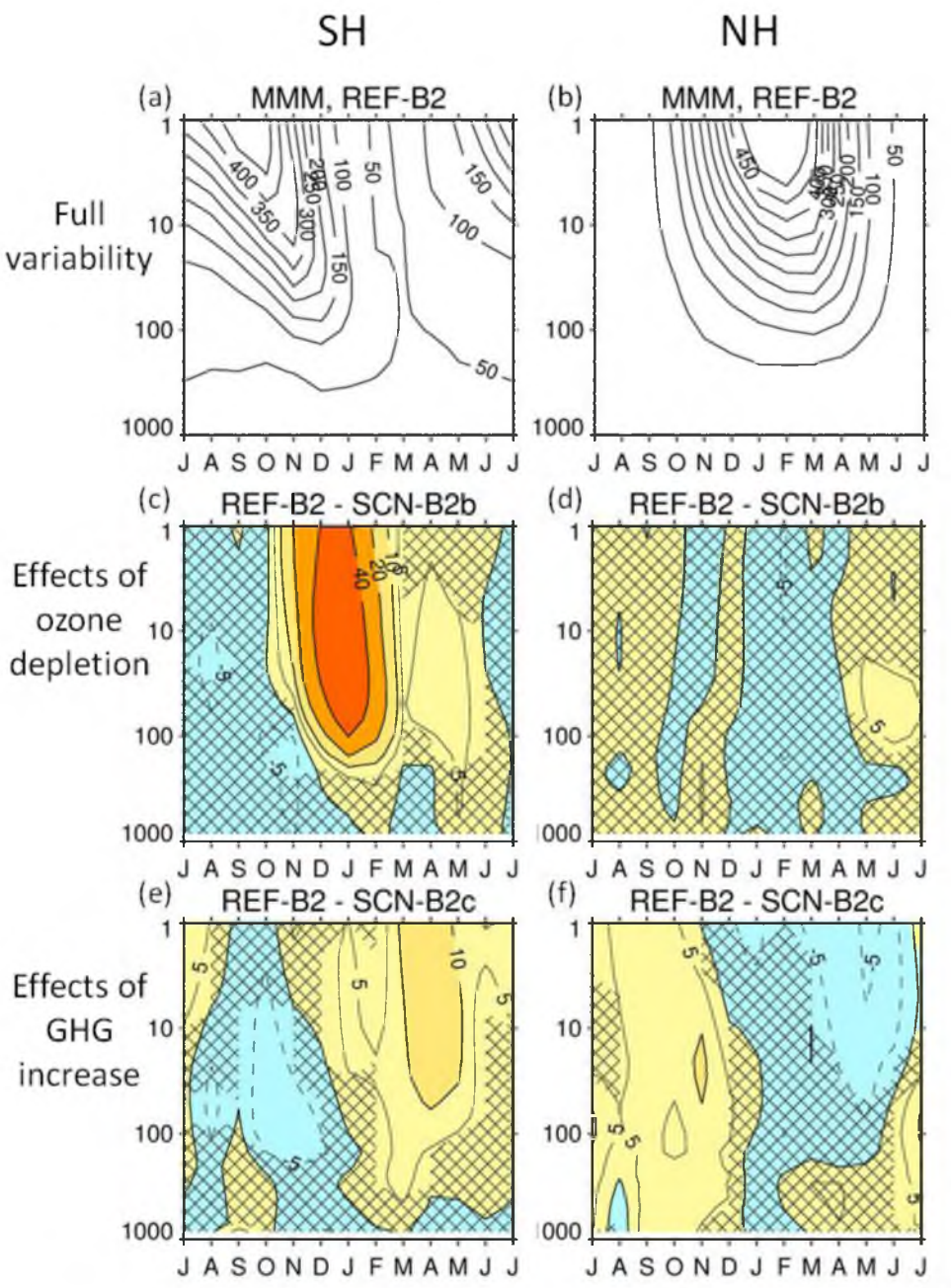

Figure 19 An interannual variability of geopotential height for the (a) SH and (b) NH. (c-f) percent change of the variability of geopotential height (60°-90°) (c, d) between SCN-B2b and REF-B2 and (e, f) between SCN-B2c and REF-B2. The percent change is calculated in analogy to those in Figure 16. All available years from 1960 and 2100 are used. Shown are multimodel means over five selected common models. In order to remove effects of external forcings such as ozone depletions, a time varying climatology of geopotential height fields is first calculated using a low pass Lanczos filter with a 30-year window. This climatology is then subtracted from the geopotential height fields to compute anomalies. See Gerber *et al.* (2010) for details. Hatching shows insignificant (95%) results after F-test.

followed by similar increases in the troposphere. The e and f panels of Figure 19 show the interannual variability change between experiments REF-B2 (ODS and GHGs vary) and SCN-B2c (only ODSs vary), with the idea that the change should be mostly due to increasing GHG concentrations. The increase in GHGs leads to a substantial increase in stratospheric variability during March (Figure 19e). Both ozone depletion and increasing GHG emissions produce an increase in variability, although the variability peak due to GHGs is delayed by a few months with respect to the peak caused by ozone depletion. The combined effect of ozone and GHGs may explain the increase in variability over the SH during these seasons seen in DEPLO3 (Figure 16c).

Over the NH, there is almost no change in stratospheric circulation variability during winter in both ozone depletion (Figure 19b) and GHG increase (Figure 19d) experiments. The variability peak from increasing GHGs in July is not related to the vortex breakdown in spring. During July, there is very little dynamical variability in the stratosphere (Figure 19f) (Gerber *et al.*, 2010; Baldwin *et al.*, 2003b) so that even small absolute changes can result in large percentage changes.

2.5.10 Chemistry vs. nonchemistry models

We also try to detect the hypothesized feedbacks in CMIP5 type of models. This is accomplished by comparing the variability from models that provide simulations that were conducted with a nonchemistry model as well with a chemistry companion version of the same model. Two models provide such simulations. One is MIROC-ESM, and the other is CESM1. These models provide about 500-year control simulations for both model versions (Table 1). As before, Figure 20 illustrates percentage changes of AM variability between the nonchemistry and the chemistry versions. Over the SH, the

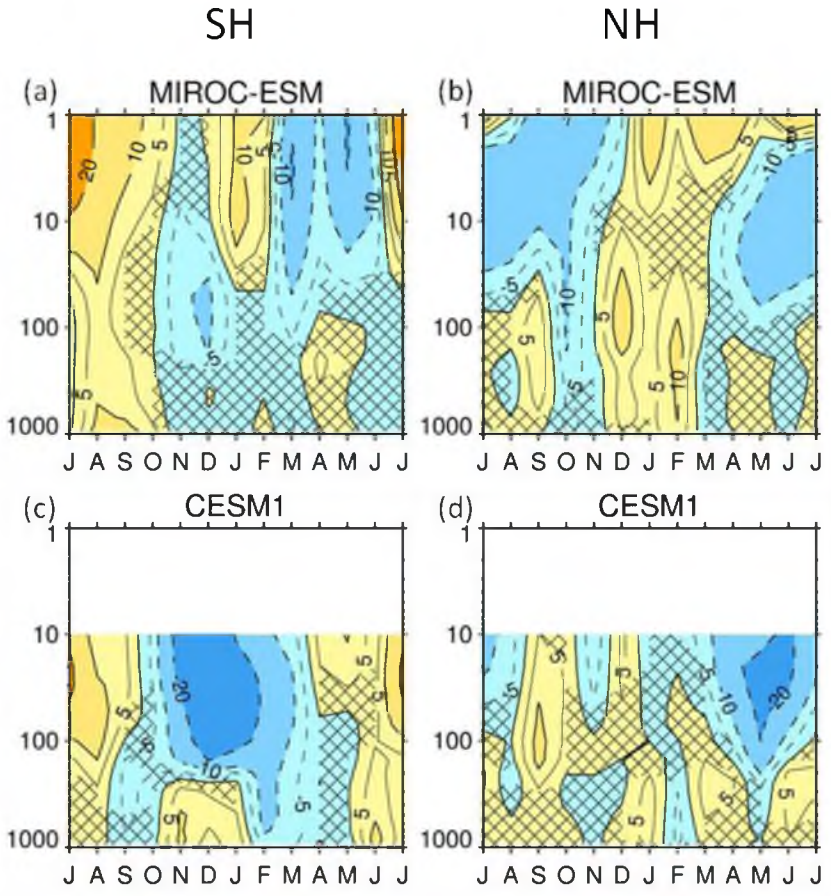

Figure 20 As Figure 19, but between nonchemistry and chemistry simulations for each CMIP5 model. Shown are (a, b) MIROC-ESM and (c, d) CESM1.

nonchemistry models exhibit broad decreases of AM variability in the stratosphere from midspring to summer (Figure 20a, b), consistent with the outcomes from our FIXO3 simulation (Figure 16e). The decrease in variability is probably related to the lack of a positive feedback in the nonchemistry models and the related stable breakdown timing of the polar vortex.

Over the NH, there is a substantial decrease in stratospheric variability from mid-spring to summer (April-August) in nonchemistry models. Such a decrease in variability is also found in our FIXO3 simulation (Figure 17e). The decrease is probably caused by

the lack of positive feedbacks between chemistry and dynamics in nonchemistry models. In particular, during late spring and summer when the NAM variability is weak (Figure 17a), a small change in the circulation will make ozone variable in chemistry models due to the positive feedbacks. Such changes in ozone in turn lead to more variations in the circulation. However, these interacting processes do not happen in nonchemistry models so that variations in the circulation are small.

2.6 Summary and conclusion

The possibility of positive feedbacks between ozone and stratospheric circulation and its influence on the tropospheric variability is investigated. We hypothesize that the chemical ozone loss feeds back into the stratospheric circulation, producing more ozone deficit, as illustrated in Figure 4. The chemically depleted stratospheric ozone during spring leads to the colder stratosphere due to less absorption of solar radiation. The cooling over the polar stratosphere makes a polar vortex stronger by thermal winds. The stronger vortex in turn results in more ozone loss, because the vortex acts to become a barrier of the meridional circulation through the BDC (Shepherd, 2007; Brasseur and Solomon, 2005). At the same time, the stronger vortex also limits the propagation and breaking of tropospheric planetary waves in the stratosphere (Charney and Drazin, 1961; Gerber, 2012), reducing the BDC (Brewer, 1949; Dobson, 1956), transporting less ozone-rich air from low to high latitudes (Holton *et al.*, 1995). The weaker BDC also reduces downwelling and adiabatic warming over the pole, hence further cooling.

In order to verify the existence of positive feedbacks, we examine the reciprocal interaction between changes in Antarctic ozone and changes in stratospheric circulation. The impact of ozone depletion on the circulation, one leg of our hypothesized feedback

(=$\partial T/\partial O_3$), is evident at long-term trends (e.g., Polvani *et al.*, 2011; Son *et al.*, 2008b). The impact of dynamics to chemistry, which is the other leg of the feedback (=$\partial O_3/\partial T$), is also well represented by interannual variations of ozone mainly due to planetary wave activities (e.g., Salby *et al.*, 2012; Salby, 2008; Manzini *et al.*, 2003).

The hypothesized feedbacks are investigated using three designed simulations from the GFDL-CM3, a coupled chemistry-climate model. By giving ozone depletion over the polar stratosphere, we attempt to intensify the suggested feedback loops in Figure 4. The feedback by ozone loss produces an enhancement of the SH stratospheric circulation until the late spring (Figure 6c). The reinforced circulation leads to the variable timing of the vortex breakdown and thus the increase in the stratospheric variability (Figure 16c). In contrast to such simulation of ozone depletion, FIXO3 exhibits no influence of dynamics on the ozone chemistry so that FIXO3 intends to break suggested feedback loops. The simulation has almost the same timing of breakdown of the polar vortex, and it will produce a small stratospheric variability (Figure 16d). Our hypothesis on positive feedbacks is confirmed by coupled chemistry-climate models taken from CCMVal-2 and CMIP5 models. Ozone depletion simulations from these models also illustrate a strong increase in atmospheric variability in the lower stratosphere. However, nonchemistry models exhibit a decrease in variability due to the lack of positive feedbacks.

Hadjinicolaou *et al.* (2002) implied from a simple chemistry model that the Arctic ozone during winter is highly connected with tropospheric variability through northern annular modes. This behavior is also seen over the Antarctic. We find from our designed simulations that midspring ozone depletion strongly affects tropospheric geopotential height with a delay of a few months. It is linked to an influence of stratospheric ozone on

the underlying tropospheric circulation. Son *et al.* (2013) also found from observational data sets that the Antarctic ozone hole has influenced the long-term climate change as well as surface climate.

Our hypothesized positive feedbacks can supplement the feedbacks suggested by Salby (2008) and Manzini *et al.* (2003). They argue that the colder temperature by the weaker meridional circulation leads to more chlorine activation and thus enhanced chemical ozone depletion over the polar stratosphere. In other words, their arguments only describe that chemical ozone depletion increases owing to less dynamical transport of ozone from the tropics to the poles. To complete the positive feedbacks, one needs to connect a loop of chemical ozone loss to the dynamical ozone loss. Such connection is represented by our hypothesized positive feedbacks.

The ozone used in FIXO3 is based on the climatological average from the atmospheric model (AM3). Although the atmospheric model is the same as in the coupled model (CM3) and all other forcings are the same between them, it is unfortunate that ozone between FIXO3 and CTRL is not exactly same. Also, there might be some differences such as lack of an El Nino and southern oscillation (ENSO) cycle and different sampling of the interannual variability from the atmospheric model.

It is important to understand the response of a reciprocal interaction between stratospheric ozone and the circulation to the extratropical variability in both hemispheres. We have suggested a positive feedback between ozone and the circulation. In the presence of such positive feedback, a small external forcing can cause large change in the variability. With understanding of the feedback, we can faithfully predict how variable the atmospheric circulation will be in the future with the expected recovery of ozone.

CHAPTER 3

THE ANNULAR MODE TIME SCALE AND THE ROLE OF THE STRATOSPHERE

3.1 Abstract

The proper simulation of the annular mode (AM) time scale may be regarded as an important benchmark for the ability of climate models. Previous research demonstrated that climate models systematically overestimate the AM time scale, which may imply that the model's climate circulation is overly sensitive to external forcing, as suggested by the fluctuation-dissipation theorem. Previous research has made it clear that the AM time scale converges very slowly, thus necessitating relatively long time simulations. Here we address the problem of stability of the AM time scale and investigate the robustness of a time scale derived from the 50-year historical reanalysis record.

We use a 4000-year control simulation with the GFDL climate model CM2.1 and investigate the AM time scale from individual 50-year segments. We find that some segments exhibit hardly any resemblance to the observations in the simulated time scale, but there are also cases that agree well with the observations. This sampling variability attaches large uncertainty to AM time scales diagnosed from decadal records. Even under the fixed climate forcing conditions of our control run, at least 100 years of data are required in order to keep the uncertainty in the northern AM time scale to 10%; for the

southern AM the required length increases to 200 yrs. If nature's AM time scale is similarly variable, there is no guarantee that the 50-year historical reanalysis record is a fully representative target for model evaluation.

We further investigate whether a relationship can be found between the structure of the AM time scale in the stratosphere and that in the troposphere. For the northern AM time scale, we find that the stratospheric peak leads the tropospheric peak. It takes, on average, about a month for the stratospheric peak to reach the surface, although there is almost no delay (just a few days) from the stratospheric peak to the tropospheric peak in observations. For the southern AM, we find a robust relationship between the magnitude and the seasonal timing of the AM time scale in both the troposphere and the stratosphere, confirming and extending earlier results of a dynamical coupling between the stratosphere and the troposphere and of influences of stratospheric variability on variability in the troposphere.

3.2 Introduction

Intense research on the sensitivity of the Earth's climate system has now continued for decades. Traditionally, climate sensitivity is estimated using data from past observations (Hegerl *et al.*, 2006) or from model simulations (Randall *et al.*, 2007). However, the ranges of climate sensitivity and associated uncertainty have essentially remained unchanged over the past decades (Knutti *et al.*, 2006; Houghton *et al.*, 2001; Randall *et al.*, 2007), mainly because of the lack of reliable observations and uncertainties in the formulation of models. Climate sensitivity is a remarkably important model characteristic because it is almost linearly scaled by many simulated aspects of climate change (Meehl *et al.*, 2007).

Recently, it has been suggested that the persistence time scale of major modes of extratropical variability in the atmosphere, also known as the annular modes (AMs) (Thompson and Wallace, 2001), could provide another measure of climate sensitivity (Gerber *et al.*, 2008b; Ring and Plumb, 2008; Chen and Plumb, 2009). As predicted by the fluctuation-dissipation theorem (Leith, 1975), the equilibrium response to external forcings and thus climate sensitivity should be proportional to the persistence time scale of the AMs. This time scale (hereafter simply AM time scale or tau) is given by the time for the auto-correlation function of the AM index time series to cross a value of 1/e (Gerber *et al.*, 2008b; Baldwin *et al.*, 2003b).

Since the climate response to external forcings should be proportional to the AM time scale, comparing the time scale between simulations and observations could represent a useful alternative for understanding how realistic the climate sensitivity of a model is. Previous studies already investigated the AM time scale from observational (Baldwin *et al.*, 2003b) and modeling (Gerber *et al.*, 2008a; 2008b; Son *et al.*, 2008a) data. Gerber *et al.* (2008a; 2010) found that the AM time scale is systematically overestimated in the intergovernmental panel on climate change (IPCC) 4th assessment report (AR4) and the chemistry-climate model validation activity (CCMVal-2) models, particularly in the Southern Hemisphere (SH). Likewise, the AM time scale seems to be unrealistically long in more simple models (Gerber *et al.*, 2008b).

In order to test the climate sensitivity using the AM time scale, one needs to determine the AM time scale robustly. However, there are several reasons to suspect that the reliable estimation of the AM time scale is not easy. For example, Chan and Plumb (2009) argued that determining the AM time scale in idealized models is interrupted by

irregular and unpredictable regime shifts of the jet stream. Further, Gerber *et al.* (2008b) suggested a quantitative measure of uncertainty in the AM time scale and estimated that about 30 years of data are required to determine a time scale of 25 days at a 10% accuracy. However, their measure is an approximation and does not take into account complicating effects from an annual cycle in the AM time scale. From their uncertainty estimate, about 30 years of the widespread satellite data, which are reliable, may not be long enough to derive robust estimates of AM time scale.

The difficulty in determining tau becomes evident, when we compute tau from the reanalysis during two different 25-year nonoverlapping periods. The tau structure is displayed as a function of season and height in Figure 21. Although the two resulting tau structures are similar, there are also important differences. For example, the results from the first half period suggest that the wintertime peak in tau occurs first in the stratosphere and then in the troposphere, but the second half period shows the opposite behavior. A similar analysis conducted by Baldwin *et al.* (2003b) using the same data but for the longer period 1958-2002 suggests that the stratospheric peak in tau precedes that in the troposphere. Some of the differences seen in the reanalysis might be related to artifacts in observations or trends associated with climate change. However, given the slow convergence of tau, it is also likely that 25 years of observed data are not enough for deriving a reliable estimate of tau.

In the present study we therefore try to answer the question of how many years of data are actually required for a stable estimate of tau, and whether the differences in tau between models and reanalysis seen in previous studies are real or due to sampling uncertainty. We address these questions using a 4000-year control simulation with a

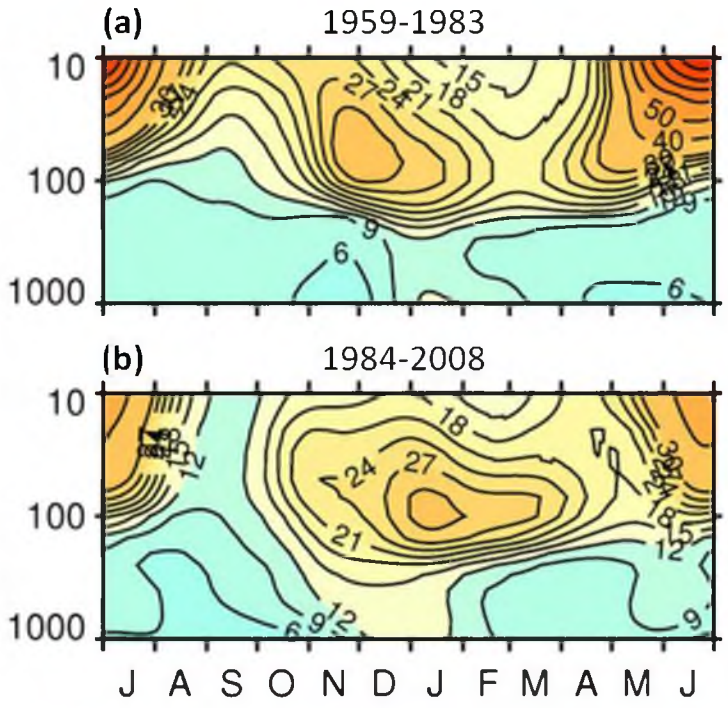

Figure 21 NAM time scale structure (in days) as a function of season and pressure, derived from the first (a, 1959-1983) and last 25 years (b, 1984-2008) of the National Centers for Environmental Prediction/National Center for Atmospheric Research (NCEP/ NCAR) reanalysis data. Contour interval is 3 days up to 30 days, and 10 days thereafter.

coupled climate model, which because of its length allows us to provide useful information about the uncertainty in tau as a function of the length of the underlying data sample. As we will further show, selected examples of tau in simulations show good agreement with the observations, with respect to the magnitude and width of the stratospheric and tropospheric peaks in the winter. We further use this long data set to find out whether there is detectable influence of the stratosphere on the troposphere in terms of tau, as previously suggested by Baldwin *et al.* (2003b). Such a connection helps make tropospheric time scales lengthen, and the long tropospheric time scales have been found in a coupled model (Simpson *et al.*, 2011).

The outline of this paper is as follows. In section 3.3, we present the methods to

calculate the AM time scale along with a detailed description of observations and simulations. Section 3.4.1 compares the AM time scale derived from observations with that from simulations. In section 3.4.2, the uncertainty of the annular mode time scale is investigated and it is shown that the relatively long simulations are important to get a robust time scale. Section 3.4.3 shows both well-performed and poorly performed examples of model derived AM time scale, compared to the observed AM time scale. Section 3.4.4 investigates the connection between the stratosphere and troposphere, and suggests that the stratosphere leads the troposphere in a view of the AM time scale. In section 3.4.5, we look over uncertainty of AM time scale structure as a function of length of underlying index time series. The final section offers a summary and partial interpretation of the results.

3.3 Data and methods

3.3.1 Data

We use daily zonal mean geopotential height fields poleward of 20° from National Centers for Environmental Prediction/National Center for Atmospheric Research (NCEP/ NCAR) reanalysis (Kalnay *et al.*, 1996), which is widely employed in AM studies (Baldwin and Thompson, 2009; Thompson and Wallace, 2000; Baldwin and Dunkerton, 2001; Baldwin *et al.*, 2003b; Gerber *et al.*, 2008a). The calculation of the AM time scale is based on a 50-year period from 1959 to 2008. The reanalysis dataset is available at 17 vertical levels from 1000 hPa to 10 hPa.

For the simulations, we employ an advanced version of coupled climate model CM2.1, developed at the Geophysical Fluid Dynamics Laboratory (Delworth *et al.*, 2006). The resolution of the atmosphere model is 2 degrees latitude by 2.5 degrees longitude

with 24 vertical levels up to 10 hPa. The ocean model is run at a horizontal resolution of 1 degree in the zonal direction and increasing in the meridional direction from 1/3 degree at the equator to 1 degree at the pole. The vertical resolution is 50 levels with 22 levels of 10 m thickness each in the top 220 meters. It is identical to the atmospheric model used for the IPCC AR4. We use the 4000-year equilibrium climate simulations.

3.3.2 Methods

Our procedure to compute the AM exactly follows the method employed by Baldwin and Dunkerton (2001), i.e., the AM is defined as the leading empirical orthogonal function (EOF) of daily geopotential height fields at each pressure level. The AM index is defined as the corresponding principal component time series to the leading EOF. In contrast to Baldwin and Dunkerton (2001), we base our calculations on zonal mean data, not on two-dimensional longitude-latitude fields (Baldwin and Thompson, 2009).

As in previous studies (Gerber *et al.*, 2008a; Baldwin *et al.*, 2003b), the AM time scale is calculated from the decorrelation time of the AM index. The daily index is correlated with itself at lags from 0 to 90 days. However, since the autocorrelation function of the index is far from exponential (Ambaum and Hoskins, 2002) and since the e-folding time scale are only acceptable when the autocorrelation function drops off exponentially, the least-square fit of an exponential curve to the autocorrelation function is used for the calculation of the time scale. In short, the AM time scale is defined as the day when the best-fitted autocorrelation function drops to a value of 1/e. We also make the autocorrelation to vary with season. Gaussian weighting with a full width at half maximum of 60 days is applied to the AM index at each day of year.

The AM time scale from the simulations is calculated by splitting the 4000-year

simulation into several N-year segments (hereafter model segments). In most cases, we use N=50 years, which enables a direct comparison with the observations and which results in 80 individual 50-year segments. We derive the AM time scale individually for each segment and then use the overall mean as our best estimate. The variability of the AM time scale is derived from the standard deviation across all segments.

3.4 Results

3.4.1 Comparison of model time scales with observed time scales

We now compare the AM time scale derived from reanalysis data sets with that from the model, and discuss major similarities and differences between them. This discussion is based on Figure 22, which shows the time scale structure of the northern and southern annular mode (NAM and SAM) derived from the reanalysis and model simulations. We note that the AM time scale calculated from zonal mean fields is very similar to that from two-dimensional fields (see Figure 1 of Baldwin *et al.*, 2003b), which justifies the use of the zonal mean fields. Comparison of model-derived time scales with reanalysis-derived time scales shows that key features of the observations are well captured by the model, including the tropospheric peaks in the boreal winter in the NAM time scale and in the austral spring in the SAM time scale. In the stratosphere, both observation and model exhibit much longer time scales than in the troposphere. The NAM time scale exhibits distinct maxima at 10 hPa in summer and at 100 hPa in winter, whereas for the SAM the time scale is always large throughout the year.

The AM time scales from simulations also exhibit important differences from reanalysis-derived time scales. First, the seasonal cycle in the troposphere is much broader in the model compared to the reanalysis, which is a possible deficiency that

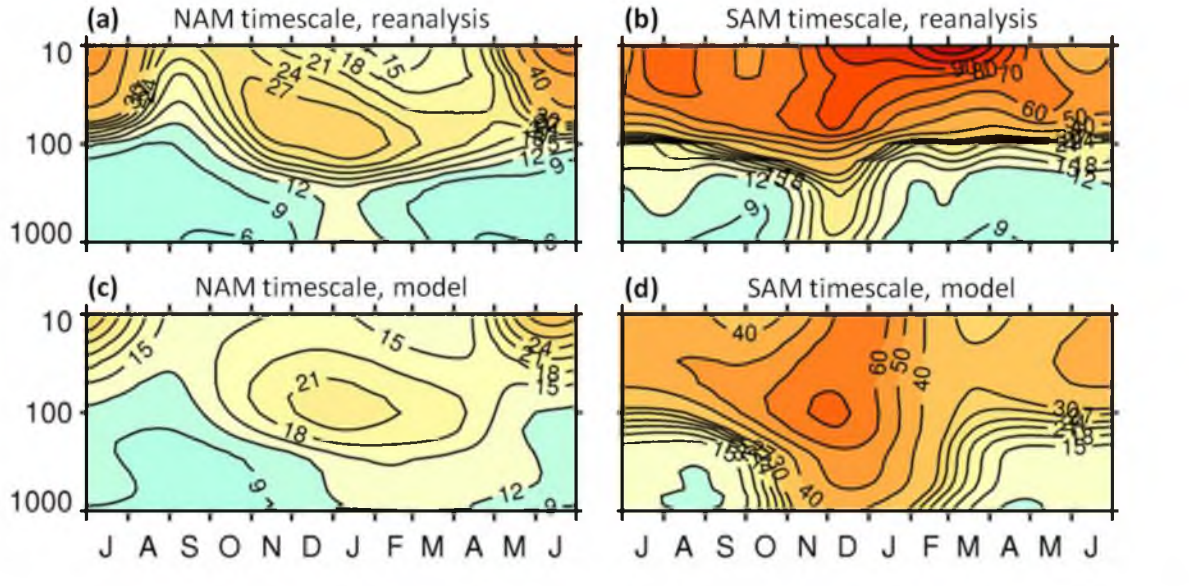

Figure 22 NAM and SAM time scale structure (in days) as a function of season and pressure. Results are shown for (a, b) NCEP/NCAR reanalysis (1959-2008) and (c, d) model (mean over 80 50-year model segments). The time scale at 1000 hPa is derived from zonal mean sea level pressure. For all other levels, zonal mean geopotential heights are used. Contour interval is 3 days up to 30 days, and 10 days thereafter.

appears to be common to most models (Gerber *et al.*, 2008a). Second, the tropospheric peak of the NAM time scale in the models occurs in mid-February, which is about 1 to 2 months delayed with respect to reanalysis. Third, the model generally underestimates the stratospheric AM time scale over both hemispheres as compared to the reanalysis, whereas it overestimates the tropospheric time scale, particularly in the Southern Hemisphere. Since there is a linear relationship between the AM time scale and the climate sensitivity as predicted by the fluctuation-dissipation theorem, the stratospheric (tropospheric) climate sensitivity in the model is expected to be small (large) with the short (long) annular mode time scale. Lastly, the model's SAM time scale exhibits a pronounced minimum in the stratosphere from March to April, whereas the reanalysis shows a maximum time scale in these months.

3.4.2 Uncertainty of the AM time scale

We next examine how variable the AM time scale is. We use 50-year segments from the model to calculate the AM time scale. The standard deviation of the AM time scales among 80 segments, which is a measure of AM time scale variability, is shown in the top panels of Figure 23. The variability structure of the NAM time scale displays distinct maxima at 100 hPa in the early winter and at 10 hPa in the summer, which closely resembles the mean structure of the NAM time scale. In the lower stratosphere and troposphere, the large variability of NAM time scale persists up to the spring. However, the variability of the SAM time scale exhibits even larger maxima than the NAM in the stratosphere due to the large magnitude of time scale itself. In the lower stratosphere and troposphere, the time scales are the most variable in the late spring and early summer.

The large variability of the NAM time scale in the lower stratosphere in the winter may result from the existence of stratospheric sudden warmings (SSWs). The SSWs are a complete breakdown of the polar vortex, which leads to the long AM time scale in the lower stratosphere (Simpson *et al.*, 2011; Baldwin *et al.*, 2003b). The SSWs occur during the different times of the winter from November to March among 80 model segments, and this is associated with the large variability of the AM time scale there. On the other hand, there are no SSWs in the Southern Hemisphere in the middle of winter, but there exists the breakdown of the polar vortex in late spring. The lack of the SSWs can explain the large magnitude of SAM time scale shown in Figure 22d. Moreover, slightly different timing of the breakdown of the polar vortex leads to the large variability of the AM time scale. Note that while the effect of stratospheric variability is limited to late spring and early summer in the Southern Hemisphere, it can happen throughout the winter-spring

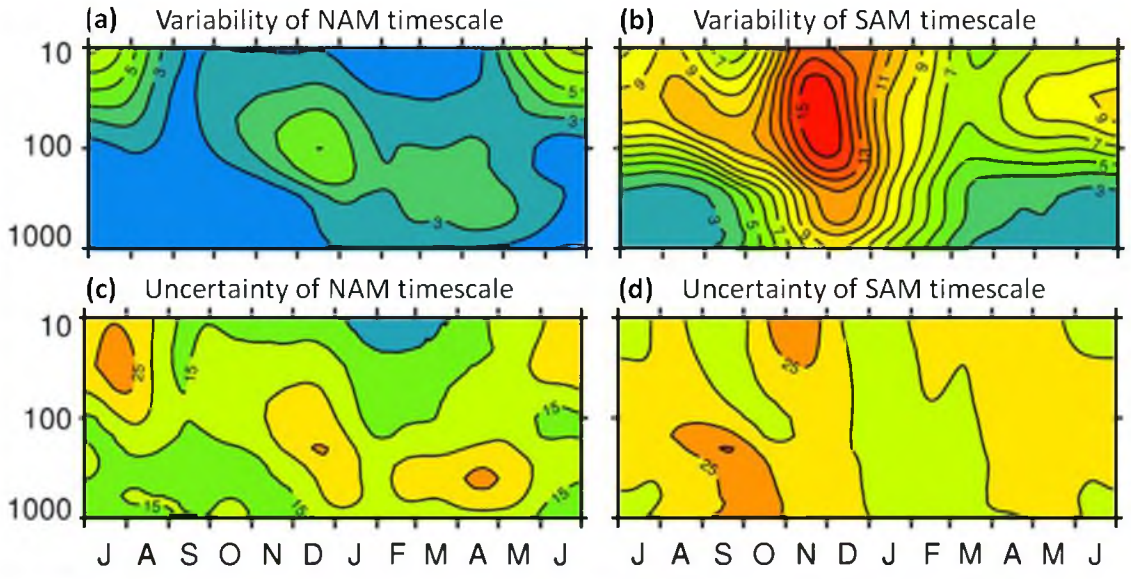

Figure 23 Variability and uncertainty of model derived time scales. Shown are (a, b) standard deviation of NAM and SAM time scale (in days), derived from 80 samples of 50-year segments and (c, d) uncertainty of timescale (in %), given by the standard deviation of time scale divided by the mean time scale.

season in the Northern Hemisphere, with the seasonality of peak time scales showing considerable variability among individual 50-year selections of the same simulation (Simpson *et al.*, 2011).

The uncertainty of the AM time scale in the present study is measured by the ratio of the standard deviation to the mean of AM time scale, which is an inverse form of a signal-to-noise ratio. It is expressed as a percentage, after being multiplied by 100%, as shown in c and d panels of Figure 23. This ratio is useful because the variability of AM time scale could be understood in the context of the mean of AM time scale. The uncertainty exceeds 10% in most cases, even 20% in some cases. We note that the uncertainty structure of the NAM time scale closely resembles the variability structure of the NAM time scale, whereas SAM does not show this behavior.

One may ask whether or not the large variability can explain some of the differences in tau between the model and reanalysis as seen in Figure 22. We note for example that the location of maximum stratospheric low-frequency variability in the simulations coincides with the location of maximum AM time scale in the observations. Indeed, selected examples of simulated time scale derived from individual segments (top panels of Figure 24) show better agreement with the observations than the mean time scale derived from all segments. This is particularly true with respect to the magnitude and width of the stratospheric and tropospheric peaks. However, some examples from the coupled model hardly capture the observed seasonal cycle of the NAM time scale; some show different phasing of peaks, multiple peaks, too broad peaks, or no peaks at all (Figure 24c). Moreover, the overall differences in SAM time scale between simulations and observations are almost everywhere large both in the stratosphere and in the troposphere (Figure 24d).

3.4.3 How realistic are model-derived AM time scales?

We now investigate the similarity of tau structure between model segments and reanalysis. Figure 25a and 25b illustrates the scatter plot of root-mean-square errors (RMSEs) of tau structure in the stratosphere and troposphere. We use the tau structure over 200-30 hPa levels for stratospheric RMSE calculations, and 1000-500 hPa for troposphere. Here, we use 8 months from September to April for NAM time scales, because they exhibit artificially large time scales in the stratosphere during the summer when the annular mode is not active (Gerber *et al.*, 2010). We find that the NAM RMSEs do not show any connection between stratosphere and troposphere (r=-0.01). However, enhanced SAM RMSEs in the stratosphere are associated with large RMSEs in the

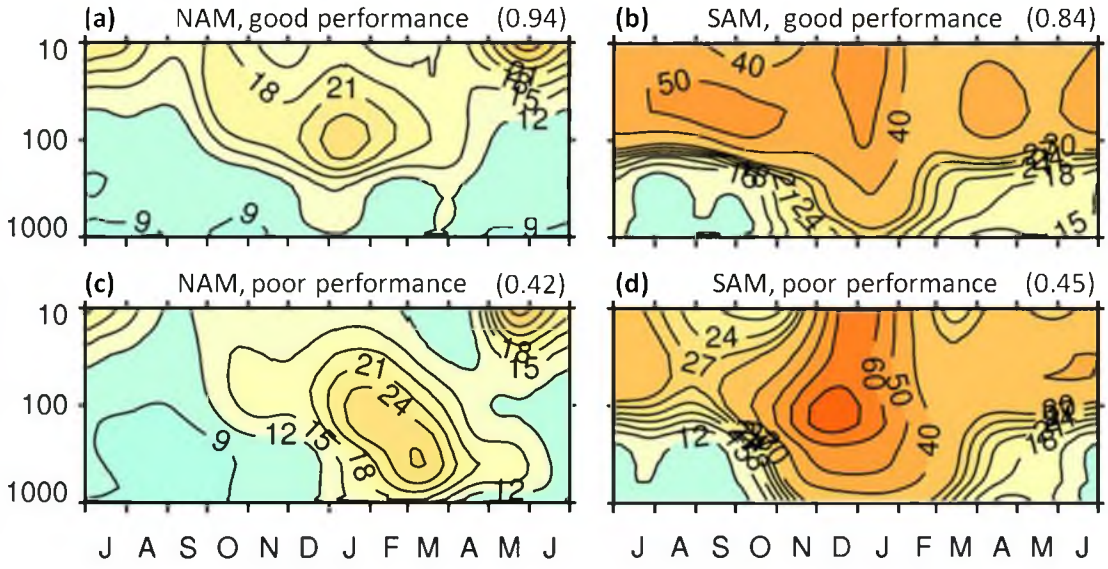

Figure 24 Time scale structure computed from selected 50-year segments. The panels a, b are examples in reasonably good agreement with the NCEP/NCAR reanalysis, whereas the panels c, d examples show poor agreement with the reanalysis. Numbers on top right of each panel indicate the correlation coefficient between time scale from NCEP/NCAR reanalysis (1959-2008) and time scale from model segments.

troposphere (r=0.65). This is even clearer in the shape of the ellipse, which represents the range of four standard deviations of the samples. In addition to separated stratospheric and tropospheric RMSEs, we display correlation coefficients calculated over all levels from 1000 to 10 hPa throughout all seasons with colors. The large variation of the correlation coefficients in the NAM time scale indicates that some model segments show good agreement with the reanalysis. On the other hand, the dominant bluish colors in correlations of SAM time scale indicate that models are not successful in reproducing the observed SAM time scale structure.

The large variation of the distribution in the NAM time scales seems to arise from the different peak timing of time scales. In the NH, the occurrence of the polar vortex in the lower stratosphere is variable due to SSWs, which involve a complete breakdown of

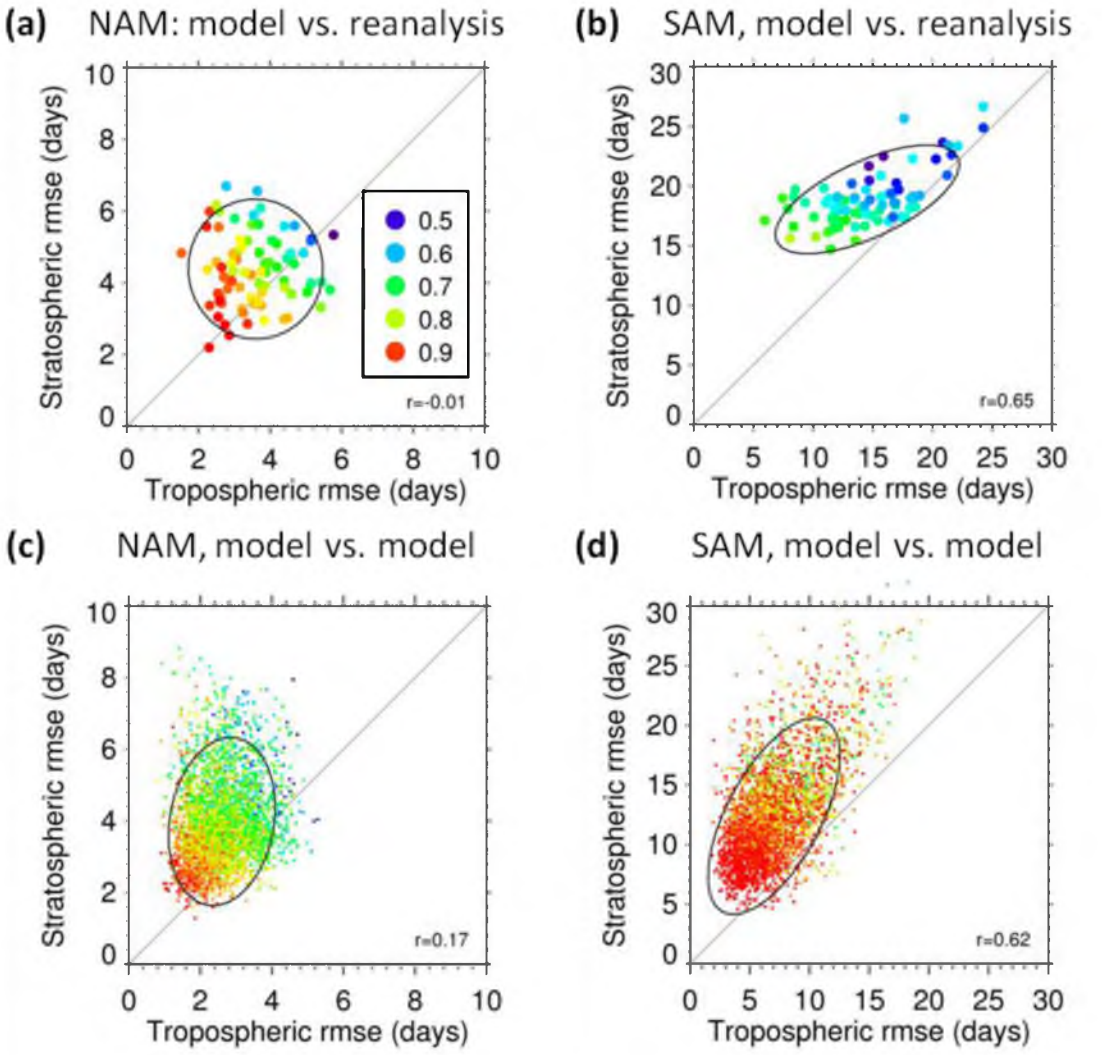

Figure 25 Relationship between tropospheric (1000-500 hPa, September-April) and stratospheric (200-30 hPa, September-April) time scale structure. (a, b) Root-mean-square errors between 80 model segments and reanalysis. (c, d) Root-mean-square errors between all paired combinations of 80 model segments. Color denotes correlations calculated over all levels (1000-10 hPa, Jan-Dec). Ellipses are centered on the mean, oriented along the direction of maximum scatter, with the two axes showing four standard deviations along the major and minor direction. Lines represent the diagonal where tropospheric and stratospheric correlations match. Numbers at the left bottom are correlations between stratospheric and tropospheric scatters.

the polar vortex, and finally leads the long AM time scale (Simpson *et al.*, 2011). This long AM time scale propagates downward at any time of the winter because the SSW events can happen broadly from November to March. Thus, the different peak timing of the AM time scale leads to the large variations in the time scale. In contrast, the SH vortex in the lower stratosphere is too steady in the early winter due to the lack of wave activity, and tends to remain variable too late; that is reflected in the general lack of breakdown of the polar vortex in the early winter in the model.

The different characteristics of the tau structure between stratosphere and troposphere are even clearer in scattered patterns among model segments. The bottom panels in Figure 25 show the stratospheric and tropospheric RMSEs of the AM time scales among model segments, which are composed of 3160 (=80x79÷2) combinations. The RMSEs of the tau structure in the stratosphere are more variable than in the troposphere, and this is also clear in the shape of the ellipse. The large variation appears to come from different timings of the breakdown of the polar vortex in the stratosphere among model segments as discussed before. We also find that NAM RMSEs exhibit a wide distribution of the correlation coefficients (from 0.5 to 1), indicating that the tau structure of the NAM time scales are variable among model segments due to mainly different timings of SSWs in the winter and spring. However, the tau structure in the SAM is close to each other ($r > 0.9$) because of the late breakdown of the polar vortex.

3.4.4 Linkages between stratosphere and troposphere

As seen before (Figure 22), both NAM and SAM time scales exhibit a distinct seasonal structure. Tropospheric peaks in τ are accompanied by coincident peaks in the lower stratosphere. From finding this agreement also in the reanalyses, Baldwin *et al.*

(2003) argued that the long tropospheric time scale could be influenced by persistent anomalies in the lower stratosphere.

Here, we further investigate this issue by examining the temporal relationship between the lower tropospheric and lower stratospheric peaks in τ. For multiple 50-year simulation segments we determine the date and the strength of maximum τ in both the lower troposphere and the lower stratosphere. Lower tropospheric and stratospheric maxima are defined as the longest time scale from 1000 to 500 hPa and from 200 to 30 hPa through the year, respectively. The selection of these levels is related to the mean τ structure for the two modes (Figure 22), and our results are not sensitive to the specific choice of these vertical limits.

We first focus on the result for the NAM time scales. Figure 26a and 26b compare the stratospheric and tropospheric values for the date and the strength of maximum τ, which are individually derived from all 80 segments. Both stratospheric and tropospheric peak dates mostly range between November and March (Figure 26a). The ellipses indicate the four standard deviation limits in the directions of maximum scatter. As shown by the orientation of the ellipses, the dates of the tropospheric peaks are weakly correlated with the dates of the stratospheric peaks. Their correlation coefficient is 0.19. Also, most scatter symbols are located above the dotted line, indicating that the troposphere usually lags the stratosphere. By taking the mean peak dates over all segments (filled symbols in the center of the ellipses), we find a lag of several weeks between the stratosphere and the troposphere. Interestingly, this time scale is similar in length to the time it takes for dynamical anomalies to propagate downward from the stratosphere into the troposphere, a phenomenon that has been extensively described in

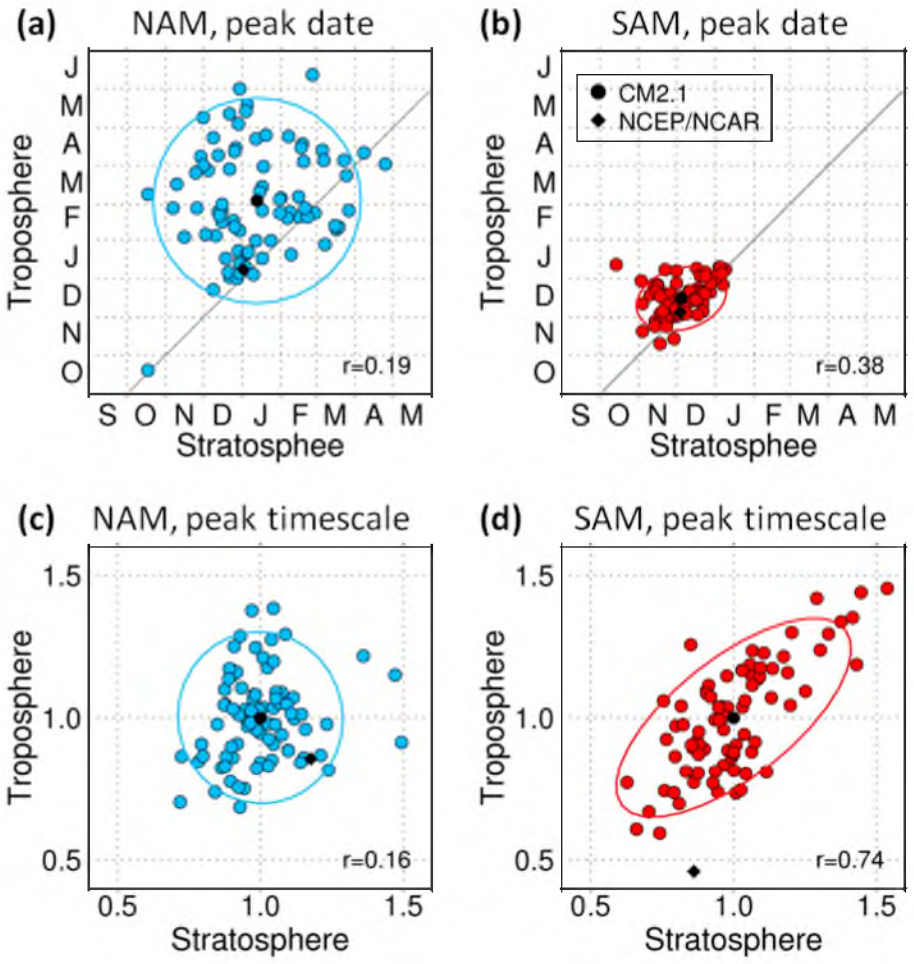

Figure 26 Relationship between stratospheric and tropospheric time scale maxima derived from 80 model segments. (a-b) Date of lower stratospheric (200-30 hPa) and lower tropospheric (1000-500 hPa) time scale maxima. (c-d) Relative strength of time scale maxima, given by the ratio of time scale maxima and the mean of all maxima (23 days for stratospheric NAM, 15 for tropospheric NAM, 71 for stratospheric SAM, and 47 for tropospheric SAM). Colored circles show outcomes from individual model segments and black circles indicate the mean. Ellipses are centered on the mean, oriented along the direction of maximum scatter, with the two axes showing four standard deviations along the major and minor direction. Numbers at the right bottom are correlations between stratospheric and tropospheric scatters. Black diamonds show outcomes from NCEP/NCAR reanalysis (1959-2008). Lines in panels a, b represent matching stratospheric and tropospheric date.

previous literatures (Baldwin and Dunkerton, 2001; Christiansen, 2001). Examining the strength of maximum τ (Figure 26c), we also find a weak connection between the stratosphere and the troposphere (r=0.16). In contrast to the simulations, the reanalyses (black triangles) exhibit about a week delay from the stratosphere into the troposphere, and the peak date occurs about 1 month earlier.

For the SAM, the peak dates (Figure 26b) are centered at late November in the stratosphere and at December in the troposphere. Comparing to the NAM peaks and taking into account the seasonal shift of 6 months between the two hemispheres, these dates are shifted early by about by 1-2 months, an issue that has also been noted by Gerber *et al.* (2008a). Similarly to the NAM, the stratospheric peak mostly leads the tropospheric peak, but narrowly ranges in the 2 months from November to December. Here, the stratospheric peak timing is significantly correlated to the tropospheric peak, (r=0.38). The narrow range and the weak correlation between the stratospheric and tropospheric peak timings in the SH may result from limiting eddy-mean flow feedback due to the nonexistence of topography there (Thompson *et al.*, 2005). Also, the maximum τ for the SAM exhibits much stronger and broader scatters than the NAM maximum, but shows a significant correlation between the stratospheric and tropospheric peak (r = 0.74).

3.4.5 Uncertainty estimates

From the large uncertainties seen in Figure 23 it is clear that the 50-year observation period from the reanalysis is likely to be too short to derive a robust estimate for τ. Since our simulations are much longer, we can use them to derive an empirical relationship between uncertainty and length of the simulation period. In this case, one has to keep in mind that the overall simulation period is limited to 4000 years, which means that the

number of individual segments decreases with increasing length of the simulation period per segment.

For an increasing number of years per segment (L) and for the coupled models, we calculate the τ uncertainties and investigate its distribution over all vertical levels and days of the year (Figure 27). For L=10 years, the uncertainties are very large and range from 30-50%. As expected, the uncertainty and its range become smaller as L increases. For example, for the both NAM and SAM time scales one can see that L must be at least 200 years if the tolerable uncertainty is 10%. Further, the curves in Figure 27 show that the uncertainty in time scales is approximately $L^{-1/2}$, which makes sense if one assumes that calculating τ over increasing L is equivalent with taking the mean τ from multiple (=L/10) 10-year segments.

Figure 27 also indicates that the SAM uncertainty is larger than the NAM uncertainty. From knowing that the SAM time scale is longer than the NAM time scale (Figure 22), this result is consistent with the findings by Gerber *et al.* (2008b). Their independent analysis suggests that the absolute τ uncertainty increases as the magnitude of τ increases.

3.5 Summary and discussion

In this study we examine and compare the AM time scale in the general circulation model and NCEP/NCAR reanalysis. The simulation exhibits important differences with respect to the observation. The seasonal cycle of the AM time scale in the troposphere is much broader in the models in comparison with the reanalysis, a possible deficiency that seems to be common to most IPCC AR4 models (Gerber *et al.*, 2008a) and the CCMVal-2 models (Gerber *et al.*, 2010). In spite of these differences, our model simulations suggest that the timing of tropospheric peaks in observations is well captured.

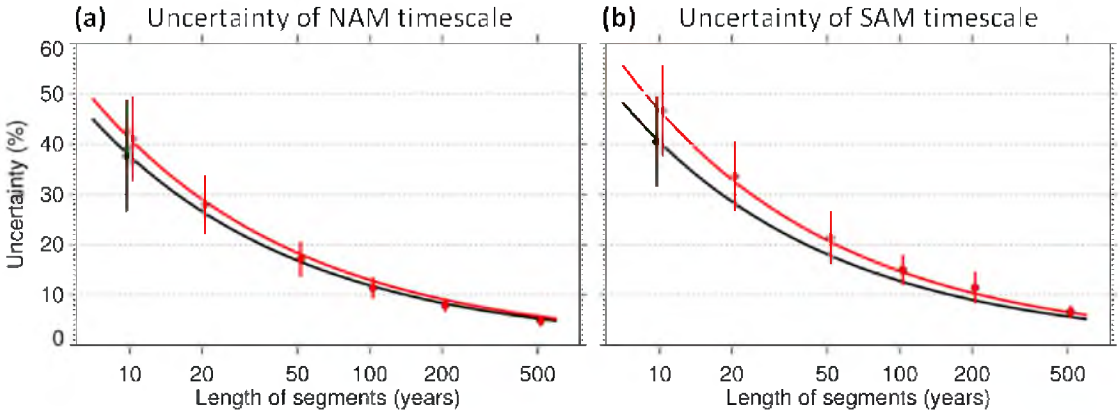

Figure 27 Uncertainty of (a) NAM and (b) SAM time scale structure as a function of length of underlying index time series for (black) NCEP/NCAR reanalysis and (red) coupled model. Uncertainty is defined as in Figure 23. Circles are actual values (slightly shifted along the x-axis for clarity), and lines represent extrapolations using the analytical expression (inversely proportional to the square root of the length of the segment, see text) and the calculated result for 10 years as initial value. Error bars denote 95% confidence intervals, calculated from bootstrapping by randomly selecting 5 samples with replacement and repeating this 100 times.

One issue of concern is that the τ uncertainty is significantly large when short years of integration are used. Our result agrees with Gerber *et al.* (2008b), who found that model integration of 2000-3000 days are sufficient to estimate time scale in the range of plus and minus 20% accuracy. For more robustness in the time scale itself, it appears to be better to use more years of integration. For both NAM and SAM time scales, one can see that years of integration must be at least 200 years if the 10% of the τ uncertainty is tolerable. In particular, the SAM uncertainty is larger than the NAM uncertainty. This result agrees with Gerber *et al.* (2008b), who suggest that the τ uncertainty increases as the magnitude of τ increases, because the SAM time scale is longer than the NAM time scale. Thus, if nature's AM time scale is similarly variable, the 50-year historical reanalysis record cannot be long enough to evaluate climate models.

There has also been recent discussion in the literature about the tropospheric

circulation response to the stratosphere (Sigmond *et al.*, 2008; Scaife *et al.*, 2005). A previous modeling study has established that the effect of stratospheric variability in lengthening tropospheric annular mode time scales is evident in both hemispheres (Simpson *et al.*, 2011). From our simulations, we investigate the possible connection of peaks in τ in the lower stratosphere and in the troposphere. For the NAM time scale, we find that the stratospheric peak leads the tropospheric peak. It takes, on average, about a month for the stratospheric peak to reach the surface, although there is almost no delay (just a few days) from the stratospheric peak to the tropospheric peak in observations. For the SAM time scale, the tropospheric peak date and strength are clearly followed by the stratospheric peaks.

CHAPTER 4

A STRATOSPHERIC CONNECTION TO ATLANTIC CLIMATE VARIABILITY

4.1 Abstract

The stratosphere is connected to tropospheric weather and climate. In particular, extreme stratospheric circulation events are known to exert a dynamical feedback on the troposphere. However, it is unclear whether the state of the stratosphere also affects the ocean and its circulation. A covariability of decadal stratospheric flow variations and conditions in the North Atlantic Ocean has been suggested, but such findings are based on short simulations with only one climate model. Here, we assess ocean reanalysis data and find that, over the previous 30 years, the stratosphere and the Atlantic thermohaline circulation experienced low-frequency variations that were similar to each other. Using climate models, we demonstrate that this similarity is consistent with the hypothesis that variations in the sequence of stratospheric circulation anomalies, combined with the persistence of individual anomalies, significantly affect the North Atlantic Ocean. Our analyses identify a previously unknown source for decadal climate variability and suggest that simulations of deep layers of the atmosphere and the ocean are needed for realistic predictions of climate.

4.2 Introduction

The ocean has a large thermal inertia and is dominated by variability on time scales of years to decades. Traditionally, atmospheric influences on the ocean are understood from the stochastic climate model paradigm, in which the troposphere is thought to provide a white-noise forcing that is integrated by the ocean to yield a low-frequency response (Hasselmann, 1976). In this study we propose another relevant influence, which is related to the stratosphere. The stratosphere is characterized by persistent flow dynamics (Baldwin *et al.*, 2003b) and considerable multidecadal energy (Cohen *et al.*, 2009; Gillett *et al.*, 2002; Butchart *et al.*, 2000). Variations in the strength of the wintertime northern hemispheric stratospheric vortex, so called 'polar vortex events,' are known to last for many weeks, as does their impact on the troposphere (Baldwin and Dunkerton, 2001). An example is stratospheric sudden warmings (SSWs), prolonged time periods with an unusually weak and warm polar vortex. SSWs occur on average every second year, but observations over the past 30 years reveal an intriguing quasidecadal rhythm in the year-to-year occurrence of such events: during the 1990s, the Arctic winter stratosphere was characterized by an almost complete absence of SSWs, but during the 1980s and also during the 2000s the stratosphere experienced a record number of such events (Figure 28a).

A connection between the stratosphere and the ocean can be established by the North Atlantic Oscillation (NAO), a large-scale pattern of near-surface circulation anomalies over the North Atlantic. Polar vortex events modulate the NAO polarity, with a strong vortex leading to a positive and a weak vortex to a negative NAO (Baldwin and Dunkerton, 2001). NAO variations in turn are linked to circulation variability in the

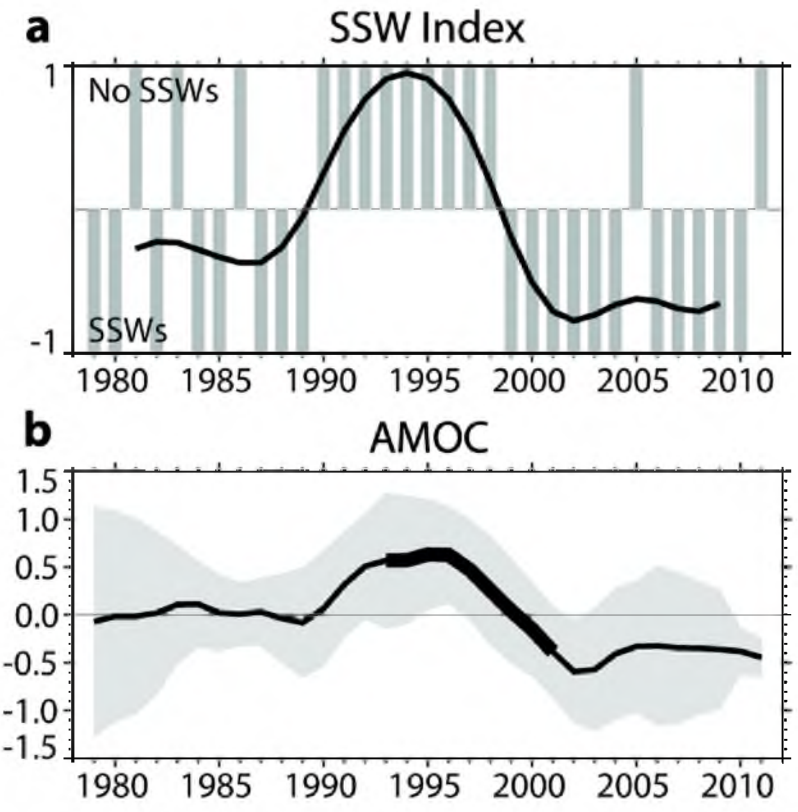

Figure 28 Observed stratospheric flow variations and their relationship to AMOC. (a) Annual time series of the SSW index; grey bars mark years with (−1) and without (1) major SSWs; the black line is a smoothed version of this. (b) Multireanalysis estimate of annual mean AMOC variations at 45° N; thick black line denotes the common period for all 12 reanalyses and grey shading is the $\pm 1\sigma$ uncertainty interval.

North Atlantic. The NAO induces anomalous fluxes of heat, momentum, and freshwater at the air–sea interface, driving or perhaps enhancing intrinsic variability in the North Atlantic gyre system (Hakkinen and Rhines, 2004) and the Atlantic Meridional Overturning Circulation (AMOC) (Delworth and Greatbatch, 2000; Eden and Jung, 2001). Thus, variations in the strength of the polar vortex and their projection on the NAO might influence the North Atlantic circulation. This is supported by a reconstruction of past AMOC variations using 12 different ocean reanalyses, revealing a similarity between variations in the AMOC (Figure 28b) and the frequency of SSWs (Figure 28a).

4.3 Data and methods

4.3.1 Data

4.3.1.1 Observations

The NCEP/NCAR reanalysis (1958–2011) are used as observations of geopotential height, surface fluxes and SSTs.

4.3.1.2 GFDL-CM2.1

The main model of this study is the Geophysical Fluid Dynamics Laboratory climate model GFDL-CM2.1. It has a horizontal resolution of 2 degrees latitude by 2.5 degrees longitude, and 24 vertical levels concentrated in the troposphere, leading to a relatively poorly resolved stratosphere. The model produces realistic simulations of tropospheric climate (Reichler and Kim, 2008) and self-sustained AMOC oscillations with a central period of ~ 20 years (Figure 29). Such oscillations may be connected to the Atlantic multidecadal oscillation (AMO) (Delworth and Mann, 2000), a pattern of North Atlantic SST variations with a period of 60–80 years (Schlesinger and Ramankutty, 1994). The fact that the period of the observed AMO is longer than the period of the simulated AMOC is not surprising given the many simplifying physics in climate models and the uncertainty in observing the AMO.

Figure 29 presents for GFDL-CM2.1 (panel a) an arbitrarily chosen 200-year AMOC time series and (panel b) the spectrum of the AMOC from using the full 4000 years of data. The spectrum from GFDL-CM2.1 exhibits a pronounced ~20 year peak, which can be compared against (panel c) the CMIP5 multimodel spectrum, derived from the standardized and concatenated AMOC time series of all 18 CMIP5 models, leading to 12944 years worth of simulation data. The AMOC spectrum in the CMIP5 models as a

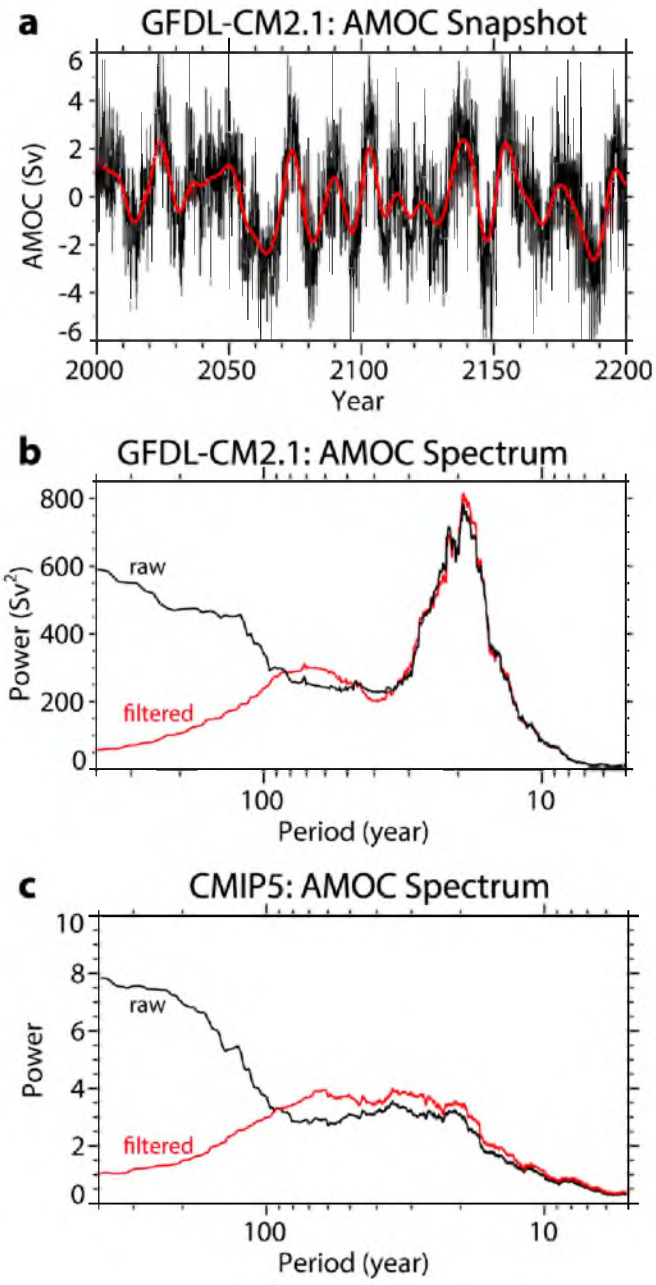

Figure 29 Model simulated AMOC. (a) 200-year snapshot of GFDL-CM2.1 AMOC time series. Black curve shows monthly values and red curve low-pass filtered version. The standard deviation of the 4000 yr long low-pass filtered time series (red curve) is 1.3 Sv. (b) Power spectra of monthly GFDL-CM2.1 AMOC time series. Black is for raw data and red is after removing slowly varying trend. (c) as (b), but for the 18 member CMIP5 multimodel ensemble, using a standardized and concatenated AMOC time series.

whole has no preferred peak; instead, power varies broadly between ca. 20-100 years. Note that the units of power in Figure 29b and 29c are different because of the standardization. Also note that the filtering effectively removes spurious slowly varying trends at periods of more than 100 years, which can be found in most models.

4.3.1.3 CMIP5

CMIP5 data are based on monthly means from the preindustrial control experiment. We consider models that provide at least 500 years of data and the quantities needed for our analysis. This leads to 18 models with a total of 12944 years of simulation data. Table 4 lists the CMIP5 model simulations that are used for the analysis. We perform analysis on the concatenated NAM and AMOC time series from models belonging to either the high-top or the low-top group; time series from each model are standardized before concatenation.

4.3.2 Statistics

4.3.2.1 Statistical analysis

In all our analysis we take the same nonparametric approach to establish statistical significance at the two-sided 95% level. In this approach, we randomly subsample elements from the entire population and take averages. The number of elements selected equals the number included in the quantity to be tested. We repeat this procedure 10000 times, leading to a distribution of outcomes that is the result of pure chance. The upper and lower 2.5 percentiles of this distribution are our empirically determined confidence limits.

Table 4 CMIP5 models and simulation lengths.

Model	Modeling group	Years
BCC-CSM1.1	Beijing Climate Center, China Meteo. Admin.	500
CANESM2	Canadian Centre for Climate Modeling and Analysis	996
CCSM4	National Center for Atmospheric Research, USA	501
CNRM-CM5	CNRM CERFACS, France	850
GFDL-CM3	NOAA GFDL, USA	500
GFDL-ESM2G	NOAA GFDL, USA	500
GFDL-ESM2M	NOAA GFDL, USA	500
GISS-E2-H	NASA GISS, USA	531
GISS-E2-R	NASA GISS, USA	1163
HADGEM2-ES	Met Office Hadley Centre, Great Britain	576
INMCM4	Institute for Numerical Mathematics, Russia	500
IPSL-CM5A-LR	Institute Pierre-Simon Laplace, France	1000
MIROC5	JAMSTEC, Univ. of Tokyo, and National Institute for Environmental Studies, Japan	670
MPI-ESM-LR	Max Planck Institute for Meteorology, Germany	1000
MPI-ESM-MR	Max Planck Institute for Meteorology, Germany	1000
MPI-ESM-P	Max Planck Institute for Meteorology, Germany	1156
MRI-CGCM3	Meteorological Research Institute, Japan	500
NORESM1-M	Norwegian Climate Centre, Norway	501

4.3.2.2 Event selection

The events selected for the composites are based on the dates on which the smoothed annual November–March means of the NAM at 10 hPa (Gaussian filter, σ~2 years) exceed a value of ±1; selected events are separated by at least 30 years.

4.3.2.3 Detrending

To account for long-term trends we first remove from all quantities a low-pass filtered (101-year running means) version of the data. Daily atmospheric quantities are filtered by removing a slowly varying trend climatology, following a procedure that accounts for seasonality of trends (Gerber *et al.*, 2010), except that a running mean filter of 101 years is applied.

4.3.3 Climate indices

4.3.3.1 SSWs

SSWs are defined when the daily mean zonal mean zonal wind at 10 hPa becomes easterly. Only the first SSW in a given winter is chosen; final warmings are excluded.

4.3.3.2 SSW index

The binary SSW index is defined by assigning years with (without) a SSW a value of −1 (+1).

4.3.3.3 Vortex index

The model derived 'vortex index' is similar to the 'SSW index'; both measure whether a polar vortex event occurs. Introducing the vortex index is necessary because most low-top models have positive stratospheric wind biases, causing wind reversals and SSWs to become rare. The vortex index is based on the daily normalized NAM at 10 hPa and a threshold of +2 (−3) to identify strong (weak) vortex years. The index is assigned a value of +1 (−1) if a strong (weak) vortex is detected; other years (neutral) are assigned a value of zero.

4.3.3.4 NAM

The NAM is based on empirical orthogonal function (EOF) analysis performed individually at each level using daily zonal mean geopotential heights poleward of 20° N; the NAM is the standardized EOF time series at any level.

4.3.3.5 NAO

The NAO is the leading EOF time series of daily sea level pressure over 20° N–80° N and 90° W–40° E.

4.3.3.6 AMOC

The AMOC is the maximum of the North Atlantic meridional overturning streamfunction at 45° N. For some models, the streamfunction is available as a pre-calculated CMIP5 quantity. For other models and for the reanalyses, the streamfunction is derived by vertically integrating the meridional sea water velocity. The reanalysis derived AMOC (1979–2010) stems from the mean over 12 products. Table 5 lists the ocean reanalysis products used to calculate the observational estimate of the AMOC over the past 30 years, shown in Figure 28. Before taking the multireanalysis mean, time series from each reanalysis are normalized, annually averaged, and smoothed (Gaussian filter, σ~1.3 years). All 12 reanalyses are only available for the 1993–2001 period. Outside this period, fewer reanalyses exist, creating spurious discontinuities at the interface between the full and the reduced set. We adjust for this by removing from the reduced set the difference between the full and reduced set at the interface.

4.3.3.7 AMO

The AMO is the monthly mean SST average over 0° N–60° N and 75° W–7.5° W (Ottera *et al.*, 2010).

Table 5 Ocean reanalyses.

Name	Institute	Model	Period	Reference
CERFACS	CERFACS	OPA8.2/NEMO	1979-2005	Daget *et al.* (2008)
ECCO_JPL	NASA-JPL	MITgcm and MOM4	1993-2011	Stammer *et al.* (2002) ECCO model products are available at http://www.ecco-group.org
GECCO	Center for Marine and Atmospheric Sciences (ZMAW)	MITgcm	1979-2001	Köhl *et al.* (2006) Köhl and Stammer (2008)
GFDL-ODA	GFDL	MOM4	1979-2007	Zhang *et al.* (2007)
GODAS	NCEP	MOMv3	1980-2011	Huang *et al.* (2011)
IFM-GEOMAR	Leibniz Institute of Marine Sciences at the University of Kiel	MPI	1979-2005	Keenlyside *et al.* (2005)
INGV	INGV	OPA8.2	1979-2005	Bellucci *et al.* (2007)
METOFFICE	METOFFICE	Ocean model of HadGEM2	1979-2004	Ingleby and Huddleston (2007)
NEMOVAR – COMBINE	ECMWF	NEMO3.0	1979-2008	Balmaseda *et al.* (2010)
ORA_S3	ECMWF	HOPE	1979-2009	Balmaseda *et al.* (2008)
PEODAS	Centre for Australian Weather and Climate Research	ACOM2	1979-2010	Yin *et al.* (2011)
SODA v2.2.4	University of Maryland	POP2.x	1979-2008	Carton and Giese (2008)

4.4 Results

4.4.1 Influences of strong polar vortex on surface

The observational record is too short for a rigorous analysis of multidecadal variability. Therefore, we examine outcomes from the climate model GFDL-CM2.1, which is integrated for 4000 years with constant forcings, approximately representative for preindustrial conditions (Wittenberg, 2009). A connection between the stratosphere and the ocean depends on the downward coupling into the troposphere. We examine this coupling by comparing the simulation against atmospheric reanalysis (hereafter simply observations). Focusing on periods when the polar vortex is unusually strong, we define events during which the northern annular mode index (NAM) at 10 hPa crosses a threshold of 2.5. Our outcomes are not very sensitive to the exact threshold, but our choice limits the number of events and captures sufficiently strong events. In the observations, we find 22 events, which is an average of 4.0 per decade. At 3.8 per decade, the model produces similar statistics. We form composites of observed and simulated events in terms of anomalies in the NAM at pressure levels between 1000 and 10 hPa and for various lags. The model captures well the structure of downward propagating stratospheric NAM anomalies seen in the observations (Figure 30a, b). However, the NAM is normalized and thus not an absolute measure of circulation anomaly. This is important, because the model does not have a well-resolved stratosphere, and, compared to the observations, it underestimates the day-to-day variability of zonal mean zonal winds in the stratosphere by about 40%. A more objective response measure is the zonal wind stress (τ) over our North Atlantic study region (15° W–60° W, 45° N–65° N). For the selected events, the simulated τ anomalies are considerably smaller than in the

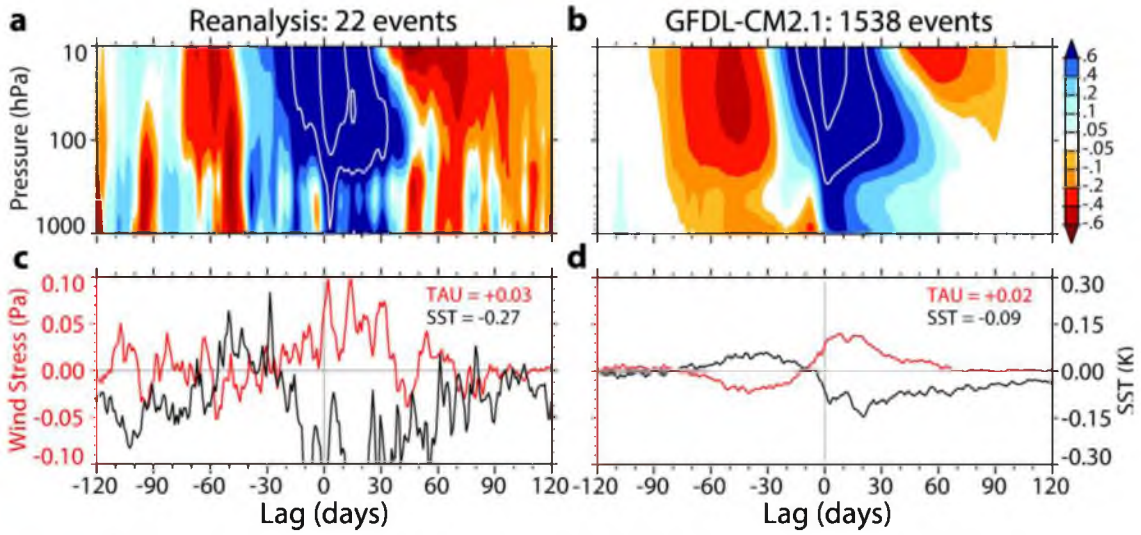

Figure 30 Strong polar vortex composites and their surface impact. (a, b) Time–height development of the NAM index; white contours indicate NAM values of 1 and 2. Horizontal time axis indicates the lead or lag (in days) with respect to the date of the events. The events are determined by the dates on which the NAM at 10 hPa exceeds +2.5. (c, d) Associated (red) zonal wind stress and (black) SST anomalies over the North Atlantic study region; numbers at the upper right are averages over days 0–60.

observations (Figure 30c, d), which is probably a consequence of the inadequate treatment of the model's stratosphere. However, it is reassuring that the model reproduces the observed sign and temporal structure of τ.

The surface impacts of the events examined in Figure 30 include a north–south dipole in sea level pressure, which is a positive phase of the NAO (Figure 31). The nodal point of this dipole is located to the south of Greenland. There, the changes in wind stress amplify the climatological mean westerlies and heat fluxes that extract thermal energy from the ocean. The model produces a heat flux pattern (Figure 31 shading) that is very similar to the observations, but the sea surface temperature (SST) cooling over the study region is three times smaller (Figure 30c, d). This muted SST response is related to the weak wind stress forcing, but also to the model's heat distribution in a 10 m thick top

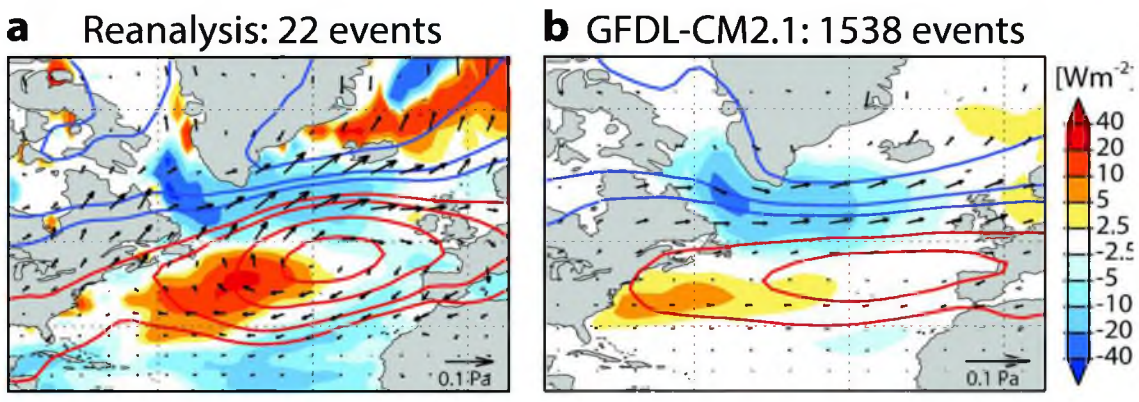

Figure 31 Spatial pattern of surface impact from the stratosphere. Shown are composite anomalies averaged from day 0 to 60 following the strong vortex events of Figure 30 for (a) reanalysis and (b) GFDL-CM2.1 model. Sea-level pressure anomalies are contoured at ±0.5, ±1, ±2, ±3, ±4 hPa; red and blue lines indicate positive and negative values, respectively. Shading shows the sum of latent and sensible heat flux anomalies (in W m^{-2}), with positive and negative anomalies indicating oceanic heat gain and loss, respectively. Vectors represent the magnitude and direction of surface wind stress anomalies.

ocean layer. The cooling to the south of Greenland is dynamically relevant because it is colocated with sites of significant deepwater formation in the Labrador and Irminger Seas and with the model's subpolar gyre (SPG; Figure 32). Figure 32 presents the climatological mixed layer depth and barotropic stream function of the ocean component of GFDL-CM2.1. This illustrates the geographical locations of the model's downwelling region and gyre system over the North Atlantic.

4.4.2 Impact of persistent stratospheric flow variations

We now study the ocean response in GFDL-CM2.1 to the stratospherically induced cooling. Because low-frequency forcing should be most effective in driving the ocean (Hasselmann, 1976), we composite on a low-pass filtered stratospheric NAM (see Methods) using a threshold of ±1. From the 4000 years, we identify 75 strong and 70

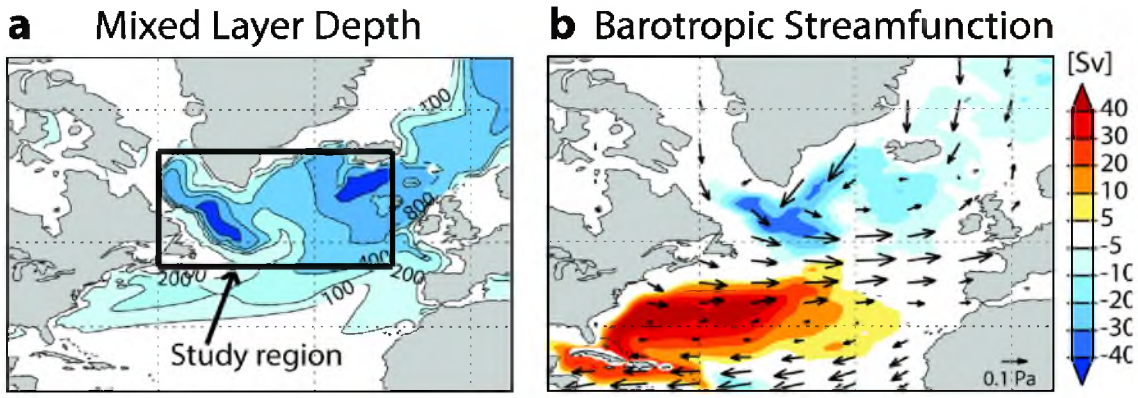

Figure 32 GFDL-CM2.1 simulated climatological mean (November-March) ocean fields. (a) Ocean mixed layer depth, contoured at 100, 200, 400, 800, and 1600 m. The rectangular box denotes our North Atlantic study region (15°W to 60°W, 45°N to 65°N). (b) (shading) Barotropic stream-function and (vectors) surface wind stress vectors.

weak events. Results from weak events are multiplied by −1 and combined with the strong events to form a single composite. The vortex index (Figure 33a), which reflects the likelihood for a vortex event to occur, shows the outcome of the compositing in terms of stratospheric circulation anomalies: the compositing favors strong polar vortex events that happen for several consecutive years centered on year zero. This situation is comparable to the one seen in the observations over the past 30 years (Figure 28a).

Over our study region, the vortex events induce a ~0.1°K cooling at the ocean surface (Figure 33b). Over the course of a few years, this signal penetrates into the deep ocean. The speed and depth of the penetration suggest that deep convection, which prevails over this region, is responsible. The cooling is followed by regular oscillations, which have a similar periodicity as the model's AMOC (Figure 29). This suggests that the oscillations are connected to the AMOC, which is confirmed when compositing the AMOC on the stratospheric events (Figure 33c). Following the central date, the AMOC undergoes regular fluctuations that are coherent with the ocean temperatures.

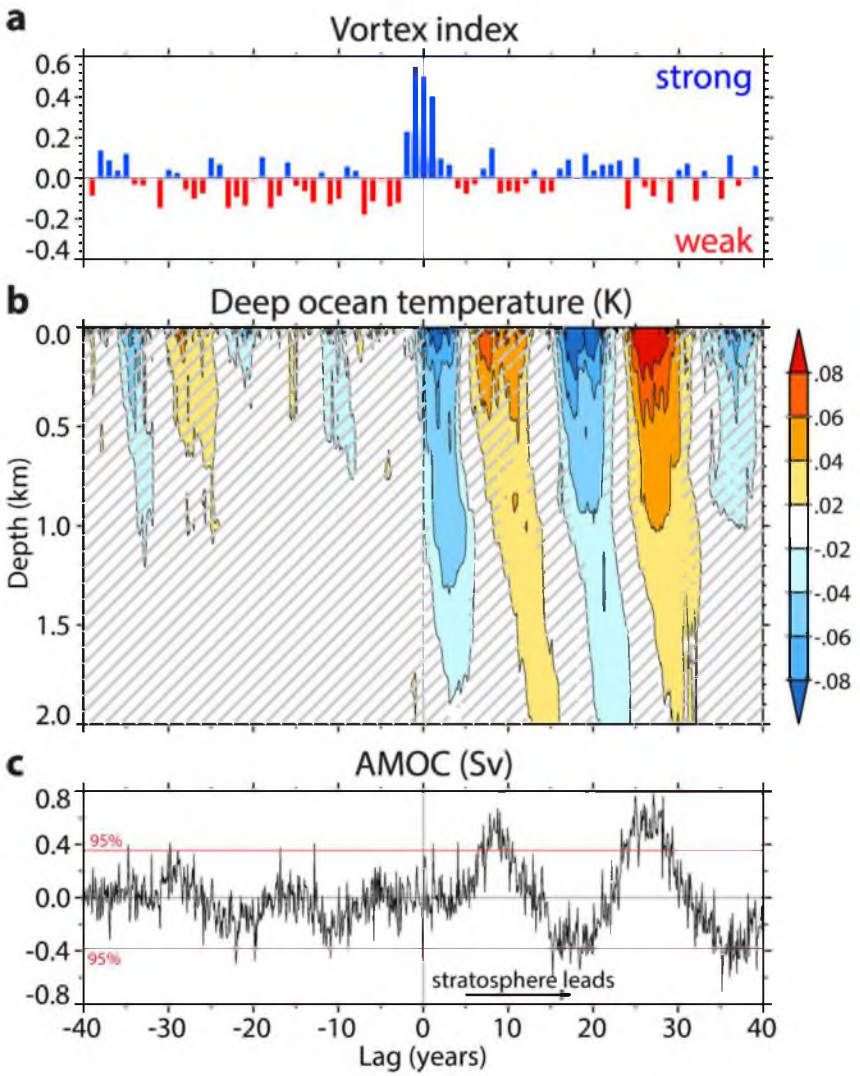

Figure 33 Impact of persistent stratospheric flow variations. Shown are GFDL-CM2.1 derived composites of periods during which the polar vortex was either persistently strong (75 events) or persistently weak (70 events, multiplied by −1). (a) Composite time series of the vortex index, measuring the likelihood that a vortex event happens during a given year. The index represents a composite and therefore varies smoothly between +1 and −1. (b) Corresponding monthly time–depth development of ocean temperature anomalies (K) over the study region (15° W–60° W, 45° N–65° N); hatching shows insignificant (95%) results. (c) Corresponding monthly anomalies in AMOC strength (Sv).

The standard deviation of the low-pass filtered AMOC fluctuations following the central date amounts to ~ 0.23 Sv (Figure 33c). However, for certain strong events this value exceeds ~ 0.5 Sv (Figure 34), which can be compared to the ~ 1.3 Sv of the model's total AMOC standard deviation. In other words, forcing from the stratosphere contributes to a large portion of total AMOC variability. The vigorous intrinsic tendency of the model's AMOC to oscillate suggests that the stratosphere acts as a trigger for such oscillations and that forcing at the resonant frequency is most effective in driving it. This is supported by analysis presented in Figure 34, which shows for GFDL-CM2.1 how low frequency stratospheric fluctuations at specific frequencies affect the AMOC. The increased density of reddish colors at ~20 years and at large thresholds demonstrates that strong stratospheric forcing at the resonant frequency of the AMOC is most influential in driving the AMOC.

4.4.3 Verification from CMIP5 models

We generalize our results by investigating further simulations taken from the preindustrial control experiment of the Fifth Coupled Model Intercomparison Project (CMIP5). For each CMIP5 model, we examine the surface anomalies that develop over the study region in response to vortex events (Figure 35a). As before, strong events are associated with increased τ and colder SSTs, but there is a large intermodel spread. We divide the models into two classes: high-top models with a well-resolved stratosphere, and low-top models with a relatively simple stratosphere. The surface response of the combined (black) high-top models is significantly stronger than that of the (grey) low-top models, confirming our previous assumption about the role of stratospheric representation. Using criteria identical to that in Figure 33, we composite the AMOC

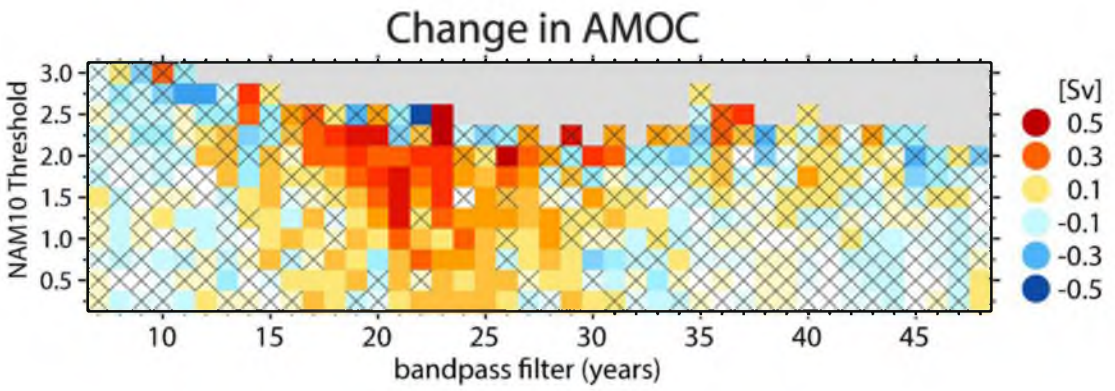

Figure 34 Resonant forcing is most effective in AMOC driving. Colors show changes in GFDL-CM2.1 AMOC strength using different compositing criteria. The criteria are similar to that in Figure 33, except that different band pass filtered versions of the NAM at 10 hPa and different NAM thresholds are used. Color shows the difference in composite low-pass filtered AMOC standard deviation between the 20 years following and preceding the composite date. Crosshatching indicates outcomes that are not significantly different (at 95%) from randomly chosen events. The number of events in each composite varies between ~250 (lower left) and 10; outcomes from less than 10 events are omitted and shown in grey.

time series from all high-top (Figure 35b) and all low-top (Figure 35c) models on low-frequency vortex events. As in GFDL-CM2.1, the AMOC of both multimodel ensembles starts to oscillate after the vortex events. However, whereas the oscillations persist for decades in GFDL-CM2.1, they vanish after several years in the CMIP5 ensembles. This is due to the widely differing spectral characteristics of the AMOC in the models, leading the composite outcome to decorrelate relatively fast. The magnitude of the AMOC anomalies after the events reaches ~ 20% of the climatological standard deviation. It is about the same for the two model classes, despite the differences in forcing strength at the surface. This similarity might be related to model differences that go beyond our simple high-top/low-top classification and the complicated response of the AMOC, which involves nonlinear dynamics.

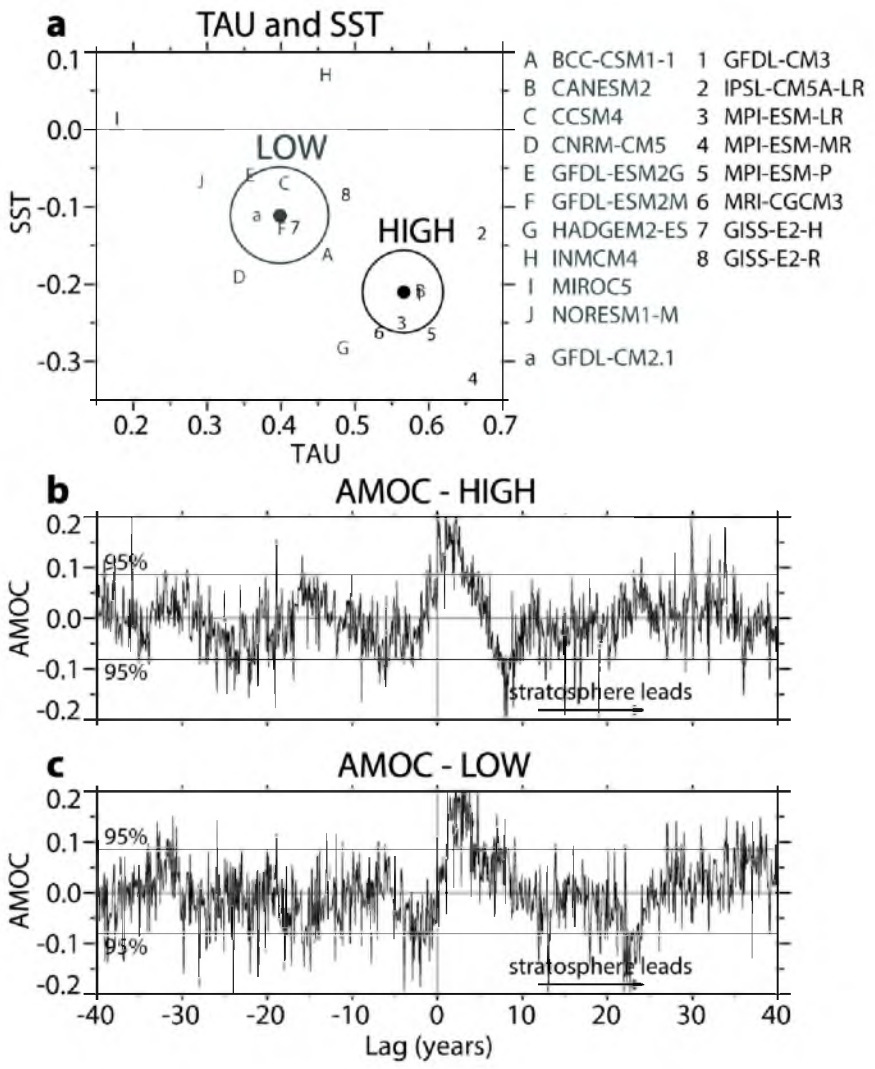

Figure 35 CMIP5 composites on stratospheric NAM. (a) Standardized τ and SST anomalies over the study region for individual models and mean of all low-top and all high-top models; the anomalies are averages over months 1–2 (τ) and 1–3 (SST) following the NAM events. Thresholds of +2.5 and −3 in monthly NAM define the events. Circles are 95% uncertainty intervals (see Methods). (b, c) Standardized AMOC anomalies from the high-top (low-top) models composited on persistent NAM events; the events are defined as in Figure 33 and contain 127 (143) strong and 133 (144) weak events for LOW (HIGH).

4.4.4 Stratospheric influences on the oceanic circulation

The analysis in the main part of the paper is based on composites of events for selected stratospheric events. This was done to continue a tradition of stratosphere related work and to unequivocally relate the stratosphere to tropospheric and oceanic signals. However, statistical regression analysis leads to very similar but much clearer results than the composites because all available data are used. This is demonstrated in Figure 36, which shows lagged regressions of various time series on the AMOC for (panel a) GFDL-CM2.1 and for (panel b) the low-top and high-top CMIP5 multimodel ensembles. For GFDL-CM2.1, the regression of the AMOC on itself (panel a, black curve) simply demonstrates that the AMOC is an oscillatory phenomenon that decorrelates over time. The result for the NAM at 10 hPa (blue) confirms that stratospheric oscillations that precede the AMOC and that have a 20-year period provide the optimal forcing. The regressions for the NAO (red) are similar, but the values become smaller with increasing lead and they lag the stratosphere by a few years. The decrease in NAO regressions with increasing negative lag suggests that the temporal coherence of low-frequency oscillations is weaker in the troposphere than in the stratosphere. The interesting temporal lag of a few years between stratospheric NAM and tropospheric NAO may be due to the combined effects of forcing from the stratosphere and forcing from the increasingly positive AMOC on the NAO. Also, note that the regression values for positive lags exhibit small but coherent oscillations with a 20-year period, hinting again that AMOC related SST variations weakly feedback into the atmosphere. This explanation is supported by previous findings about weak feedbacks of the North Atlantic Ocean on the atmosphere. The outcomes for (panel b) the two CMIP5 ensembles are similar: in both

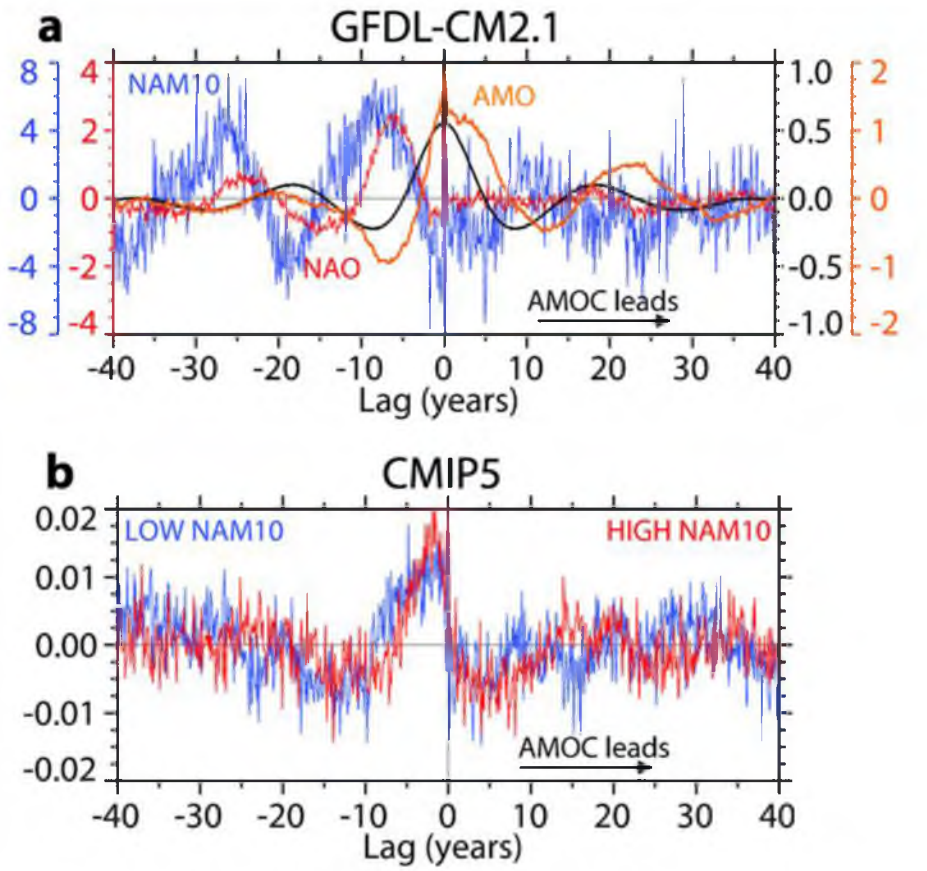

Figure 36 Lagged regressions on monthly AMOC index. All data are monthly means. (a) For GFDL-CM2.1, with (blue) showing the NAM at 10 hPa (10^{-3} Sv^{-1}), (red) the NAO (10^{-2} Sv^{-1}), (orange) the AMO index (10^{-2} K/Sv), and (black) the AMOC index itself. As in Msadek *et al.* (2011), the AMO index is defined as the monthly mean SSTs averaged over the region 0°N-60°N and 75°W-7.5°W. (b) For the NAM at 10 hPa (unitless) from the CMIP5 multimodel ensemble and using a standardized AMOC index, with (blue) showing the outcome from the low-top and (red) the high-top group of models.

cases, strong (weak) stratospheric vortex events are followed by a positive (negative) AMOC, implying that the stratosphere is causal.

4.4.5 Relationship between the NAM and the AMOC

In Figure 37 we further investigate the lead-lag relationship among the NAM at 10 hPa, the NAO, and the AMOC, using a multitaper spectral coherence analysis. The top three panels (a-c) are for GFDL-CM2.1, and the bottom panel (d) is for the CMIP5 multi-model ensembles. The results for GFDL-CM2.1 demonstrate that at periods of ~20 years, variations among the NAM at 10 hPa, NAO, and AMOC are coherent at statistically significant levels. Further, variations in the NAM at 10 hPa lead variations in the NAO by about 20 degrees (ca. 1 year) (Figure 37a), and variations in the NAM at 10 hPa and the NAO lead variations in the AMOC by about 90 degrees (ca. 5 years) (Figure 37b, c). The outcome for the CMIP5 ensembles (Figure 37d) indicates that the coherence between the stratospheric NAM and the AMOC is very large and significant at three spectral intervals (ca. 12, 20, and 40 years). At most periods the stratospheric NAM leads variations in the AMOC by phases between 0 and 90 degrees.

4.5 Conclusion

Our analysis suggests a significant stratospheric impact on the ocean. Recurring stratospheric vortex events create long-lived perturbations at the ocean surface, which penetrate into the deeper ocean and trigger multidecadal variability in its circulation. This leads to the remarkable fact that signals that emanate from the stratosphere cross the entire atmosphere–ocean system. The propagation into the deeper ocean can be explained from the well-known impact of the NAO on the SPG and AMOC (Hakkinen, 1999;

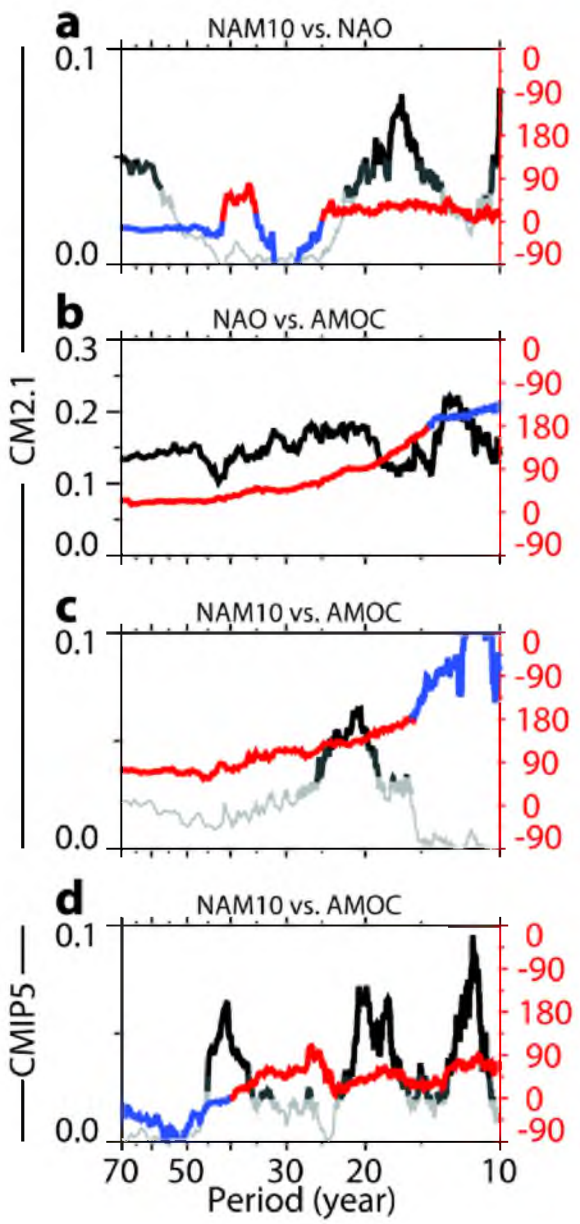

Figure 37 Spectral coherence between annual mean time series. Black-and-white curves (left axis) indicate spectral coherence, with values below the 90% significance level shown in light grey, and values above the 95% (99%) level shown in dark-grey (black). Red-blue curves (right axis) indicate phase (in degrees); red color means that the first index leads the second ($0° \leq$ phase $< 180°$); blue color means that the first index lags the second ($-180° \leq$ phase $< 0°$). Panels (a) to (c) are for GFDL-CM2.1, and (d) is for the CMIP5 multimodel ensemble.

Lohmann *et al.*, 2009). The oscillatory behavior of the ocean following stratospheric events is probably related to a delayed negative feedback of the AMOC on itself (Eden and Jung, 2001; Lohmann *et al.*, 2009; Delworth *et al.*, 1993). A number of factors promote the stratosphere–ocean connection: the persistence of individual stratospheric events; a stratospheric rhythm that matches the resonant frequency of the AMOC; the dynamical coupling from the stratosphere to the troposphere; the collocation between the NAO nodal point and regions of downwelling; and the intrinsic instability of the AMOC.

We do not advocate the stratosphere as the sole or primary source of AMOC variability. However, the stratosphere seems to contain a significant amount of low-frequency energy capable of modulating the AMOC. The source of this energy may be related to coupling with other subcomponents of climate (Msadek *et al.*, 2011; Mosedale *et al.*, 2006; Cohen *et al.*, 2007) or variations in external forcings (Ottera *et al.*, 2010; Ineson *et al.*, 2011). However, in our simulations external forcings are held constant in time, and our analysis (Figures 33, 36, and 37) leads to the conclusion that at low frequencies the stratosphere drives the AMOC. It seems most likely to us that the stratospheric multidecadal energy is related to stochastic forcing from the troposphere (Scaife *et al.*, 2005; Plumb and Semeniuk, 2003), which may involve variations in the dynamical wave forcing (Butchart *et al.*, 2000), or in the frequency of blockings (Hakkinen *et al.*, 2011) and their influence on SSWs (Martius *et al.*, 2009).

Our results have implications for the prediction of decadal climate, a subject that has gained increasing attention recently (Keenlyside *et al.*, 2008; Smith *et al.*, 2010; Mehta *et al.*, 2011). As it is impossible to accurately predict variations in the strength of the polar vortex beyond several days, it is likely that the new mechanism acts to limit the skill of

decadal predictions. However, representing the coupling between stratosphere, troposphere, and ocean in modeling systems should refine estimates of decadal climate predictability and improve the skill of short-term climate predictions after strong stratospheric events. Our results add to an increasing body of evidence that the stratosphere forms an important component of climate and that this component should be represented well in models.

CHAPTER 5

CONCLUSION

Changes in the stratospheric circulation influence weather and climate in the troposphere, especially at high latitudes. This dissertation intends to improve our understanding of stratospheric influences on variability in the troposphere and the ocean on intraseasonal to interdecadal time scales. The dissertation is comprised of three major parts. In the first part, Chapter 2, we examine a possible positive feedback between stratospheric ozone and the circulation. In the second part, Chapter 3, we quantify the uncertainty of the persistence time scale of the annular mode and further investigate the role of the stratosphere for the troposphere. In the third part, Chapter 4, we investigate influences of low-frequency stratospheric variability on the ocean.

In Chapter 2, we hypothesize the existence of a positive feedback between stratospheric ozone and the circulation. The suggested feedback consists of the following processes: natural or man-made variations in stratospheric ozone lead to anomalous absorption of solar radiation and cause at some lag temperature anomalies in the polar lower stratosphere during spring. The heating or cooling alters the strength of the polar vortex, which is an important barrier for meridional transports from the tropics to the poles. A strong vortex also limits the propagation and breaking of planetary waves from the troposphere, a process which in turn weakens the Brewer-Dobson circulation and

again reduces the poleward transport of ozone-rich air from the tropical upper stratosphere to the high latitudes. Interactions between chemical and dynamical changes may reinforce each other and create our hypothesized positive feedback. The feedback is evident through variability increases of the extratropical circulation.

In Chapter 3, we emphasize the importance of the annular mode persistence time scale, which apparently is systematically overestimated by many climate models. This raises the concern that the models are overly sensitive to external forcings and that future projections based on those models are unreliable. However, we find that the current 50-year record of global historical observations may be too short to judge the ability of climate models to reproduce faithfully the observed annular mode time scale. We also find a robust relationship between the magnitude and the seasonal timing of the annular mode time scale in both the stratosphere and the troposphere, confirming and extending earlier results of a dynamical coupling between the stratosphere and the troposphere and of influences of stratospheric variability on the troposphere.

In Chapter 4, we propose that at long interdecadal time scales changes in the stratospheric circulation and those in the oceanic circulation over the North Atlantic Ocean are connected. This connection is established by the North Atlantic oscillation (NAO), a large-scale pattern of near-surface circulation anomalies over the North Atlantic. Persistent disturbances of the stratospheric polar vortex modulate the NAO, and the NAO in turn drives the Atlantic meridional overturning circulation (AMOC) through anomalous surface fluxes. This connection is suggested by our analysis of atmospheric and oceanic reanalyses: over the past 30 years, the stratosphere and the AMOC experienced low-frequency variations that were similar to each other. Using coupled

atmosphere-ocean models, we demonstrate that this similarity is consistent with the hypothesis that variations in the sequence of stratospheric circulation anomalies significantly influence the North Atlantic Ocean. The analysis of climate model simulations confirms the existence of a covariability between stratospheric and oceanic circulation. This covariability provides evidence that the stratosphere is important for climate and climate change.

Since the stratosphere plays an important role in shaping the tropospheric climate and the oceanic circulation on various time scales, we conclude that models should faithfully represent the stratosphere as it forms an important component of climate.

REFERENCES

Albers, J. R. and T. R. Nathan, 2012: Pathways for communicating the effects of stratospheric ozone to the polar vortex: Role of zonally asymmetric ozone. *J. Atmos. Sci.*, **69**, 785-801.

Albers, J. R., J. P. McCormack, and T. R. Nathan, 2013: Stratospheric ozone and the morphology of the northern hemisphere planetary waveguide. *J. Geophys. Res.*, **118**, 563-576.

Albers, J. R. and T. R. Nathan, 2013: Ozone loss and recovery and the preconditioning of upward-propagating planetary wave activity. *J. Atmos. Sci.*, **70**, 3977-3994.

Ambaum, M. H. P. and B. J. Hoskins, 2002: The NAO troposphere-stratosphere connection. *J. Climate*, **15**, 1969-1978.

Athanasiadis, P. J. and M. H. P. Ambaum, 2009: Linear contributions of different time scales to teleconnectivity. *J. Climate*, **22**, 3720-3728.

Baldwin, M. P. and T. J. Dunkerton, 1999: Propagation of the Arctic oscillation from the stratosphere to the troposphere. *J. Geophys. Res.*, **104**, 30937-30946.

Baldwin, M. P. and T. J. Dunkerton, 2001: Stratospheric harbingers of anomalous weather regimes. *Science*, **244**, 581-584.

Baldwin, M. P., T. Hirooka, A. O'neill, and S. Yoden, 2003a: Major stratospheric warming in the Southern Hemisphere in 2002: Dynamical aspects of the ozone hole split. *SPARC Newsl.*, **20**.

Baldwin, M. P., D. B. Stephenson, D. W. J. Thompson, T. J. Dunkerton, A. J. Charlton, and O. N. Alan, 2003b: Stratospheric memory and skill of extended-range weather forecasts. *Science*, **301**, 636-640.

Baldwin, M. P. and D. W. J. Thompson, 2009: A critical comparison of stratosphere-troposphere coupling indices. *Quart. Jour. Royal. Met. Soc.*, **135**, 1661-1672.

Balmaseda, M., K. Mogensen, F. Molteni, and A. Weaver, 2010: The NEMOVAR-COMBINE ocean reanalysis. *COMBINE Technical Report*, **No. 1**.

Balmaseda, M. A., A. Vidard, and D. L. T. Anderson, 2008: The ECMWF ocean analysis system: ORA-S3. *Mon. Wea. Rev.*, **136**, 3018-3034.

Bellucci, A., S. Masina, P. DiPietro, and A. Navarra, 2007: Using temperature-salinity relations in a global ocean implementation of a multivariate data assimilation scheme. *Mon. Wea. Rev.*, **135**, 3785-3807.

Braesicke, P. and J. A. Pyle, 2003: Changing ozone and changing circulation in northern mid-latitudes: possible feedbacks? *Geophys. Res. Lett.*, **30**, 1059.

Brasseur, G. P. and S. Solomon, 2005: *Aeronomy of the Middle Atmosphere, 3rd ed.* D. Reidel Company, Dordrecht, Netherlands, 646 p pp.

Brewer, A. W., 1949: Evidence for a world circulation provided by the measurements of helium and water vapour distribution in the stratosphere. *Quart. Jour. Royal. Met. Soc.*, **75**, 351-363.

Butchart, N., J. Austin, J. R. Knight, A. A. Scaife, and M. L. Gallani, 2000: The response of the stratospheric climate to projected changes in the concentrations of well-mixed greenhouse gases from 1992 to 2051. *J. Climate*, **13**, 2142-2159.

Carton, J. A. and B. S. Giese, 2008: A reanalysis of ocean climate using simple ocean data assimilation (SODA). *Mon. Wea. Rev.*, **136**, 2999-3017.

Chan, C. J. and R. A. Plumb, 2009: The response to stratospheric forcing and its dependence on the state of the troposphere. *J. Atmos. Sci.*, **66**, 2107-2115.

Charlton, A. J. and L. M. Polvani, 2007: A new look at stratospheric sudden warmings. Part I: Climatology and modeling benchmarks. *J. Climate*, **20**, 449-469.

Charlton, A. J., L. M. Polvani, J. Perlwitz, F. Sassi, E. Manzini, K. Shibata, S. Pawson, J. E. Nielsen, and D. Rind, 2007: A new look at stratospheric sudden warmings. Part II: Evaluation of numerical model simulations. *J. Climate*, **20**, 470-488.

Charney, J. G. and P. G. Drazin, 1961: Propagation of planetary-scale disturbances from the lower into the upper atmosphere. *J. Geophys. Res.*, **66**, 83-109.

Chen, G. and R. A. Plumb, 2009: Quantifying the eddy feedback and the persistence of the zonal index in an idealized atmospheric model. *J. Atmos. Sci.*, **66**, 3707-3720.

Christiansen, B., 2001: Downward propagation of zonal mean zonal wind anomalies from the stratosphere to the troposphere: model and reanalysis. *J. Geophys. Res.*, **106**, 27307-27322.

Cohen, J., D. Salstein, and K. Saito, 2002: A dynamical framework to understand and predict the major Northern Hemisphere mode. *Geophys. Res. Lett.*, **29**, 51.

Cohen, J., M. Barlow, P. J. Kushner, and K. Saito, 2007: Stratosphere-troposphere coupling and links with Eurasian land surface variability. *J. Climate*, **20**, 5335-5343.

Cohen, J., M. Barlow, and K. Saito, 2009: Decadal fluctuations in planetary wave forcing

modulate global warming in late boreal winter. *J. Climate*, **22**, 4418-4426.

Crutzen, P. J. and F. Arnold, 1986: Nitric acid cloud formation in the cold Antarctic stratosphere: A major cause for the springtime ozone hole. *Nature*, **324**, 651-655.

Daget, N., A. T. Weaver, and M. A. Balmaseda, 2008: An ensemble three-dimensional variational data assimilation system for the global ocean: Sensitivity to the observation and background-error variance formulation. *Tech. Memo.*, **No. 562**, ECMWF: Reading, UK. Available at [http://www.ecmwf.int/publications/library/do/references/list/14].

Dee, D. P., S. M. Uppala, A. J. Simmons, P. Berrisford, P. Poli, S. Kobayashi, U. Andrae, M. A. Balmaseda, G. Balsamo, P. Bauer, P. Bechtold, A. C. M. Beljaars, L. van de Berg, J. Bidlot, N. Bormann, C. Delsol, R. Dragani, M. Fuentes, A. J. Geer, L. Haimberger, S. B. Healy, H. Hersbach, E. V. Hólm, L. Isaksen, P. Kållberg, M. Köhler, M. Matricardi, A. P. McNally, B. M. Monge-Sanz, J. J. Morcrette, B. K. Park, C. Peubey, P. de Rosnay, C. Tavolato, J. N. Thépaut, and F. Vitart, 2011: The ERA-interim reanalysis: Configuration and performance of the data assimilation system. *Quart. Jour. Royal. Met. Soc.*, **137**, 553-597.

Delworth, T., S. Manabe, and R. J. Stouffer, 1993: Interdecadal variations of the thermohaline circulation in a coupled ocean-atmosphere model. *J. Climate*, **6**, 1993-2011.

Delworth, T. L. and R. J. Greatbatch, 2000: Multidecadal thermohaline circulation variability driven by atmospheric surface flux forcing. *J. Climate*, **13**, 1481-1495.

Delworth, T. L. and M. E. Mann, 2000: Observed and simulated multidecadal variability in the Northern Hemisphere. *Clim. Dyn.*, **16**, 661-676.

Delworth, T. L., A. J. Broccoli, A. Rosati, R. J. Stouffer, V. Balaji, J. A. Beesley, W. F. Cooke, K. W. Dixon, J. Dunne, K. A. Dunne, J. W. Durachta, K. L. Findell, P. Ginoux, A. Gnanadesikan, C. T. Gordon, S. M. Griffies, R. Gudgel, M. J. Harrison, I. M. Held, R. S. Hemler, L. W. Horowitz, S. A. Klein, T. R. Knutson, P. J. Kushner, A. R. Langenhorst, H.-C. Lee, S.-J. Lin, J. Lu, S. L. Malyshev, P. C. D. Milly, V. Ramaswamy, J. Russell, M. D. Schwarzkopf, E. Shevliakova, J. J. Sirutis, M. J. Spelman, W. F. Stern, M. Winton, A. T. Wittenberg, B. Wyman, F. Zeng, and R. Zhang, 2006: GFDL's CM2 global coupled climate models. Part I: Formulation and simulation characteristics. *J. Climate*, **19**, 643-674.

Dickinson, R. E., 1968: Planetary Rossby waves propagating vertically through weak westerly wind wave guides. *J. Atmos. Sci.*, **25**, 984-1002.

Dobson, G. M. B., 1956: Origin and distribution of the polyatomic molecules in the atmosphere. *Proc. R. Soc. Lond.*, **236**, 187-193.

Donner, L. J., B. L. Wyman, R. S. Hemler, L. W. Horowitz, Y. Ming, M. Zhao, J.-C. Golaz, P. Ginoux, S. J. Lin, M. D. Schwarzkopf, J. Austin, G. Alaka, W. F. Cooke, T. L. Delworth, S. M. Freidenreich, C. T. Gordon, S. M. Griffies, I. M. Held, W. J. Hurlin, S. A. Klein, T. R. Knutson, A. R. Langenhorst, H.-C. Lee, Y. Lin, B. I. Magi, S. L.

Malyshev, P. C. D. Milly, V. Naik, M. J. Nath, R. Pincus, J. J. Ploshay, V. Ramaswamy, C. J. Seman, E. Shevliakova, J. J. Sirutis, W. F. Stern, R. J. Stouffer, R. J. Wilson, M. Winton, A. T. Wittenberg, and F. Zeng, 2011: The dynamical core, physical parameterizations, and basic simulation characteristics of the atmospheric component AM3 of the GFDL global coupled model CM3. *J. Climate*, **24**, 3484-3519.

Duchon, C. E., 1979: Lanczos filtering in one and two dimensions. *J. Appl. Meteorol.*, **18**, 1016-1022.

Eden, C. and T. Jung, 2001: North Atlantic interdecadal variability: Oceanic response to the North Atlantic oscillation (1865-1997). *J. Climate*, **14**, 676-691.

Eyring, V., M. P. Chipperfield, M. A. Giorgetta, D. E. Kinnison, E. Manzini, K. Matthes, P. A. Newman, S. Pawson, T. G. Shepherd, and D. W. Waugh, 2008: Overview of the new CCMVal reference and sensitivity simulations in support of upcoming ozone and climate assessments and the planned SPARC CCMVal. *SPARC Newsl.*, **30**, 20-26.

Eyring, V., T. G. Shepherd, and D. W. Waugh (Eds.), 2010: SPARC report on the evaluation of chemistry-climate models. *SPARC Report No. 5*, WCRP-132, WMO/TD-No. 1526. Available at [http://www.atmosp.physics.utoronto.ca/SPARC].

Eyring, V., J. M. Arblaster, I. Cionni, J. Sedláček, J. Perlwitz, P. J. Young, S. Bekki, D. Bergmann, P. Cameron-Smith, W. J. Collins, G. Faluvegi, K. D. Gottschaldt, L. W. Horowitz, D. E. Kinnison, J. F. Lamarque, D. R. Marsh, D. Saint-Martin, D. T. Shindell, K. Sudo, S. Szopa, and S. Watanabe, 2013: Long-term ozone changes and associated climate impacts in CMIP5 simulations. *J. Geophys. Res.*, **118**, 5029-5060.

Farman, J. C., B. G. Gardiner, and J. D. Shanklin, 1985: Large losses of total ozone in Antarctica reveal seasonal ClOx/NOx interaction. *Nature*, **315**, 207-210.

Fioletov, V. E. and T. G. Shepherd, 2003: Seasonal persistence of midlatitude total ozone anomalies. *Geophys. Res. Lett.*, **30**, 1417.

Gerber, E. P., L. M. Polvani, and D. Ancukiewicz, 2008a: Annular mode time scales in the intergovernmental panel on climate change fourth assessment report models. *Geophys. Res. Lett.*, **35**, L22707.

Gerber, E. P., S. Voronin, and L. M. Polvani, 2008b: Testing the annular mode autocorrelation time scale in simple atmospheric general circulation models. *Mon. Wea. Rev.*, **136**, 1523-1536.

Gerber, E. P., M. P. Baldwin, H. Akiyoshi, J. Austin, S. Bekki, P. Braesicke, N. Butchart, M. Chipperfield, M. Dameris, S. Dhomse, S. M. Frith, R. R. Garcia, H. Garny, A. Gettelman, S. C. Hardiman, A. Karpechko, M. Marchand, O. Morgenstern, J. E. Nielsen, S. Pawson, T. Peter, D. A. Plummer, J. A. Pyle, E. Rozanov, J. F. Scinocca, T. G. Shepherd, and D. Smale, 2010: Stratosphere-troposphere coupling and annular mode variability in chemistry-climate models. *J. Geophys. Res.*, **115**, D00M06.

Gerber, E. P., 2012: Stratospheric versus tropospheric control of the strength and structure of the Brewer-Dobson circulation. *J. Atmos. Sci.*, **69**, 2857-2877.

Gillett, N. P., M. R. Allen, R. E. McDonald, C. A. Senior, D. T. Shindell, and G. A. Schmidt, 2002: How linear is the Arctic oscillation response to greenhouse gases? *J. Geophys. Res.*, **107**, 4022.

Gillett, N. P. and D. W. J. Thompson, 2003: Simulation of recent Southern Hemisphere climate change. *Science*, **302**, 273-275.

Griffies, S. M., M. Winton, L. J. Donner, L. W. Horowitz, S. M. Downes, R. Farneti, A. Gnanadesikan, W. J. Hurlin, H.-C. Lee, Z. Liang, J. B. Palter, B. L. Samuels, A. T. Wittenberg, B. L. Wyman, J. Yin, and N. Zadeh, 2011: The GFDL CM3 coupled climate model: Characteristics of the ocean and sea ice simulations. *J. Climate*, **24**, 3520-3544.

Hadjinicolaou, P., A. Jrrar, J. A. Pyle, and L. Bishop, 2002: The dynamically driven long-term trend in stratospheric ozone over northern middle latitudes. *Quart. Jour. Royal. Met. Soc.*, **128**, 1393-1412.

Hakkinen, S., 1999: Variability of the simulated meridional heat transport in the North Atlantic for the period 1951–1993. *J. Geophys. Res.*, **104**, 10991-11007.

Hakkinen, S. and P. B. Rhines, 2004: Decline of subpolar North Atlantic circulation during the 1990s. *Science*, **304**, 555-559.

Hakkinen, S., P. B. Rhines, and D. L. Worthen, 2011: Atmospheric blocking and Atlantic multidecadal ocean variability. *Science*, **334**, 655-659.

Hartmann, D. L., J. M. Wallace, V. Limpasuvan, D. W. J. Thompson, and J. R. Holton, 2000: Can ozone depletion and global warming interact to produce rapid climate change? *Proc. Natl. Acad. Sci.*, **97**, 1412-1417.

Hasselmann, K., 1976: Stochastic climate models Part I. Theory. *Tellus A*, **28**.

Haynes, P., 2005: Stratospheric dynamics. *Ann. Rev. Fluid Mech.*, **37**, 263-293.

Hegerl, G. C., T. J. Crowley, W. T. Hyde, and D. J. Frame, 2006: Climate sensitivity constrained by temperature reconstructions over the past seven centuries. *Nature*, **440**, 1029-1032.

Holton, J. R., 1980: The dynamics of sudden stratospheric warmings. *Ann. Rev. Fluid Mech.*, **8**, 169-190.

Holton, J. R., P. H. Haynes, M. E. McIntyre, A. R. Douglass, R. B. Rood, and L. Pfister, 1995: Stratosphere-troposphere exchange. *Rev. Geophys.*, **33**, 403-439.

Houghton, J. T., Y. Ding, D. J. Griggs, M. Noguer, P. J. van der Linden, X. Dai, K. Maskell, and C. A. Johnson, 2001. *Climate Change 2001: The Scientific Basis*,

Cambridge University Press, 994 pp.

Huang, B., Y. Xue, A. Kumar, and D. Behringer, 2011: AMOC variations in 1979–2008 simulated by NCEP operational ocean data assimilation system. *Clim. Dynam.*, 1-13.

Hurrell, J. W., 1995: Decadal trends in the Northern Atlantic oscillation: Regional temperature and precipitation. *Science*, **269**, 676-679.

Ineson, S., A. A. Scaife, J. R. Knight, J. C. Manners, N. J. Dunstone, L. J. Gray, and J. D. Haigh, 2011: Solar forcing of winter climate variability in the Northern Hemisphere. *Nature Geos.*, **4**, 753-757.

Ingleby, B. and M. Huddleston, 2007: Quality control of ocean temperature and salinity profiles: Historical and real-time data. *J. Mar. Sys.*, **65**, 158-175.

Kalnay, E., M. Kanamitsu, R. Kistler, W. Collins, D. Deaven, L. Gandin, M. Iredell, S. Saha, G. White, J. Woollen, Y. Zhu, A. Leetmaa, B. Reynolds, M. Chelliah, W. Ebisuzaki, W. Higgins, J. Janowiak, K. C. Mo, C. Ropelewski, J. Wang, R. Jenne, and D. Joseph, 1996: The NCEP/NCAR 40-year reanalysis project. *Bull. Amer. Meteor. Soc.*, **77**, 437-471.

Karpechko, A. Y., N. P. Gillett, L. J. Gray, and M. Dall'Amico, 2010: Influence of ozone recovery and greenhouse gas increases on Southern Hemisphere circulation. *J. Geophys. Res.*, **115**, D22117.

Keeley, S. P. E., N. P. Gillett, D. W. J. Thompson, S. Solomon, and P. M. Forster, 2007: Is Antarctic climate most sensitive to ozone depletion in the middle or lower stratosphere? *Geophys. Res. Lett.*, **34**, L22812.

Keeley, S. P. E., R. T. Sutton, and L. C. Shaffrey, 2009: Does the North Atlantic oscillation show unusual persistence on intraseasonal timescales? *Geophys. Res. Lett.*, **36**, L22706.

Keenlyside, N. S., M. Latif, M. Botzet, J. Jungclaus, and U. Schulzweida, 2005: A coupled method for initializing El Niño Southern oscillation forecasts using sea surface temperature. *Tellus*, **57A**, 340-356.

Keenlyside, N. S., M. Latif, J. Jungclaus, L. Kornblueh, and E. Roeckner, 2008: Advancing decadal-scale climate prediction in the North Atlantic sector. *Nature*, **453**, 84-88.

Knutti, R., G. A. Meehl, M. R. Allen, and D. A. Stainforth, 2006: Constraining climate sensitivity from the seasonal cycle in surface temperature. *J. Climate*, **19**, 4224-4233.

Köhl, A., D. Dommenget, K. Ueyoshi, and D. Stammer, 2006: The global ECCO 1952 to 2001 ocean synthesis. *ECCO Report*, **No. 40**.

Köhl, A. and D. Stammer, 2008: Variability of the meridional overturning in the North

Atlantic from the 50-year GECCO state estimation. *J. Phys. Oceanogr.*, **38**, 1913-1929.

Kuroda, Y. and K. Kodera, 2005: Solar cycle modulation of the southern annular mode. *Geophys. Res. Lett.*, **32**, L13802.

Leith, C. E., 1975: Climate response and fluctuation dissipation. *J. Atmos. Sci.*, **32**, 2022-2026.

Lohmann, K., H. Drange, and M. Bentsen, 2009: A possible mechanism for the strong weakening of the North Atlantic subpolar gyre in the mid-1990s. *Geophys. Res. Lett.*, **36**, L15602.

Manzini, E., B. Steil, C. Brühl, M. A. Giorgetta, and K. Krüger, 2003: A new interactive chemistry-climate model: 2. Sensitivity of the middle atmosphere to ozone depletion and increase in greenhouse gases and implications for recent stratospheric cooling. *J. Geophys. Res.*, **108**, 4429.

Martius, O., L. M. Polvani, and H. C. Davies, 2009: Blocking precursors to stratospheric sudden warming events. *Geophys. Res. Lett.*, **36**, L14806.

Matsuno, T., 1971: A dynamical model of the stratospheric sudden warming. *J. Atmos. Sci.*, **28**, 1479-1494.

McLandress, C., T. G. Shepherd, J. F. Scinocca, D. A. Plummer, M. Sigmond, A. I. Jonsson, and M. C. Reader, 2011: Separating the dynamical effects of climate change and ozone depletion. Part II: Southern Hemisphere troposphere. *J. Climate*, **24**, 1850-1868.

Meehl, G. A., T. F. Stocker, W. D. Collins, P. Friedlingstein, A. T. Gaye, J. M. Gregory, A. Kitoh, R. Knutti, J. M. Murphy, A. Noda, S. C. B. Raper, I. G. Watterson, A. J. Weaver, and Z.-C. Zhao, 2007: Global Climate Projections. *In: Climate Change 2007: The Physical Science Basis. Contribution of Working Group I to the Fourth Assessment Report of the Intergovernmental Panel on Climate Change*, [Solomon, S., D. Qin, M. Manning, Z. Chen, M. Marquis, K.B. Averyt, M. Tignor and H.L. Miller (eds.)]. Cambridge University Press, Cambridge, United Kingdom and New York, NY, USA.

Mehta, V., G. Meehl, L. Goddard, J. Knight, A. Kumar, M. Latif, T. Lee, A. Rosati, and D. Stammer, 2011: Decadal climate predictability and prediction: Where are we? *Bull. Amer. Meteor. Soc.*, **92**, 637-640.

Mosedale, T. J., D. B. Stephenson, M. Collins, and T. C. Mills, 2006: Granger causality of coupled climate processes: Ocean feedback on the North Atlantic oscillation. *J. Climate*, **19**, 1182-1194.

Msadek, R., C. Frankignoul, and L. X. Li, 2011: Mechanisms of the atmospheric response to North Atlantic multidecadal variability: A model study. *Clim. Dyn.*, **36**, 1255-1276.

Nathan, T. R. and E. C. Cordero, 2007: An ozone-modified refractive index for vertically

propagating planetary waves. *J. Geophys. Res.*, **112**, D02105.

Norton, W. A., 2003: Sensitivity of Northern Hemisphere surface climate to simulation of the stratospheric polar vortex. *Geophys. Res. Lett.*, **30**, 1627-1630.

Ottera, O. H., M. Bentsen, H. Drange, and L. Suo, 2010: External forcing as a metronome for Atlantic multidecadal variability. *Nature Geos.*, **3**, 688-694.

Perlwitz, J., S. Pawson, R. L. Fogt, J. E. Nielsen, and W. D. Neff, 2008: Impact of stratospheric ozone hole recovery on Antarctic climate. *Geophys. Res. Lett.*, **35**, L08714.

Plumb, R. A. and K. Semeniuk, 2003: Downward migration of extratropical zonal wind anomalies. *J. Geophys. Res.*, **108**, 4223.

Polvani, L. M., D. W. Waugh, G. J. P. Correa, and S.-W. Son, 2011: Stratospheric ozone depletion: The main driver of twentieth-century atmospheric circulation changes in the Southern Hemisphere. *J. Climate*, **24**, 795-812.

Pyle, J. A., P. Braesicke, and G. Zeng, 2005: Dynamical variability in the modelling of chemistry-climate interactions. *Faraday Discuss.*, **130**, 27-39.

Randall, D. A., R. A. Wood, S. Bony, R. Colman, T. Fichefet, J. Fyfe, V. Kattsov, A. Pitman, J. Shukla, J. Srinivasan, R. J. Stouffer, A. Sumi, and K. E. Taylor, 2007: Cilmate Models and Their Evaluation. *In: Climate Change 2007: The Physical Science Basis. Contribution of Working Group I to the Fourth Assessment Report of the Intergovernmental Panel on Climate Change* [Solomon, S., D. Qin, M. Manning, Z. Chen, M. Marquis, K.B. Averyt, M.Tignor and H.L. Miller (eds.)]. Cambridge University Press, Cambridge, United Kingdom and New York, NY, USA, 996pp.

Randel, W. J. and F. Wu, 1999: Cooling of the Arctic and Antarctic polar stratospheres due to ozone depletion. *J. Climate*, **12**, 1467-1479.

Reichler, T., P. J. Kushner, and L. M. Polvani, 2005: The coupled stratosphere-troposphere response to impulsive forcing from the troposphere. *J. Atmos. Sci.*, **62**, 3337-3352.

Reichler, T. and J. Kim, 2008: How well do coupled models simulate today's climate? *Bull. Amer. Meteor. Soc.*, **89**, 303-311.

Ring, M. J. and R. A. Plumb, 2008: The response of a simplified GCM to axisymmetric forcings: Applicability of the fluctuation-dissipation theorem. *J. Atmos. Sci.*, **65**, 3880-3898.

Salby, M. L., 2008: Involvement of the Brewer-Dobson circulation in changes of stratospheric temperature and ozone. *Dyn. Atmos. Oceans*, **44**, 143-164.

Salby, M. L., E. A. Titova, and L. Deschamps, 2012: Changes of the Antarctic ozone hole: Controlling mechanisms, seasonal predictability, and evolution. *J. Geophys. Res.*, **117**,

D10111.

Scaife, A. A., J. R. Knight, G. K. Vallis, and C. K. Folland, 2005: A stratospheric influence on the winter NAO and North Atlantic surface climate. *Geophys. Res. Lett.*, **32**, L18715.

Schlesinger, M. E. and N. Ramankutty, 1994: An oscillation in the global climate system of period 65-70 years. *Nature*, **367**, 723-726.

Shepherd, T. G., 2007: Transport in the middle atmosphere. *J. Meteor. Soc. Japan*, **85B**, 165-191.

Shine, K. P., 1986: On the modelled thermal response of the Antarctic stratosphere to a depletion of ozone. *Geophys. Res. Lett.*, **13**, 1331-1334.

Sigmond, M., J. F. Scinocca, and P. J. Kushner, 2008: Impact of the stratosphere on tropospheric cliamte change. *Geophys. Res. Lett.*, **35**, L12706.

Simpson, I. R., P. Hitchcock, T. G. Shepherd, and J. F. Scinocca, 2011: Stratospheric variability and tropospheric annular-mode timescales. *Geophys. Res. Lett.*, **38**, L20806.

Smith, D. M., R. Eade, N. J. Dunstone, D. Fereday, J. M. Murphy, H. Pohlmann, and A. A. Scaife, 2010: Skilful multi-year predictions of Atlantic hurricane frequency. *Nature Geos.*, **3**, 846-849.

Solomon, S., R. R. Garcia, F. S. Rowland, and D. J. Wuebbles, 1986: On the depletion of Antarctic ozone. *Nature*, **321**, 755-758.

Solomon, S., 1999: Stratospheric ozone depletion: A review of concepts and history. *Rev. Geophys.*, **37**, 275-316.

Son, S.-W., S. Lee, S. B. Feldstein, and J. E. Ten Hoeve, 2008a: Time scale and feedback of zonal-mean-flow variability. *J. Atmos. Sci.*, **65**, 935-952.

Son, S.-W., L. M. Polvani, D. W. Waugh, H. Akiyoshi, R. Garcia, D. Kinnison, S. Pawson, E. Rozanov, T. G. Shepherd, and K. Shibata, 2008b: The impact of stratospheric ozone recovery on the Southern Hemisphere westerly jet. *Science*, **320**, 1486-1489.

Son, S.-W., N. F. Tandon, L. M. Polvani, and D. W. Waugh, 2009: Ozone hole and Southern Hemisphere climate change. *Geophys. Res. Lett.*, **36**, L15705.

Son, S.-W., A. Purich, H. H. Hendon, B.-M. Kim, and L. M. Polvani, 2013: Improved seasonal forecast using ozone hole variability? *Geophys. Res. Lett.*, **40**, 6231-6235.

Son, S. W., E. P. Gerber, J. Perlwitz, L. M. Polvani, N. P. Gillett, K. H. Seo, V. Eyring, T. G. Shepherd, D. Waugh, H. Akiyoshi, J. Austin, A. Baumgaertner, S. Bekki, P. Braesicke, C. Brühl, N. Butchart, M. P. Chipperfield, D. Cugnet, M. Dameris, S. Dhomse, S. Frith, H. Garny, R. Garcia, S. C. Hardiman, P. Jöckel, J. F. Lamarque, E. Mancini, M.

Marchand, M. Michou, T. Nakamura, O. Morgenstern, G. Pitari, D. A. Plummer, J. Pyle, E. Rozanov, J. F. Scinocca, K. Shibata, D. Smale, H. Teyssèdre, W. Tian, and Y. Yamashita, 2010: Impact of stratospheric ozone on Southern Hemisphere circulation change: A multimodel assessment. *J Geophys. Res.*, **115**, D00M07.

Stammer, D., C. Wunsch, I. Fukumori, and J. Marshall, 2002: State estimation improves prospects for ocean research. *Eos Trans. AGU*, **83**.

Taylor, K. E., R. J. Stouffer, and G. A. Meehl, 2012: An overview of CMIP5 and the experiment design. *Bull. Amer. Meteor. Soc.*, **93**, 485-498.

Thompson, D. W. J. and J. M. Wallace, 1998: The Arctic oscillation signature in the wintertime geopotential height and temperature fields. *Geophys. Res. Lett.*, **25**, 1297-1300.

Thompson, D. W. J. and J. M. Wallace, 2000: Annular modes in the extratropical circulation. Part I: Month-to-month variability. *J. Climate*, **13**, 1000-1016.

Thompson, D. W. J., J. M. Wallace, and G. C. Hegerl, 2000: Annular modes in the extratropical circulation. Part II: Trends. *J. Climate*, **13**, 1018-1036.

Thompson, D. W. J. and J. M. Wallace, 2001: Regional climate impacts of the Northern Hemisphere annular mode. *Science*, **293**, 85-89.

Thompson, D. W. J., M. P. Baldwin, and S. Solomon, 2005: Stratosphere-troposphere coupling in the Southern Hemisphere. *J. Atmos. Sci.*, **62**, 708-715.

Thompson, D. W. J., S. Solomon, P. J. Kushner, M. H. England, K. M. Grise, and D. J. Karoly, 2011: Signatures of the Antarctic ozone hole in Southern Hemisphere surface climate change. *Nature Geosci*, **4**, 741-749.

Watanabe, S., T. Hajima, K. Sudo, T. Nagashima, T. Takemura, H. Okajima, T. Nozawa, H. Kawase, M. Abe, T. Yokohata, T. Ise, H. Sato, E. Kato, K. Takata, S. Emori, and M. Kawamiya, 2011: MIROC-ESM: model description and basic results of CMIP5-20c3m experiments. *Geosci. Model Dev. Discuss.*, **4**, 1063-1128.

Waugh, D. W., W. J. Randel, S. Pawson, P. A. Newman, and E. R. Nash, 1999: Persistence of the lower stratospheric polar vortices. *J. Geophys. Res.*, **104**, 27191-27201.

Weber, M., S. Dikty, J. P. Burrows, H. Garny, M. Dameris, A. Kubin, J. Abalichin, and U. Langematz, 2011: The Brewer-Dobson circulation and total ozone from seasonal to decadal time scales. *Atmos. Chem. Phys.*, **11**, 11221-11235.

Wittenberg, A. T., 2009: Are historical records sufficient to constrain ENSO simulations? *Geophys. Res. Lett.*, **36**, L12702.

Yin, Y., O. Alves, and P. R. Oke, 2011: An ensemble ocean data assimilation system for seasonal prediction. *Mon. Wea. Rev.*, **139**, 786-808.

Zhang, S., M. J. Harrison, A. Rosati, and A. Wittenberg, 2007: System design and evaluation of coupled ensemble data assimilation for global oceanic climate studies. *Mon. Wea. Rev.*, **135**, 3541-3564.